NNLO mixed QCD-EW corrections to the Drell-Yan production of Z and W bosons

Zhaoting Pan

UNIVERSITÉ DE GRENOBLE

THÈSE

Pour obtenir le grade de

DOCTEUR DE L'UNIVERSITÉ DE GRENOBLE

Spécialité : **Physique Subatomique et Astroparticules**

Arrêté ministériel : 7 août 2006

Présentée par

Zhaoting Pan

Thèse dirigée par **Roberto Bonciani**

préparée au sein **Laboratoire de Physique Subatomique et de Cosmologie**
et de **l'École Doctorale de Physique de Grenoble**

Corrections mixtes QCD-EW au niveau NNLO à la production Drell-Yan de bosons Z et W.

Thèse soutenue publiquement le **25 Octobre 2013**,
devant le jury composé de :

Dr. Malek Fairouz
Directeur de recherche CNRS, LPSC, Université de Grenoble , Président
Pr. Degrassi Giuseppe
Professor, University of Roma Tre, Rome, Italy, Rapporteur
Pr. Teubner Thomas
Professor, University of Liverpool, Liverpool, United Kingdom, Rapporteur
Dr. Roberto Bonciani
University of Roma " La Sapienza" and INFN Sezione di Roma, Rome, Italy , Directeur de thèse

First I would like to thank Prof. Giuseppe Degrassi and Prof. Thomas Teubner for doing me the honor of being my referees and for having attended my defense. Their remarks will be very useful for my project. Then, I would like to thank Malek Fairouz for making me the pleasure to chair my thesis jury.

I am greatful to Roberto Bonciani, my supervisor, for giving me the opportunity to work with him and giving me his support, confidence and frienship during this project. His determination and encouragement were valuable during these three years and helped me to overcome many difficulties.

I am also grateful to Serge Kox, Director of the LPSC, for hosting me in the laboratory, as well as to all the administrative staff for guiding me patiently.

Many thanks to my co-supervisor, Ingo Schienbein, especially for guiding me during my first teaching experiences and during the last year. I thank Sabine Kraml, head of the theoretical physics group for her support.

Then, my gratitude goes to all the members of the group for the time I passed with them during these three years: they made in such a way that to come to LPSC has always been a pleasure. I would particularly like to thank the PhD students: Beranger Dumont, Tomas Jezo, Florian Lyonnet, Quentin le Boulc'h, Josselin Proudom, and Jeremy Bernon for the great atmosphere.

Finally, I thank the CSC for the financial support during these three years and my family, especially my parents, for their constant support and encouragement.

Résumé

La thèse porte sur les corrections mixtes QCD-EW au niveau NNLO à la production Drell-Yan de bosons Z et W. Le processus Drell-Yan est un processus fondamental permettant de tester avec précision le Modèle Standard (MS) de physique des particules au sein de collisionneurs hadroniques, car ce dernier présente une section efficace importante, une signature expérimentale très propre, ainsi qu'une très haute sensibilité aux propriétés des bosons de jauge. En particulier, la production Drell-Yan de Ws est importante pour une détermination précise (via distribution en masse transverse et distribution en p_T) de la masse du W, m_W, un paramètre d'entrée du MS. La masse du W sera mesurée au LHC de façon très précise ($\Delta m_W \sim 10$MeV). Ce niveau de précision requiert un contrôle théorique d'une précision équivalente sur les distributions cinématiques. La production Drell-Yan de bosons Z permet quant à elle une mesure précise d'un autre paramètre important du MS, $\sin^2\theta_W$. Une prédiction théorique précise de l'asymétrie Forward-backward dans le canal de désintégration $Z \to l^+l^-$ peut ainsi permettre au LHC d'égaler la performance du LEP. Par ailleurs, le Drell-Yan est un processus de fond pour de nombreuses réactions importantes comme, par exemple, la production de paires top-antitop ou la production de nouvelles résonances vectorielles, Z' et W', présentes dans des nombreuses extensions du MS. Enfin, le mécanisme de Drell-Yan peut être utilisé pour la calibration des détecteurs et la détermination de la luminosité au LHC. Pour toutes ces raisons, une prédiction théorique précise et fiable, siginfiant ici que l'on garde sous contrôle les termes provenant des corrections perturbatives d'ordre supérieur de la section efficace et des distributions du mécanisme de production de Drell-Yan, est exigée pour mener à bien des études de physique au niveau de collisionneurs hadroniques.

L'état de l'art pour les prédictions théoriques inclut les corrections QCD au niveau NNLO, avec la resommation de termes logarithmiques provenant de l'émission des gluons *softs*. Toutefois, afin de correspondre à la précision requise pour la détermination des paramètres du MS, les corrections mixtes, fortes-électrofaibles, peuvent jouer un rôle important. Dans cette thèse, nous étudions les corrections mixtes QCD-EW au niveau NNLO, en accordant une attention particulière aux contributions virtuel-réel et double-réel à la section efficace totale de production d'un boson Z ou W on shell. Le calcul est effectué analytiquement, en utilisant une méthode introduite il y a quelques années par C. Anastasiou K. Melnikov, et dont l'algorithme est décrit ci-dessous. Nous générons des diagrammes de Feynman impliqués dans ce processus, avec un générateur (par exemple `Qgraf`) . En utilisant les règles de Cutkosky, nous pouvons re-écrire l'intégration sur l'espace des phases des termes d'interférence (diagrammes à une boucle $2 \to 2$ interférés avec les diagrammes *tree-level* $2 \to 2$ et diagrammes au niveau de l'arbre $2 \to 3$ au carré) en fonction d'une combinaison d'intégrales avec propagateurs ayant la correcte prescription de causalité et propagateurs avec la prescription opposée. Ces intégrales peuvent être traitées de la même manière que les

corrections virtuelles. En particulier, nous réduisons le nombre d'intégrales scalaires, dont les divergences sont régularisées en régularisation dimensionnelle, à un petit ensemble d'intégrales indépendantes appelées Master Integrals (MIs) . Cette réduction est réalisée en utilisant l'algorithme de Laporta, basé sur les identités d'intégration par partie, implémentées dans un programme C++ nommé Reduze 2. Le calcul des MIs est effectué en utilisant la méthode de résolution par équations différentielles. En conséquence, nous obtenons les MIs exprimées comme une série de Laurent en $(D-4)$, où D est la dimension de l'espace-temps, qui multiplie un facteur qui tient compte de la limite souple de l'intégrale exacte en D. Dans cette thèse, nous donnons les expressions analytiques explicites pour les MIs des contributions virtuel-réel et double-réel, nécessaires pour le calcul de la section efficace totale.

Abstract

The thesis concerns the NNLO mixed QCD-EW corrections to the Drell-Yan (DY) production of Z and W bosons, via the following reactions: $pp(\bar{p}) \to Z+X \to l^+l^-+X$ and $pp(\bar{p}) \to W + X \to l\nu + X$. This is a fundamental process for an accurate test of the Standard Model (SM) at hadron colliders, since it has a large cross section, a clean experimental signature, and it is very sensitive to the properties of the gauge bosons. In particular, the Drell-Yan production of Ws is important for an accurate determination (via transverse mass and p_T distributions) of the W mass, m_W, an input parameter of the model. The W mass is supposed to be measured at the LHC very accurately ($\Delta m_W \sim 10\,\text{MeV}$). This level of accuracy requires an equally accurate theoretical control on the kinematic distributions. Drell-Yan production of Z bosons allows for a precise measurement of another important parameter of the SM, $\sin^2\theta_W$. An accurate theoretical prediction for the forward-backward asymmetry in the $Z \to l^+l^-$ decay channel can allow the LHC to match the performance of LEP. Furthermore, Drell-Yan is a background process for many important reactions, like for instance, the production of top-antitop pairs or the production of new vector resonances, Z' and W', present in many extensions of the SM. Finally, the Drell-Yan mechanism can be used for detector calibration and determination of the collider luminosity at the LHC. Because of all these reasons, an accurate and reliable theoretical prediction for the cross section and the distributions of the Drell-Yan production mechanism, that means control on the higher-order perturbative corrections, is demanded for physics studies at hadron colliders.

The state of the art for the theoretical predictions includes the NNLO QCD corrections, together with the resummation of logarithmic terms originating from soft gluon emission, and the NLO EW corrections. All these corrections are implemented in ad hoc Monte Carlo event generators. However, in order to match the required accuracy for the determination of the SM parameters, the mixed strong-electroweak corrections can play an important role and have to be considered. In this thesis, we study the mixed QCD-EW corrections to Drell-Yan processes at the NNLO. Let us consider the production of leptons in the final state (l^+l^- pairs or $l\nu$). The exact NNLO corrections involve two-loop corrections to the $2 \to 2$ process (virtual corrections), one-loop corrections to the $2 \to 3$ process, where the leptonic pair is produced with an additional photon or gluon in the final state (virtual-real corrections) and

tree-level $2 \to 4$ processes, in which the leptonic pair is produced together with a photon and a gluon in the final state (double-real corrections). From a technical point of view, the calculation of such a set of corrections would involve the calculation of very complicated Feynman diagrams, such as two-loop box diagrams with massive propagators, one-loop pentagons, as well as the corresponding IR subtraction counter-terms. However, if we consider sufficiently inclusive observables it is known that the biggest contribution comes from the diagrams in which the decaying particle (Z or W boson) is nearly on-shell. The remaining contribution is of order $\mathcal{O}(\Gamma/M)$, where Γ is the decay width of the boson and M its mass (in our case this ratio is very small, at the percent level). In this approximation, we can decouple the decay from the production process and consequently, the complication of the calculation is far reduced. We, then, concentrate on the production of an on-shell Z (or W) boson, paying particular attention to the virtual-real and double-real contributions to the total cross section. The calculation is performed analytically, using a method introduced some years ago by C. Anastasiou and K. Melnikov for the calculation of the NNLO QCD corrections to the total cross section of production of a Higgs boson. This method consists in what follows. We generate the Feynman diagrams, involved in the process under consideration, with a diagram generator (for instance `Qgraf`). Using the Cutkosky rules, we can re-write the integration over the phase-space of the interference terms (one-loop $2 \to 2$ diagrams interfered with the tree-level $2 \to 2$ and tree $2 \to 3$ diagrams squared) in terms of a combination of integrals with propagators having the right causality prescription and propagators with the opposite one. These integrals can be treated in the same way as the virtual corrections. In particular, we reduce the large number of scalar integrals, whose divergences are regulated in dimensional regularization, to a small set of independent integrals called Master Integrals (MIs). This reduction is done using the "Laporta Algorithm", based on the Integration-by-Parts Identities, implemented in a `C++` computer program called `Reduze`. The calculation of the MIs is performed using the method of differential equations. As a result, we get the MIs expressed as a Laurent series in $\epsilon = (4-D)/2$, where D is the dimension of the space-time, multiplying a factor which takes into account the soft limit of the integral in D dimensions.

We performed the complete reduction to the set of MIs in the two cases: the production of an on-shell Z boson and the production of a on-shell W boson. The double-real contributions (diagrams with three cuts) can be expressed in terms of 11 MIs, 8 of which were already present in the literature. Nevertheless, we performed again their calculation, in order to validate our approach. We found complete agreement with the 8 MIs used in the case of the Higgs boson production. Moreover, we provide the analytic expression of the 3 MIs that were not present in the case of the Higgs production. Since we are dealing with electroweak corrections, we have to consider also the contribution coming from diagrams in which a massive virtual boson (Z or W) is exchanged. The three additional MIs refer indeed to these kind of diagrams,

and have two massive propagators (one of which is a cut propagator). The virtual-real contributions (diagrams with two cuts) are expressed in terms of 26 MIs. Out of them, 5 contain a single massive (cut) propagator and were already known in the literature. Also in this case, we performed again by scratch the calculation finding complete agreement. The remaining 22 MIs were not present in the literature. 13 contain two massive propagators (one is cut) and 8 contain three massive propagators (again, one of them is a cut propagator). The main difference between the NNLO QCD corrections to Higgs boson production and the corrections we are considering in this thesis lies in the fact that in the latters it is possible to exchange virtual massive bosons. Correspondingly, the Feynman diagrams contain massive propagators and the analytic structure of the results is more rich and also more involved. In particular, topologies with many entangled MIs appear. In the case of the two-cut diagrams, we encountered one topology with three entangled MIs in the set of masters with two massive propagators and one topology with four entangled masters belonging to the set with three massive propagators. While we suceeded to decouple (partially) in the limit $\epsilon \to 0$ the system of three linear differential equations corresponding to the case with three entangled MIs, we are still working on the system of four entangled MIs.

An additional note concerns the set of basis functions used to express the analytic results present in the thesis. The subset of diagrams involved in the NNLO QCD corrections to the Higgs boson production can be expressed entirely in terms of harmonic polylogarithms (HPLs), *i.e.* in terms of generalized polylogarithms with weights $(-1, 0, 1)$. This is also the case of the majority of the MIs with two massive propagators. However, two MIs with two massive propagators present an additional denominator, which introduces an additional fractional weight to the set of the HPLs. Moreover, the system of differential equations of the four entangled MIs seems to present again additional denominators and the set of weights results augmented by two complex numbers and relative complex conjugates. This would clearly mean that for the calculation of the diagrams with more masses, the basis of HPLs is not sufficient and the functional basis of generalized polylogarithms is needed. These results are still preliminary and need further investigation.

Aside from the expressions of the 13 three-cut and two-cut diagrams involved in the calculation of the NNLO QCD corrections to the Higgs boson production, which were already known in the literature and that we re-calculated in order to check our approach, in the thesis we include the expressions of 3 new MIs with three cuts (2 massive propagators), 7 new MIs with two cuts (2 massive propagators) and 1 MI with two cuts and 3 massive propagators. In the case of 2 entangled MIs with two massive propagators, at the moment we do not have the result for the soft limit, and the masters are expressed in terms of explicit integration constants, still unconstrained.

The other MIs are work in progress. We have the corresponding systems of first-order linear differential equations and, at least in the case with two massive propagators, their solution should be only matter of time. In the three-massive case,

instead, the bottleneck is constituted by the four entangled MIs, that needs further investigation.

The present work is structured as follows.

In Chapter 1, we introduce the Drell-Yan process and we describe briefly the physical motivation for Drell-Yan studies at hadron colliders. The measurements of the Drell-Yan production of W and Z bosons are performed very accurately at LHC by ATLAS and CMS collaborations. We discuss the importance of equally accurate theoretical predictions for the relevant observables and we review the status of the theoretical calculations present in the literature. Moreover, we present our notations and conventions.

In Chapter 2, we discuss the full set of Feynman diagrams needed for the calculation of the mixed QCD-EW corrections to the DY production of Z and W bosons. We describe the narrow-width approximation, which allows us to perform the calculation disentangling the production of the gauge boson from its subsequent decay. Finally, we list the set of corrections on which we will focus in the rest of the thesis.

In Chapter 3, we present in some details the method on which we based our calculations: the reduction to the MIs of the problem, using the Laporta algorithm implemented in the computer program Reduze, publicly released, and the calculation of the MIs by means of the Differential Equations method. We further discuss the solution of the differential equations in two cases: exact solution in D dimensions, expressing the result in terms of hypergeometric-like functions, or solution in Laurent expansion of $(D-4)$.

In Chapter 4, we focus on the reduction of the diagrams corresponding to the double real and virtual-real emissions of photons and gluons. Following the method introduced for the NNLO QCD corrections to the total cross section of production of a Higgs boson, we use the Cutkosky rules in order to treat the real emission in the same way as the virtual corrections. We reduce the big number of dimensionally regularized scalar integrals to a small set of MIs and we discuss their soft limit, needed to constraint the arbitrary constants in the solution of the differential equations.

In Chapter 5, we present the calculation of the MIs using the differential equations and we collect our results.

Finally, in Chapter 6, we draw our conclusions and outlook.

Two appendices are added at the end of the text. In Appendix 1, we give our notations and relevant Feynman rules. In Appendix 2, we remind the reader with some basic property of the set of functions used to express the results of the MIs: the set of harmonic polylogarithms (HPLs).

Contents

Chapter 1

The Drell-Yan Process

1.1 Introduction

1.1.1 Discovery of Drell-Yan process and application

The first dimuon experiment [1] for the observation of massive muon pairs in hadron collisions was done using the reaction $p + U \rightarrow \mu^+ + \mu^- + X$. Data were taken at incident proton energies of 22, 25, 28.5, and 29.5 GeV/c and the muon pair mass of 1-6.7 GeV. This experiment was originally designed to search for intermediate weak bosons. No such a resonant structure was found. The result of the experiment was given by a fall in the cross section with increasing dilepton mass over almost 10 orders of magnitude, as is shown in the left plot of Fig. 1.1.

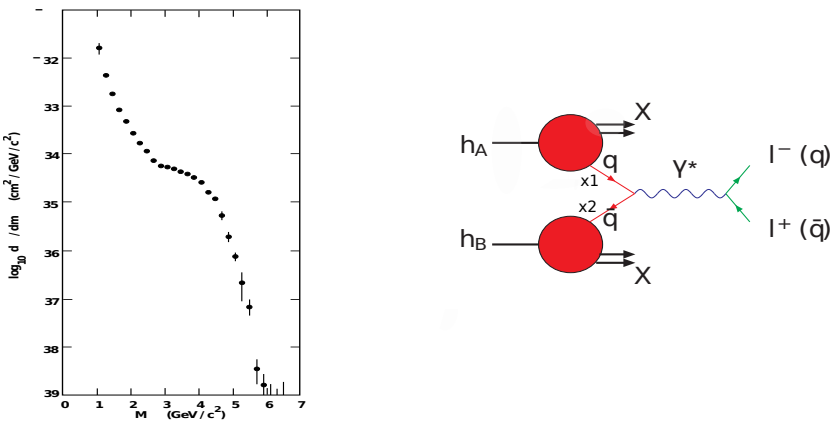

Figure 1.1: The left plot is the result of the first dimuon experiment, the right one is Drell-Yan process with single intermediate photon

In 1970, Sidney Drell and Tung-Mow Yan proposed [20] that the continuum of the opposite-sign dileptons was produced in hadron-hadron collision by the process

depicted on the right picture of Fig. 1.1, applying in fact to the first dimuon experiment the concept of "Parton Model" [2]. In the first step an antiquark from one hadron annihilates against a quark from the other hadron to give a virtual photon. Subsequently this photon converts to a pair of (opposite-sign) leptons: $\mu^+\mu^-$,e^+e^-, ... The process is an electromagnetic process. The hard matrix element can be calculated in perturbation theory and then convoluted with the parton distribution functions, that include the non perturbative long distance information. The generated virtual photon contributes with a factor M^{-4} in the cross section and this leads to the rapid fall of the cross section with increasing delipton mass.

Since 1970, the Drell-Yan (DY) mechanism was studied extensively, both in fixed-target and collider experiments. It provides valuable pieces of informations about the parton distribution functions (PDFs), which describe the way the momentum of an incoming high-energy nucleon is partitioned among its constituent partons. These PDFs are basic ingredients for calculating essentially all processes at hadron colliders. Measurements of Drell-Yan production cross sections allow the extraction of the structure functions of the beam hadron. Since experimentally the detection of a lepton pair is relatively simple, the lepton pair production data have become an integral component of the global fits, together with the deep inelastic lepton-nucleon scattering, in determining the parton distributions inside a nucleon (see Fig. 1.2). Moreover, the J/Ψ(charm) and Υ families of resonances were discovered with DY

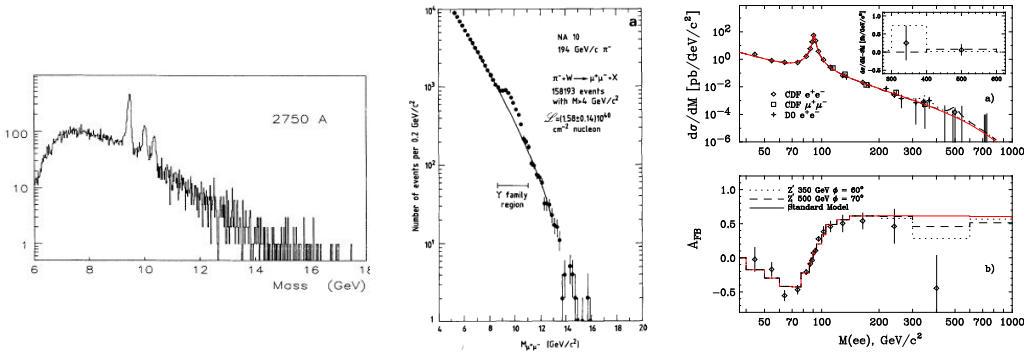

Figure 1.2: The first plot is the $p + W \to \mu^+\mu^- X$ probing antiquark distribution at 800 GeV/c , the second one is $\pi^- + W \to \mu^+\mu^- X$ probing antiquark distribution in pion at 194 Gev/c, the last two are $\bar{p} + p \to l^+l^- X$ probing antiquark distribution in antiproton at 1.8 TeV [3].

mechanism. This mechanism was the first application of the parton model idea beyond deep inelastic scattering, and it played a crucial role in the design of the experiment at CERN, which later discovered the W and Z bosons.

1.1.2 Drell-Yan mechanism

Let us illustrate the leading order Drell-Yan process as shown on the right picture in Fig. 1.1. A high-mass lepton pair l^+l^- emerges from $q\bar{q}$ annihilation in a proton-proton collision. The quark carries a fraction x_1 of the first hadron's longitudinal momentum, and a fraction x_2 of the other hadron's longitudinal momentum is carried by the antiquark. The leading-order (LO) QCD prediction takes the form

$$\sigma(p(P_1)p(P_2) \to \ell^+\ell^- + X) = \int_0^1 dx_1 \int_0^1 dx_2 \sum_a f_a(x_1) f_{\bar{a}}(x_2) \times \\ \times \hat{\sigma}(q_a(x_1P_1) + \bar{q}_{\bar{a}}(x_2P_2) \to \ell^+\ell^- + X), \tag{1.1}$$

where the sum runs over all species of quarks and antiquarks. X denotes any hadronic final state. The parton distribution functions, $f(x)$, are defined as the probability density of finding a parton with longitudinal momentum fraction x inside the proton. Let s be the squared center-of-mass energy of the hadron-hadron collision. Then the four-momentum of the annihilating pair to the dilepton four-momentum (E, p_ℓ) gives:

$$E = (x_1 + x_2)\sqrt{s}/2, \tag{1.2}$$

and

$$p_\ell = (x_1 - x_2)\sqrt{s}/2. \tag{1.3}$$

The virtuality of the exchanged photon, or equivalently the invariant mass squared M^2 of the lepton pair, is given by[1]

$$M^2 = -(p_{l^+} + p_{l^-})^2 = E^2 - p_\ell^2 = s x_1 x_2 \,. \tag{1.4}$$

Two basic relations between the quark variables and the observable now appear:

$$\tau = M^2/s \tag{1.5}$$

and

$$x_F = 2p_\ell/\sqrt{s} = x_1 - x_2 \,. \tag{1.6}$$

Let us consider the process $q + \bar{q} \to \mu^+\mu^-$. Quantum electrodynamics yields the leading-order cross section above the threshold:

$$\sigma(q + \bar{q} \to \mu^+\mu^-) = -\frac{4\pi\alpha^2 Q_q^2}{3N_c q^2} \,, \tag{1.7}$$

where Q_q is the quark charge, q is the four-momentum of the virtual photon and N_c is the number of colors ($N_c = 3$ in the Standard Model). At leading order $\hat{s} = -q^2 = M^2$, therefore

$$\sigma(q + \bar{q} \to \mu^+\mu^-) = \frac{4\pi\alpha^2 Q_q^2}{3N_c M^2} \,. \tag{1.8}$$

[1]Note that we use the Pauli-Veltman metric tensor $(+++-)$.

The cross section for the lepton pair production is therefore

$$d^2\sigma(pp \to \mu^+\mu^- + X) = \sum_q 4\pi\alpha^2 Q_q^2 f_q(x_1) f_{\bar{q}}(x_2) dx_1 dx_2 / 3N_c M^2. \tag{1.9}$$

Re-expressing this in the measurable dilepton parameters M^2 and x_F gives

$$\frac{d^2\sigma(pp \to \mu^+\mu^- + X)}{dM^2 dx_F} = \frac{4\pi\alpha^2}{3N_c M^4} \frac{x_1 x_2}{x_1 + x_2} \sum_q Q^2 f_q(x_1) f_{\bar{q}}(x_2), \tag{1.10}$$

where

$$\begin{aligned} x_1 &= \frac{1}{2}[(x_F^2 + 4\tau)^{1/2} + x_F], \\ x_2 &= \frac{1}{2}[(x_F^2 + 4\tau)^{1/2} - x_F]. \end{aligned} \tag{1.11}$$

If we now introduce the rapidity of the lepton pair

$$Y = \frac{1}{2} \log\left(\frac{x_1}{x_2}\right), \tag{1.12}$$

we have $dY = dx_F/(x_1 + x_2)$ and thus

$$\frac{d^2\sigma(pp \to \mu^+\mu^- + X)}{dM^2 dY} = \frac{4\pi\alpha^2}{3N_c M^2 s} \sum_q Q_q^2 \{f_q(x_1) f_{\bar{q}}(x_2) + (q \leftrightarrow \bar{q})\}. \tag{1.13}$$

1.1.3 Notation and Born approximation

In this section, we discuss the lowest order contribution to the partonic cross section of production of a lepton or lepton-neutrino pair via the exchange of a weak boson.

We consider first the process $q(p_1)\bar{q}(p_2) \to Z(p) \to e^+(p_3)e^-(p_4)$ and illustrate the calculation of the cross section $\hat{\sigma}_Z^{(0)}$. The relevant Feynman diagram is shown in Fig. 1.3. The boson mass is expressed by m. The Mandelstam invariants are defined as follows:

$$s = -(p_1 + p_2)^2, \quad t = -(p_1 - p_3)^2, \quad u = -(p_2 - p_3)^2. \tag{1.14}$$

Using Feynman rules given in Appendix A, the matrix element at LO can be written as

$$\begin{aligned} \mathcal{M}_Z^B &= \frac{-i}{(2\pi)^4} \bar{u}(p_4)[i(2\pi)^4] \frac{ig\gamma_\mu}{4c_w}(c_2 - \gamma^5) v(p_3) \frac{1}{s - M_Z^2 + im_Z\Gamma_Z} \\ &\quad \times \bar{v}(p_2)[i(2\pi)^4] \frac{ig}{4c_w} \gamma^\mu (c_1 + \gamma^5) u(p_1) \delta_{ij}, \end{aligned} \tag{1.15}$$

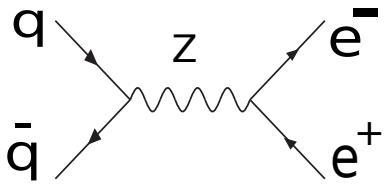

Figure 1.3: The lowest order Feynman diagram contribution to the amplitude for the reaction $q\bar{q} \to Z \to e^+e^-$. The arrows denote the flow of charged quarks and leptons.

where $s_w = \sin(\theta_W)$, $c_w = \cos(\theta_W)$, $c_1 = 1 - \frac{8}{3}s_w^2$, $c_2 = 4s_w^2 - 1$, N_c is the number of colors ($N_c = 3$ in the Standard Model), m_Z is the pole mass of the Z boson, Γ_Z its total width, $M_Z^2 = m_Z^2 - \Gamma_Z^2/4$. Then, averaging over the initial spins and colors and summing over the final spins, we find the following matrix element modulus squared: $|\mathcal{M}_Z^B|^2 = \mathcal{M}_Z^B \mathcal{M}_Z^{B*}$,

$$\begin{aligned}
\overline{|\mathcal{M}_Z^B|^2} &= \frac{1}{4N_c^2} \sum_{s_i, s_f, c} |\mathcal{M}_Z^B|^2 \\
&= \frac{(2\pi)^8 g^4}{4N_c c_w^4} \frac{1}{(s - M_Z^2)^2 + m_Z^2 \Gamma_z^2} \big[(-\frac{1}{4} + \frac{5s_w^2}{3} - \frac{8s_w^4}{3}) t^2 \\
&\quad + (\frac{1}{4} - \frac{5s_w^2}{3} + \frac{37s_w^4}{9} + \frac{32s_w^8}{9})(s^2 + 2st + 2t^2) \big], \qquad (1.16)
\end{aligned}$$

where we used the following sums over polarizations:

$$\sum_\lambda u(p)\bar{u}(p) = -i \not{p}, \qquad (1.17)$$

$$\sum_\lambda v(p)\bar{v}(p) = -i \not{p}, \qquad (1.18)$$

since we consider the quark and the electron as massless. The total cross section can be expressed by

$$\hat{\sigma}_Z^{(0)} = \frac{1}{8s} \int \frac{d^3p_3}{(2\pi)^3 p_3^0} \frac{d^3p_4}{(2\pi)^3 p_4^0} (2\pi)^{-4} \delta^4(p_1 + p_2 - p_3 - p_4) \overline{|\mathcal{M}^B|^2} \qquad (1.19)$$

and using the relations,

$$x = |\vec{p}_3|, \qquad t = \sqrt{s}|\vec{p}_3|(\cos\theta - 1); \qquad (1.20)$$

inserting Eq. (1.17) into Eq. (1.18), we find

$$\begin{aligned}\hat{\sigma}_Z^{(0)} &= \frac{1}{4N_c}\frac{1}{8s}\int \frac{x^2 dx d\Omega}{4(2\pi)^2 x^2}\frac{\delta(x-\frac{\sqrt{s}}{2})}{2}\frac{g^4}{c_w^4}\frac{1}{(s-M_Z^2)^2+m_Z^2\Gamma_z^2} \\ &\times\big[(-\frac{1}{4}+\frac{5s_w^2}{3}-\frac{8s_w^4}{3})sx^2(\cos\theta-1)^2+(\frac{1}{4}-\frac{5s_w^2}{3}+\frac{37s_w^4}{9}+\frac{32s_w^8}{9}) \\ &\times(s^2+2s\sqrt{s}x(\cos\theta-1)+2sx^2(\cos\theta-1)^2\big]. \end{aligned} \tag{1.21}$$

Finally, we have

$$\hat{\sigma}_Z^{(0)} = \frac{g^4}{192\pi N_c c_w^4}\frac{s}{(s-M_Z^2)^2+m_Z^2\Gamma_z^2}\Big[\frac{1}{4}-\frac{5s_w^2}{3}+\frac{50s_w^4}{9}-\frac{80s_w^6}{9}+\frac{64s_w^8}{9}\Big]. \tag{1.22}$$

For the W boson production, we consider the lowest order process $q(p_1)\bar{q}(p_2) \to W(p) \to l^+(p_3)\nu_l(p_4)$. We choose the same kinematic notation as for the case of the

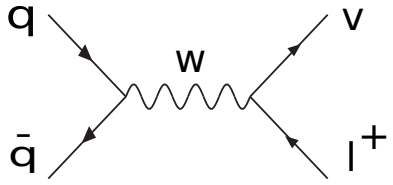

Figure 1.4: The lowest order Feynman diagram contributing to the amplitude for the reaction $q\bar{q} \to W \to l^+\nu$. The arrows denote the flow of charged quarks and leptons.

Z boson production. Then:

$$\begin{aligned}\mathcal{M}_W^B &= \frac{-i}{(2\pi)^4}\bar{u}(p_4)[i(2\pi)^4]\frac{ig}{2\sqrt{2}}\gamma_\mu(1+\gamma^5)v(p_3)\frac{1}{s-M_W^2+im_W\Gamma_W} \\ &\times\bar{\nu}(p_2)[i(2\pi)^4]\frac{ig}{2\sqrt{2}}\gamma^\mu(1+\gamma^5)V_{ud}u(p_1) \end{aligned} \tag{1.23}$$

where V_{ud} is the CKM matrix-element, m_W is the W-boson mass and Γ_W is the W decay width. We find

$$\hat{\sigma}_W^{(0)} = \frac{g^4|V_{ud}|^2}{384\pi N_c}\frac{s}{(s-M_W^2)^2+m_W^2\Gamma_W^2}\,, \tag{1.24}$$

where the weak coupling can be expressed in terms of α, the fine structure constant, and of $\sin\theta_W$, the sine of the weak mixing angle, by using the relation $4\pi\alpha = g^2\sin^2\alpha_W$. The weak mixing angle is defined as $\cos\theta_W = m_W/m_Z$, m_W is the pole mass of the W boson, Γ_W its total width, and $M_W^2 = m_W^2 - \Gamma_W^2/4$.

1.1.4 Factorization and parton distribution functions

When quarks or gluons appear in the initial state of the parton subprocess, the corrections to the process will, in general, have mass singularities that do not cancel in the subprocess total cross section. Hence, Drell-Yan cross section in QCD is a combination of short- and long-distance behavior, and it is not computable directly in perturbation theory. The factorization theorem allows us to derive predictions for these cross sections. At the Born approximation the short-distance cross section is identical to the normal parton scattering cross section. At higher orders, the short-distance cross section is derived from the parton scattering cross section by separating the long-distance pieces, which are universal, and factoring them into the parton distribution functions (PDF). The short-distance cross section, instead, is process dependent and is calculable in perturbation theory.

Consider the process $A+B \to l^+ + l^- + X$. The factorization theorem is contained in the following expression at any order in QCD:

$$\sigma_{AB\to l^+l^-+X}(S) = \sum_{a,b} \int_0^1 dz_1 dz_2 f_{aA}(z_1,\mu)\sigma_{ab}(s,\alpha_S(\mu)) f_{bB}(z_{2B},\mu)\,, \tag{1.25}$$

where in Eq. (1.24) the renormalization and factorization scales have been set equal ($\mu_F = \mu_R = \mu$). S and $s = z_1 z_2 S$ are the hadronic and partonic *c.m.* energy respectively. The PDFs f_{aA} and f_{bB} are not calculable within perturbative QCD and must be determined by experiment. They are universal quantities, *i.e.* once f_{aA} is known from an experiment, it can be used to describe the cross section in another reaction initiated by the same hadron A. The evolution of the PDFs with the factorization scale is a prediction of the theory and can be calculated in perturbative QCD. The function σ_{ab} is the hard scattering partonic cross section, process-dependent and computable in perturbation theory.

We define a renormalized (finite) partonic cross section $\bar{\sigma}_{ab}$ and transition functions Γ_{ab} such that

$$\sigma_{ab}(s) \;=\; \int dx_1 dx_2 \Gamma_{ac}(x_1) d\bar{\sigma}_{cd}(x_1 x_2 s)\Gamma_{bd}(x_2). \tag{1.26}$$

x_1 and $x_2 \in [0,1]$ give the momentum fraction of the quark after emitting a gluon. The singular terms are absorbed into the transition function in such a way that the renormalized cross section is finite. The transition functions Γ can be interpreted as the probability densities of finding a quark inside a quark. In order to predict the hadron cross section, renormalized PDFs $\bar{f}$ are needed, which are defined as

$$\bar{f}(\xi) = \int_0^1 \int_0^1 dx dz \Gamma(z)\delta(\xi - xz) = \int_\xi^1 \frac{dz}{z} f(\frac{\xi}{z}) = f(\xi) \otimes \Gamma(\xi). \tag{1.27}$$

The symbol $\otimes$ means the convolution in a compact form. Then the infrared safe hadronic cross section reads

$$\sigma_{AB\to l^+l^-+X}(s) = \sum_{a,b}\int d\xi_1 d\xi_2 \bar{f}_{cA}(\xi_1) d\bar{\sigma}_{cd}(\xi_1\xi_2 s)\bar{f}_{dB}(\xi_2). \quad (1.28)$$

The ξ_1 and $\xi_2 \in [0,1]$ are defined as $\xi_1 = x_1 z_1$ and $\xi_2 = x_2 z_2$. It is easy to find the connection between renormalized and un-renormalized hadronic cross section. Inserting the Eq. (1.27) into Eq. (1.28),

$$\sigma_{AB\to l^+l^-+X}(s) = \sum_{a,b}\int dx_1 dx_2 dz_1 dz_2 f_{aA}(x_1)\Gamma_{ac}(x_1) d\bar{\sigma}_{cd}(x_1 x_2 s)\Gamma_{bd}(x_2) f_{bB}(x_2) \quad (1.29)$$

which now contain only renormalized quantities. The Born cross section is finite, but at NLO it will be necessary to apply the renormalization prescription defined above. The quantities $\bar{\sigma}$, σ and Γ are supposed to have a perturbative expansion in α_S:

$$\begin{aligned}
\bar{\sigma}(s) &= \sum_{n=0}(\frac{\alpha_2}{\pi})^n \bar{\sigma}^{(n)}(s), \\
\sigma(s) &= \sum_{n=0}(\frac{\alpha_2}{\pi})^n \sigma^{(n)}(s), \\
\Gamma(x)_{ab} &= \delta_{ab}\delta(1-x)\sum_{n=0}(\frac{\alpha_2}{\pi})^n \Gamma^{(n)}_{ab}(x). \quad (1.30)
\end{aligned}$$

The first term in the expansion of the transition function is a delta function and $\Gamma^{(1)}_{ab}$ is the lowest order Altarelli-Parisi [4] kenel that gives the evolution of the PDFs. Putting Eq. (1.30) into Eq. (1.26), we find

$$\begin{aligned}
\sigma^{(0)}_{ab}(s) + \frac{\alpha_S}{\pi}\sigma^{(1)}_{ab}(s) &= \bar{\sigma}^{(0)}_{ab}(s) + \frac{\alpha_S}{\pi}\Bigg[\bar{\sigma}^{(1)}_{ab}(s) + \sum_c \int dx_1 \Gamma^{(1)}_{ac}(x_1) d\bar{\sigma}^{(0)}_{cb}(x_1 s) \\
&\quad + \sum_d \int dx_2 d\bar{\sigma}^{(0)}_{ad}(x_2 s)\Gamma^{(1)}_{bd}(x_2)\Bigg]. \quad (1.31)
\end{aligned}$$

At the Born level, we find $\bar{\sigma}^{(0)} = \sigma^{(0)}$. The NLO correction can be obtain by comparing the left side and right side of Eq. (1.30) at order $\mathcal{O}(\alpha_S)$,

$$\bar{\sigma}^{(1)}_{ab} = \sigma^{(1)}_{ab} - \sum_c \int dx_1 \Gamma^{(1)}_{ac}(x_1) d\sigma^{(0)}_{cb} - \sum_d \int dx_2 d\sigma^{(0)}_{ad}\Gamma^{(1)}_{bd}(x_2), \quad (1.32)$$

Thus the singularity from the $\sigma^{(1)}_{ab}$ is removed by the Born cross section with the transition functions.

1.2 Physics motivations for Drell-Yan studies at hadron colliders

From a theoretical point of view, the Drell-Yan production rates are known at the NNLO accuracy. A very interesting property of the DY resides in the nature of the final state. The Drell-Yan process as stated previously consists in the production of a lepton pair through a Z, γ or W exchange after a $q\bar{q}$ annihilation. Therefore, there are no coloured particles in the final state, and hence no uncertainties related to fragmentation functions.

From the experimental point of view, Drell-Yan is also very attractive inasmuch it has a fairly large cross section, typically of $\mathcal{O}$(nb), and thus a significant expected statistics, even after applying cuts on the kinematical variables. The experimental signature of Drell-Yan events is also extremely clean, as we require two isolated high p_T charged leptons produced back to back for the Z and γ channels, and one isolated high p_T charged lepton together with missing transverse energy for the W channel. Therefore, both charged current (CC) and neutral current (NC) Drell-Yan channels are considered as "standard candle" reactions. They are of the utmost importance for the machine luminosity monitoring and for the calibration of the detectors at the LHC. Moreover, the Drel-Yan process is also considered as one of the golden channel for extracting information on PDFs, like quark and antiquark sea distributions, or parton distributions in the extended kinematics regions.

On top of that, the Drell-Yan is also a fundamental process for an accurate check of the Standard Model at hadron colliders. In particular, the DY production of Ws is important for an accurate determination (via transverse mass and p_T distributions) of the W mass, m_W, and the W decay width Γ_W. The fermion-pair production above the Z boson or W boson poles is a rich search field for new phenomena at present and future high energy colliders. Finally, the DY process is an irreducible background to several searches beyond SM physics, like the production of additional, heavier, neutral gauge bosons, Z', whose branching ratio into charged lepton pair varies according to the model specifications.

1.3 Measurement of the Drell-Yan process at LHC

1.3.1 Measurements of inclusive W and Z production cross sections

Measurements of the inclusive cross sections of DY $W^{\pm}$ and Z/γ^* production in the electron and muon decay channels [7] are presented in Tables 1.1 and 1.2. They are based on the full data sample collected by the ATLAS experiment at LHC in 2010 at a centre-of-mass energy of 7 TeV. With an integrated luminosity of about 35 pb^{-1},

	$\sigma_W^{fid} \cdot \mathrm{BR}(W \to e\nu)$ [nb]
W^+	$2.898 \pm 0.011(stat) \pm 0.052(syst) \pm 0.099(lumi)$
W^-	$1.893 \pm 0.009(stat) \pm 0.038(syst) \pm 0.064(lumi)$
$W^\pm$	$4.791 \pm 0.014(stat) \pm 0.089(syst) \pm 0.163(lumi)$
	$\sigma_W^{tot} \cdot \mathrm{BR}(W \to e\nu)$ [nb]
W^+	$6.063 \pm 0.023(stat) \pm 0.108(syst) \pm 0.206(lumi) \pm 0.014(acc)$
W^-	$4.191 \pm 0.020(stat) \pm 0.085(syst) \pm 0.142(lumi) \pm 0.084(acc)$
$W^\pm$	$10.255 \pm 0.031(stat) \pm 0.190(syst) \pm 0.349(lumi) \pm 0.156(acc)$
	$\sigma_{Z/\gamma^*}^{fid} \cdot \mathrm{BR}(Z/\gamma^* \to ee)$ [nb]
Z/γ^*	$0.426 \pm 0.004(stat) \pm 0.012(syst) \pm 0.014(lumi)$
	$\sigma_{Z/\gamma^*}^{tot} \cdot \mathrm{BR}(Z/\gamma^* \to ee)$ [nb]
Z/γ^*	$0.952 \pm 0.010(stat) \pm 0.026(syst) \pm 0.032(lumi) \pm 0.019(acc)$

Table 1.1: Fiducial and total cross section times branching ratios for W^+, W^-, $W^\pm$ and Z/γ^* production in the electron decay channel [7].

a total of about 270,000 W boson decays into an electron or muon and associated neutrino and a total of about 24,000 Z/γ^* decays into electron or muon pairs have been observed. The results are compared with QCD predictions calculated at NNLO in the fiducial regions of the measurements which allows for maximum sensitivity to details of the parton distributions used in these calculations. Comparing the results of the CMS and ATLAS collaborations with the theoretical predictions we find that they are in agreement.

The left plot of in Fig. 1.5 presents LHCb measurements [8] and illustrate the impact of higher-order effects on the total cross section.

The most recent measurements of the inclusive W and Z production cross sections were performed at the LHC in pp collisions collected in 2012 at $\sqrt{s} = 8$ TeV and corresponding to an integrated luminosity of 18.7 ± 0.9 pb^{-1} [5]. The LHC instantaneous luminosity increased drammatically compared to the dataset used for the first measurement at 7 TeV [6, 7], from 2×10^{31} to 7×10^{33} cm^{-1}s^{-1}, and the average number of inelastic proton-proton interactions (pile-up) increased from two up to twenty. Since the precision measurements require a low pile-up and triggers with low transverse momentum thresholds, the instantaneous luminosity was decreased by approximately a factor of ten in a dedicated LHC configuration. The total inclusive cross sections are consistent for the two decay modes within their measurement uncertainties. The combination of both channels is shown in Table 1.3. The theoretical predictions of the cross section, and relative ratios, based on the program FEWZ [10], that includes NNLO QCD corrections and uses the MSTW2008 [11] set of PDFs, are 12 ± 0.32 nb for the production of W (7.32 ± 0.20 nb for W^+ and 5.18 ± 0.13 nb for W^-) and

	$\sigma_W^{fid} \cdot \mathrm{BR}(W \to \mu\nu)$ [nb]
W^+	$3.002 \pm 0.011(stat) \pm 0.050(syst) \pm 0.102(lumi)$
W^-	$1.948 \pm 0.009(stat) \pm 0.034(syst) \pm 0.066(lumi)$
$W^\pm$	$4.949 \pm 0.015(stat) \pm 0.081(syst) \pm 0.168(lumi)$
	$\sigma_W^{tot} \cdot \mathrm{BR}(W \to \mu\nu)$ [nb]
W^+	$6.062 \pm 0.023(stat) \pm 0.101(syst) \pm 0.206(lumi) \pm 0.099(acc)$
W^-	$4.145 \pm 0.020(stat) \pm 0.072(syst) \pm 0.141(lumi) \pm 0.086(acc)$
$W^\pm$	$10.210 \pm 0.030(stat) \pm 0.166(syst) \pm 0.347(lumi) \pm 0.153(acc)$
	$\sigma_{Z/\gamma^*}^{fid} \cdot \mathrm{BR}(Z/\gamma^* \to \mu\mu)$ [nb]
Z/γ^*	$0.456 \pm 0.004(stat) \pm 0.004(syst) \pm 0.015(lumi)$
	$\sigma_{Z/\gamma^*}^{tot} \cdot \mathrm{BR}(Z/\gamma^* \to \mu\mu)$ [nb]
Z/γ^*	$0.935 \pm 0.009(stat) \pm 0.009(syst) \pm 0.032(lumi) \pm 0.019(acc)$

Table 1.2: Fiducial and total cross section times branching ratios for W^+, W^-, $W^\pm$ and Z/γ^* production in the muon decay channel [7].

1.13 ± 0.04 nb for the production of Z. The uncertainties include the contribution from the strong coupling constant α_S, the choice of heavy quark masses as well as neglected higher-order corrections beyond NNLO, by allowing the renormalization and factorization scales to vary.

In order to fix the PDFs and precisely determine the input parameter such as the gauge boson mass, differential distributions have to be studied.

1.3.2 Study of differential distributions

The theoretical calculations of the differential cross section of the DY production, $d\sigma/dM$ and the double differential cross section, $d^2\sigma/dMdY$, where M is the dilepton invariant mass and Y is the absolute value of the dilepton rapidity are already known up to NNLO QCD. Comparisons between theoretical calculations and experimental measurements provide important constraints on the PDFs. The difference in predictions due to different PDFs, as shown in Fig. 1.2 (right), makes the measurement important for the PDF constraints. We will review the theoretical calculations in the following sections.

1.4 The importance of an accurate theoretical prediction

The experimental accuracy aimed at the LHC for inclusive Drell-Yan observables is of $\mathcal{O}(1\%)$. The resulting Tevatron average for the mass of the W boson is $m_W =$

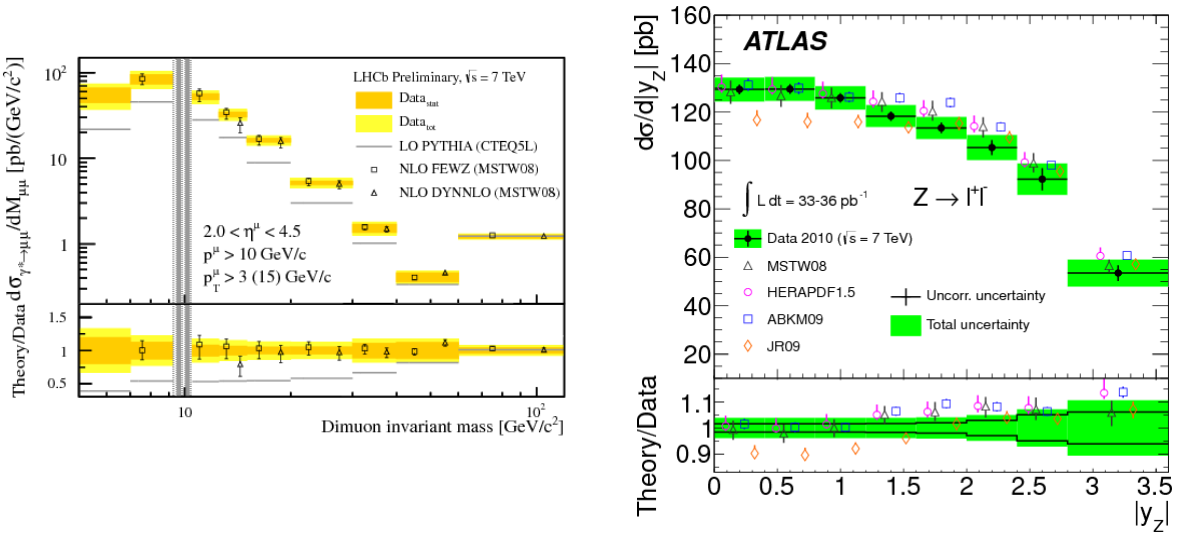

Figure 1.5: (left) The Drell-Yan invariant mass spectrum, normalized to the Z resonance region, as measured by LHCb and compared to LO, NLO and NNLO predicted. (right) The Drell-Yan cross section $(1/\sigma)d\sigma/d|Y|$ as a function of the dimuon rapidity, measured by the ATLAS experiment in the region 66-116 GeV. [9]

(80387±16) MeV. The mass of the Z boson is measured to be $m_Z = (91187 \pm 2)$ MeV. The statistical uncertainty on the Z boson cross section for 10 fb^{-1} is approximately 0.05% per lepton channel at the LHC. In order to provide a reliable accuracy for LHC data analysis, theoretical models have to reach at least 0.3% of accuracy. This is a serious challenge for theory.

The prospects for the measurement of m_W at CERN LHC are at the level of 15 MeV, or even 10 MeV [12, 13]. A measurement of m_W at the 10 MeV level is very challenging from the theoretical point of view due to the careful modeling of the production mechanism that is required. We should have the control on all the perturbative and nonperturbative corrections that can modify the shape of the relevant kinematic distribution at this level of precision [14].

The NLO QCD corrections to the Drell-Yan reaction are rather large, being about 70% at fixed target energies and about 30% for the $Sp\bar{q}S$. Therefore, higher-order corrections are necessary to put $\mathcal{O}(\alpha_S)$ predictions on a firm ground. In addition, electroweak radiative corrections play an important role in the W mass and width measurements; final state photon radiation is known to shift both quantities by $\mathcal{O}$(100 Mev). In order to measure the W mass and width accurately, the QCD mixed electroweak corrections are needed.

Process	Combination Measurement
$\sigma(pp \to WX) \cdot BR(W \to e\nu)$[nb]	$12.04 \pm 0.05(\text{stat}) \pm 0.37(syst) \pm 0.53(lumi)$
$\sigma(pp \to WX) \cdot BR(W \to \mu\nu)$ [nb]	$11.79 \pm 0.04(stat) \pm 0.27(syst) \pm 0.52(lumi)$
$\sigma(pp \to WX) \cdot BR(W \to l\nu)$[nb]	$11.88 \pm 0.03(stat) \pm 0.22(syst) \pm 0.52(lumi)$
$\sigma(pp \to W^+X) \cdot BR(W^+ \to e^+\nu)$ [nb]	$7.10 \pm 0.04(stat) \pm 0.26(syst) \pm 0.31(lumi)$
$\sigma(pp \to W^+X) \cdot BR(W^+ \to \mu^+\nu)$[nb]	$6.84 \pm 0.03(stat) \pm 0.16(syst) \pm 0.30(lumi)$
$\sigma(pp \to W^+X) \cdot BR(W^+ \to l^+\nu)$[nb]	$6.91 \pm 0.02(stat) \pm 0.14(syst) \pm 0.30(lumi)$
$\sigma(pp \to W^-X) \cdot BR(W^- \to e^-\nu)$ [nb]	$4.94 \pm 0.03(stat) \pm 0.19(syst) \pm 0.22(lumi)$
$\sigma(pp \to W^-X) \cdot BR(W^- \to \mu^-\nu)$[nb]	$4.95 \pm 0.03(stat) \pm 0.13(syst) \pm 0.22(lumi)$
$\sigma(pp \to W^-X) \cdot BR(W^- \to l^-\nu)$ [nb]	$4.95 \pm 0.02(stat) \pm 0.11(syst) \pm 0.22(lumi)$
$\sigma(pp \to ZX) \cdot BR(Z \to e^+e^-)$[nb]	$1.10 \pm 0.02(stat) \pm 0.05(syst) \pm 0.05(lumi)$
$\sigma(pp \to ZX) \cdot BR(Z \to \mu^+\nu^-)$ [nb]	$1.13 \pm 0.01(stat) \pm 0.03(syst) \pm 0.05(lumi)$
$\sigma(pp \to ZX) \cdot BR(Z \to l^+l^-)$[nb]	$1.12 \pm 0.02(stat) \pm 0.05(syst) \pm 0.05(lumi)$

Table 1.3: Averaged cross sections times leptonic branching ratios in nb for W (W^+, W^-) and Z production in the combined electron and muon final states, at $\sqrt{s} = 8$ TeV [5].

At fixed (NLO) order, EW effects are tiny, but not negligible in the view of a m_W known with a precision of $\mathcal{O}(10$ MeV). Drell-Yan is a background process for many important reactions such as, for instance, the production of the $t\bar{t}$ pairs or the production of new vector resonances, Z' and W', which appear in several extensions of the Standard Model. Drell-Yan is also a useful process for the calibration and monitoring of the detector performances, specially, the hadronic and partonic luminosities at the LHC.

For all the aforementioned reasons, an accurate and reliable theoretical prediction for the cross section and distributions of the Drell-Yan process are demanded for the precision studies at hadron colliders.

1.5 Theoretical uncertainties and status of theoretical calculations

Now let us review the theoretical uncertainties. The sources of theoretical uncertainties in the case of the Drell-Yan process are related to the kinematic variables. A realistic phenomenological study and data analysis require the inclusion of the relevant radiation corrections and their implementation into Monte Carlo event generators.

The inclusion of QCD radiation is mandatory for the simulation of any process at hadron colliders. The NLO QCD corrections to the total cross section are known since many years. They were calculated in [15], where a sizable increase of the total

cross section with respect to the leading order one is found by the authors. More exclusive observables are known in the litterature. The Z and W production at non-zero transverse momentum P_T is known at NLO accuracy in QCD [16] and in the full SM [17]. A complete calculation of the $\mathcal{O}(\alpha_S^2)$ corrections to the Drell-Yan cross section has been performed by van Neerven and collaborators [27] in the $\overline{MS}$ scheme.

Recently the two-loop QCD helicity amplitudes for the production of a Z or a W with a photon have also been calculated [35]. The rapidity distribution of a vector boson is known at the NNLO in QCD [36]. For low p_T ($p_T \ll M_W, M_Z$), the convergence of the fixed-order calculation is spoiled by large logarithmic terms $\alpha_S^n \log^m(M_W^2/p_T^2)$ that have to be resummed [18]. The generator RESBOS [19], used for data analysis at Tevatron, includes these effects.

The parton level Monte Carlo event generator described in [28], which considers the NNLO QCD radiation correction to the production of W and Z bosons in hadron collisions, includes the $\gamma - Z$ interference, finite-width effects, the leptonic decay of the vector bosons, and the corresponding spin corrections. The program allows to apply arbitrary kinematical cuts on the final-state leptons and associate jet activity.

W boson production cross section at hadron colliders including $\mathcal{O}(\alpha_S^2)$ corrections has been studied using the numerical code FEWZ [10]. The aforementioned code also includes spin corrections, finite width effects, $\gamma - Z$ interference, and allows for the application of arbitrary cuts on the leptonic final state.

In contrast with QCD, effects of electroweak corrections on precision measurements of some Standard Model observables, like the W boson mass and decay width are found to be pretty small. Nonetheless, they should not be neglected. The electroweak NLO corrections are known for the W [31] and Z [32] production cross sections, both in the Narrow-Width Approximation (NWA), and in the case of the exact calculation. Furthermore, the $\mathcal{O}(\alpha)$ EW contributions give large corrections to the tails of the transverse mass and lepton transverse momentum distributions, because of the presence of large EW Sudakov logarithms [33, 34]. These regions are important for the search of new heavy gauge bosons.

A detailed study of the production of the charged current Drell-Yan process is done in [29], which includes the exact $\mathcal{O}(\alpha)$ electroweak corrections properly matched with leading-log effects due to multiple-photon emission, as required by the experiments at Tevatron and at the LHC. This calculation has been implemented in the new version of the event generator HORACE.

The inhibition of soft parton radiation near the boundary $z \to 1$ of the phase space, where $z = x = |Q^2|/s$ for the Drell-Yan, generates large logarithms whose resummation is necessary in order to extract reliable theoretical predictions. In particular it is important for theoretical and phenomenological QCD improved parton model can be extract toward the borderline $z \simeq 1$ between perturbative and nonperturbative physics.

General arguments toward the exponentiation of all the logarithms have been given

[24, 25]. Moreover, Drell-Yan is the first process that had the resummation worked out at the NNNLL [26] and matched to NNLO fixed order calculations, because it has no colored final state particles (if γ, Z or W decay leptonically).

Most recently, the neutral current Drell-Yan with combined QCD and electroweak corrections has been implemented within the framework of the POWHEG BOX [30]. The aforementioned implementation combines both NLO electroweak and QED multiple photon corrections with native NLO and Parton Shower QCD contribution.

Even though a substantial number of higher-order corrections have already been calculated, the mixed QCD-EW corrections at NNLO are still missing. In this thesis, we study those corrections and focus on the virtual-real and double-real contributions to the total cross section of the production of on-shell Z and W bosons.

Chapter 2

The mixed QCD-EW corrections

In this chapter, we will focus on the full set of QCD-EW mixed corrections to the partonic DY mechanism. Even in the case in which we consider the leptonic decay of the gauge bosons (and therefore the particles in the final state coming from the decay of the boson carry no color), the NNLO mixed corrections involve complicated Feynman diagrams, as for instance two-loop boxes with massive propagators and one-loop pentagons. This is due to the fact that, although the initial state is prevented to exchange a gluon with the final state, it can exchange with it a virtual weak boson. These diagrams are very complicated to compute, and they constitute a challenge for the current techniques for the calculation of Feynman diagrams. Since, however, we are considering inclusive observables (in particular we are calculating the total cross section) and, moreover, for the SM weak bosons the ratio between the decay width and the mass is quite small (at the percent level), we can rely on the so-called narrow-width approximation and disentangle the production from the decay process. This approximation makes in such a way that the calculation of the total cross section is substantially simplified and affordable.

2.1 Up to two-loop contributions

We consider the partonic processes $q\bar{q} \to Z \to l^+l^-$ and $q\bar{q} \to W \to l\nu$. At tree level, there are two diagrams contributing and they are shown in Fig. 2.1.

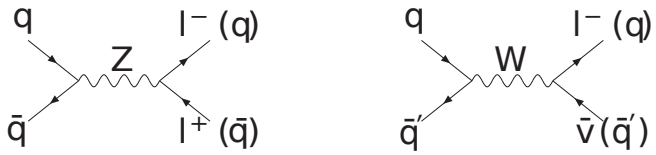

Figure 2.1: Feynman diagrams contributing to the Drell-Yan process at the partonic level.

At next-to leading order (NLO), QCD corrections affect exclusively the initial

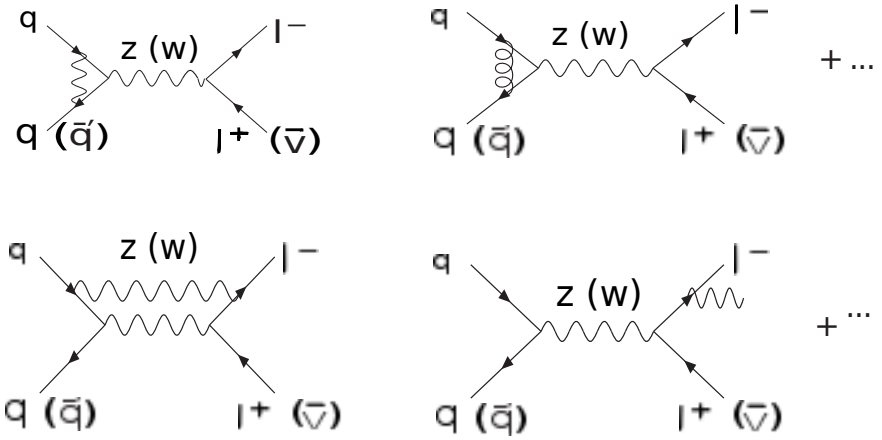

Figure 2.2: Some Feynman diagrams illustrating the NLO corrections to the Drell-Yan process at the partonic level.

state and they result at most in the calculation of massless one-loop vertex diagrams. However, when we consider the electroweak corrections, the situation changes considerably, because the final state can interfere with the initial state by the exchange of an electroweak gauge boson. Virtual corrections will include, then, the calculation of box Feynman diagrams with massive propagators (see Fig. 2.2).

At the next-to-next-to leading order (NNLO), the situation is the same as the one at the NLO. In particular, $\mathcal{O}(\alpha_S^2)$ corrections affect only the initial state. From a technical point of view, the NNLO QCD corrections involve at most two-loop massless vertices in the virtual set, while virtual-real radiation diagrams involve at most massless one-loop boxes with one external leg off-shell. Let us consider the mixed corrections, $\mathcal{O}(\alpha\alpha_S)$. Since the initial state can exchange a photon or a massive weak boson with the final state, while a gluon is exchanged between the incoming quarks, the virtual corrections involve two-loop box diagrams with massive propagators, that are extremely challenging to evaluate[1]. Furthermore, the virtual-real diagrams can involve massive pentagon Feynman diagrams (see Fig. 2.3), that have to be integrated over the entire phase space. This amount to calculate three-loops cut diagrams, and the level of difficulty is evident.

A considerable help in the calculation of the observable we are interested in comes from the fact that it can be shown that the bulk of the corrections to the cross section comes from the region of the phase space in which the decaying Z or W bosons are nearly on shell. This means that, in first approximation, we can neglect the contributions coming from diagrams in which the initial state exchanges bosons with

[1] A first partial result, concerning the massless two-loop boxes, was considered in [39]

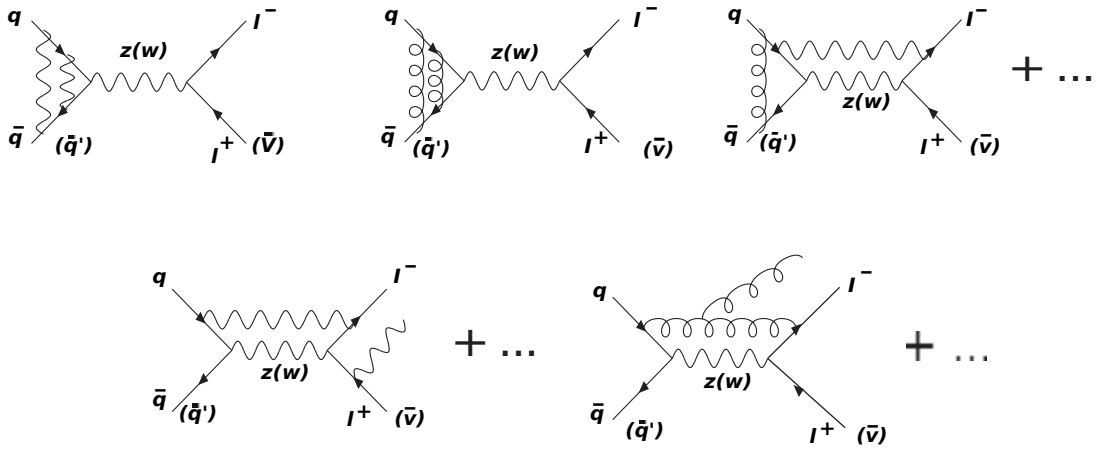

Figure 2.3: Drell-Yan process NNLO contributions.

the final state, and we can concentrate on the corrections in which an on-shell Z or W boson is first produced and then it decays in the final state particles. The neglected non-resonant contributions are of the order of $\sim \mathcal{O}(\Gamma/M)$, if Γ is the decay width of the decaying boson and M its mass. This describes the so-called "narrow-width" approximation, as discussed in the next section.

2.2 Narrow-Width approximation

The narrow-width approximation (NWA) [40] is widely applied to the calculation of the cross sections involving promptly decaying particles. The following requirements have to be met in order to apply consistently this approximation. Firstly, we have to consider inclusive observables. Then, the total decay width Γ of the resonant particle has to be much smaller than its mass, M. Furthermore, the mass of the parent particle has to be much bigger then the one of the daughter particles. Finally, the scattering energy must be much larger then the mass of the decaying particle.

In the limit $\Gamma/M \to 0$, the squared propagator

$$D(p^2) = \left[(p^2 - M^2)^2 + (M\Gamma)^2\right]^{-1} , \tag{2.1}$$

with 4-momentum p approaches a delta function:

$$\lim_{\frac{\Gamma}{M}\to 0} D(p^2) = \frac{\pi}{M\Gamma}\delta(p^2 - M^2). \tag{2.2}$$

The scattering cross section σ is expressed as follows:

$$\sigma = \frac{(2\pi)^7}{2s}\int_{p^2_{min}}^{p^2_{max}} dp^2 \int d\phi_p |\mathcal{M}_p(p^2)|^2 D(p^2) \int d\phi_d |\mathcal{M}_d(p^2)|^2. \tag{2.3}$$

When using Eq. (2.2), we have

$$\sigma \to \sigma_{NWA} = \frac{(2\pi)^7}{2s} \int d\phi_p |\mathcal{M}_p(M^2)|^2 K \int d\phi_d |\mathcal{M}_d(M^2)|^2. \tag{2.4}$$

where $K = \frac{\pi}{M\Gamma}$. The scattering cross section σ thus approximately decouples into the on-shell production (σ_p) and the decay. In our case, all the requirements are satisfied. The productions we consider are resonant scattering processes and the W and Z masses and decay width are experimentally found to be [42]:

$$m_W = (80.385 \pm 0.015)\,\text{GeV}\,, \qquad \Gamma_W = (2.085 \pm 0.042)\,\text{GeV}\,, \tag{2.5}$$

$$m_Z = (91.1876 \pm 0.0021)\,\text{GeV}\,, \qquad \Gamma_Z = (2.4952 \pm 0.0023)\,\text{GeV}\,. \tag{2.6}$$

Compared to the masses, the total decay widths are small. There is no significant interference with non-resonant processes and we can separate the resonant propagator as the Eq. (2.2) from the matrix element.

After the implementation of the narrow-width approximation, the production and the decay processes are separated, as depicted pictorially in Fig. 2.4 in the case of the Z boson. Therefore, the $\mathcal{O}(\alpha\alpha_S)$ corrections to the total cross section for the

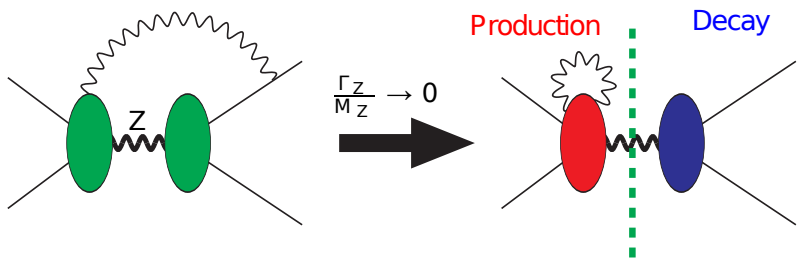

Figure 2.4: Narrow-Width approximation for the Z production

production of a lepton pair (or lepton-neutrino pair) in DY processes can be divided in two separated contributions. The first one includes the NNLO corrections to the production of an on-shell gauge boson multiplied by the branching ratio of $Z \to l^+l^-$ or $W \to l\nu$ at the LO. The NNLO corrections to the production process need the virtual two-loop corrections to the channels $q\bar{q} \to Z$ and $q\bar{q}' \to W$, the virtual-real contributions involving $2 \to 2$ diagrams with a photon or a gluon in addition to the gauge boson in the final state and the double-real contributions ($2 \to 3$ diagrams) with a photon and a gluon together with the gauge boson in the final state. The second contribution is given by the product of the $\mathcal{O}(\alpha_S)$ corrections to the production process times the $\mathcal{O}(\alpha)$ corrections to the decay of the gauge boson.

In this thesis we concentrate on the first contribution, *i.e.* the NNLO corrections to the production process.

2.3 $\mathcal{O}(\alpha\alpha_S)$ corrections to the production process

The Feynman diagrams involved in the calculation of the NNLO mixed QCD-EW corrections to the cross section of production of an on-shell Z or W boson can be generated using a generator program, as for instance FeynArts [41] or `Qgraf` [43].

According to the number of particles in the final state, the Feynman diagrams can be classified in virtual corrections (two-loop $2 \to 1$ vertex diagrams), virtual-real corrections (one-loop $2 \to 2$ box diagrams) and double-real corrections (tree-level $2 \to 4$ diagrams).

The calculation of the corrections to the cross section proceeds in the following way. Since the final state in the three groups of diagrams is constituted by a different number of particles, we have to add the relative cross sections:

$$\hat{\sigma} = \hat{\sigma}_V + \hat{\sigma}_{VR} + \hat{\sigma}_{RR} \,. \tag{2.7}$$

In the calculation of the various pieces of Eq. (2.7), we have to deal with UV and IR divergences. In $\hat{\sigma}_V$ the divergences arise from the integration with respect to the loop momenta. In $\hat{\sigma}_{VR}$ we have an overlapping of the divergences arising from the integration with respect to the one-loop momentum and the integration of the phase space of the additional unresolved gluon or photon. In $\hat{\sigma}_{RR}$, the matrix element is finite and the divergences arise from the integration of the phase space of the two unresolved additional photon and gluon in the final state. In order to manipulate divergent integrals, we have to regularize such divergences. For this purpose we use Dimensional Regularization. The divergent integral is calculated in a number of dimensions $D \neq 4$ in which is formally convergent. Then, the result becomes a function of the parameter D and the original divergence is recovered in the limit $D \to 4$, and appears as poles in $(D-4)$. The UV divergences are removed from the cross section with the renormalization procedure. IR divergences, instead, are removed only after the three cross sections are added together and the remaining initial state collinear divergences are re-absorbed in the redefinition of the parton distribution functions with which we have to convolute $\hat{\sigma}$ in order to have the hadronic cross section.

Virtual corrections

The Feynman diagrams contributing to the virtual corrections are shown in Fig. 2.5. The corresponding form factors and their contribution to the cross section of production of an on-shell Z or W boson are considered in [44, 45]. The calculation of this set of diagrams is done using the technique that will be explained in more detail in Chapter 3, *i.e.* interfering with the tree-level the two-loop diagrams (or projecting out the form factors), reducing the corresponding dimensionally regularized scalar integrals by means of the "Laporta Algorithm" to the set of MIs and solving analytically the masters with the differential equations method.

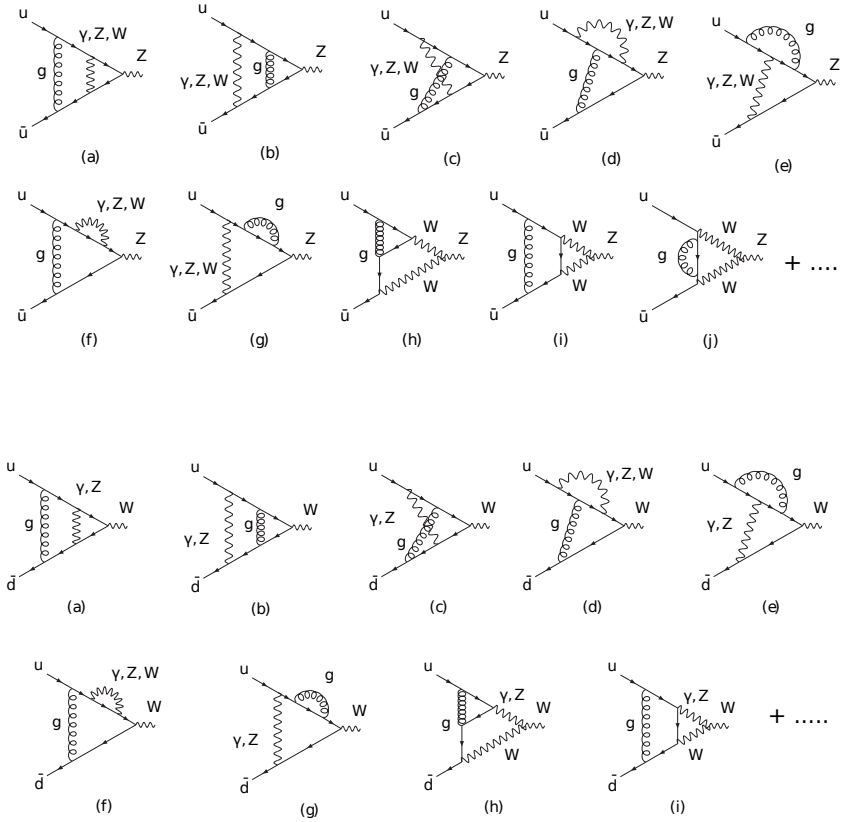

Figure 2.5: First two lines: the 40 Feynman diagrams contributing to the Drell-Yan production of an on-shell Z boson at $\mathcal{O}(\alpha\alpha_S)$. Last two lines: the 44 Feynman diagrams contributing to the Drell-Yan production of an on-shell W boson at $\mathcal{O}(\alpha\alpha_S)$. The dots stand for the diagrams that are symmetric in the exchange of the quark and anti-quark lines.

Real radiation

The Feynman diagrams contributing to the double-real corrections are shown in Fig. 2.6. The interferences among these diagrams are included in $\hat{\sigma}_{RR}$.

The Feynman diagrams for the one-loop virtual-real corrections at NNLO get contributions from the following two types of diagrams: the first one include diagrams in which an additional photon is radiated in the final state and the corresponding diagrams are shown in Fig. 2.7; the second include diagrams in which the additional particle is a gluon, as in Fig. 2.8. σ_{VR} includes, therefore, the interferences among the diagrams of Fig. 2.7 and the tree-level $2 \to 2$ diagrams $q\bar{q} \to Z\gamma$ (or $q\bar{q}' \to W\gamma$), and the interferences among the diagrams of Fig. 2.8 and the tree-level $2 \to 2$ diagrams $q\bar{q} \to Zg$ (or $q\bar{q}' \to Wg$). The calculation of the contributions coming from the double-real and virtual-real corrections is done using the technique that will be explained in

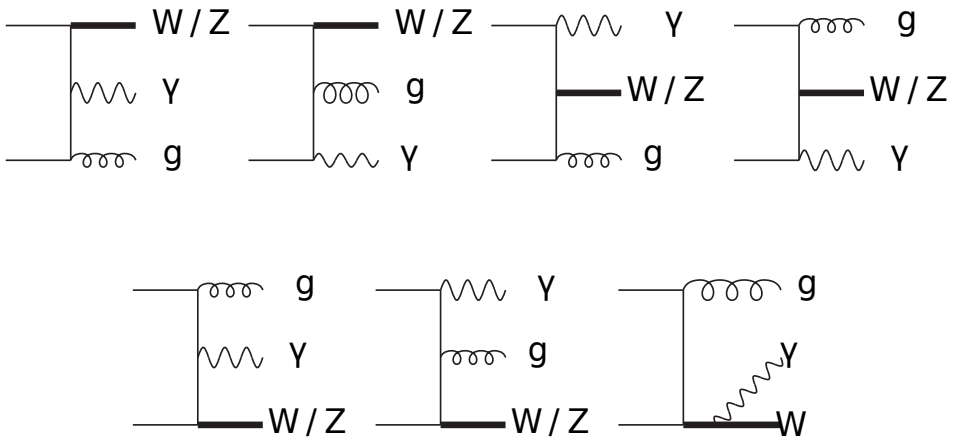

Figure 2.6: Diagrams corresponding to the double-real radiation. The Z (or W) is produced with an additional photon and gluon in the final state. The last diagram is peculiar of the W production, since the Z, being neutral, can not radiate a photon. Bold lines represent the massive bosons. Thin lines represent the light quarks.

more detail in Chapter 4.

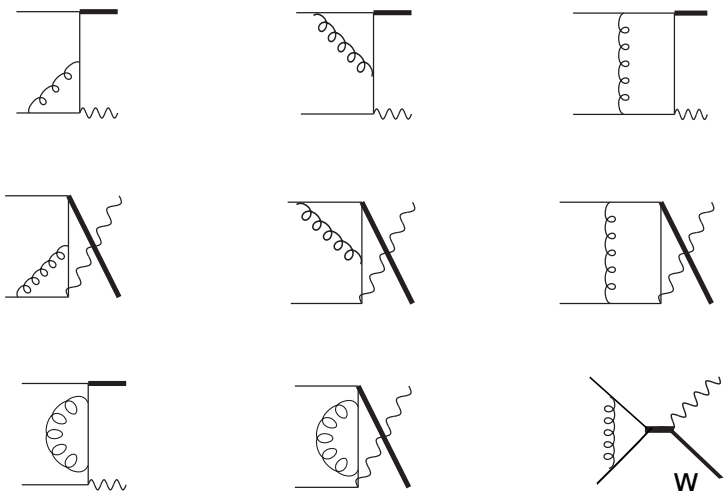

Figure 2.7: Diagrams corresponding to the virtual-real radiation. In this set the Z (or W) is produced with an additional photon in the final state, while the incoming quarks exchange a gluon. The last diagram is peculiar of the W production, since the Z, being neutral, can not radiate a photon. Bold lines represent the massive bosons. Thin lines represent the light quarks.

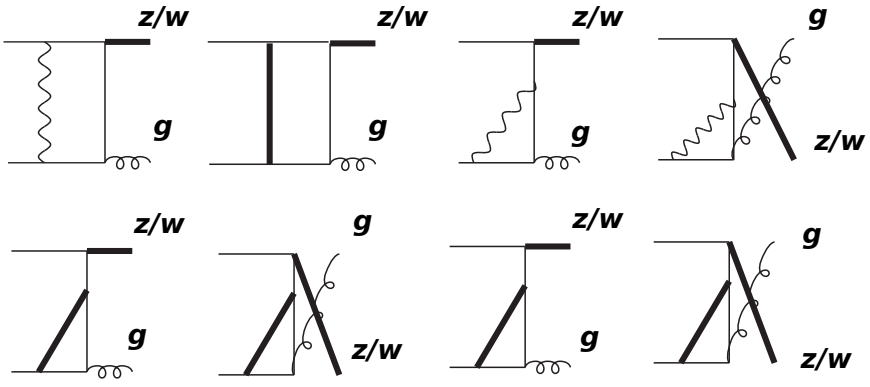

Figure 2.8: Diagrams corresponding to the virtual-real radiation. In this set the Z (or W) is produced with an additional gluon in the final state, while the incoming quarks exchange a photon or a massive weak boson. Bold lines represent the massive bosons. Thin lines represent the light quarks.

Chapter 3

The method

The importance of more and more accurate tests, which give evidence of the validity and limits of the Standard Model and which are able to point out the presence of new physics, unavoidably brings us to the necessity of the radiative corrections at higher and higher level in pQFT. This involves the calculation of multi-loop Feynman diagrams. Even though radiative corrections at the one-loop level have been know for a long time and for some simple processes three- and four-loop corrections can be calculated, the state of the art does not include, as yet, some fundamental processes at the two-loop level. The great level of complexity in the calculation of Feynman diagrams led to the development of methods alternative to the usual direct integration of loop integrals with Feynman parameters or with the use of dispersion relations. In this chapter we will describe one of these methods, proposed in [49, 50], and successively developed in [51].

Let us consider, therefore, a generic scattering process. The evaluation of the radiative corrections to the process leads to the calculation of a certain number of scalar integrals. We will work with integrals in a Euclidean space. The corresponding loop integrals in Minkowski space can be recovered by the Wick rotation.

It is well know that perturbative calculations in renormalizable quantum field theories suffer from divergences. To remove them, a procedure of regularization and then renormalization is needed.

The first step is the regularization of the loop integrals. At this stage we replace a divergent loop integral by a well-defined and finite one, which depends on a non-physical parameter Λ. The original integrals, and consequently the divergence, can be recovered in some limit of the parameter. The choice of Λ is arbitrary. A naive regularization consists, for example, in taking Λ as a cut-off in a momentum space. But for our purposes we will adopt the so-called dimensional regularization (DR) [52], in which divergent integrals are performed in a space with arbitrary D dimensions. The limit $D \to 4$ gives us back the original divergent integral. The reason for this choice is twofold. As a first point, DR preserves all the original symmetries of the Lagrangian,

e.g. gauge symmetry invariance is guaranteed. A second important reason for the use of DR lies in the properties of dimensionally regularized Feynman integrals. They are formally convergent integrals and this, from a computational point of view, is a very valuable fact. In fact we can justify some formal operations, which allow us to manipulate integrals and to apply the method we want to describe. Finally DR provides also a powerful method for dealing simultaneously with both IR and UV divergence [53]. Just to fix some notation let us follow [51] and define a generic 2-loop scalar D-dimensional integral:

$$I(p_1,\ldots,p_n) = \int \frac{d^D k_1 d^D k_2}{(2\pi)^{(D-2)}} \frac{S_1^{n_1}[\ldots]\, S_q^{n_q}}{D_1^{m_1}[\ldots]\, D_t^{m_t}} \tag{3.1}$$

In this equation we consider: n external momenta $p_1,\ldots,p_n$; t different propagators $D_1,\ldots,D_t$ which determine the topology of the integral, each one raised to the power m_i , with $m_i \geq 1$; q different scalar products $S_1,\ldots,S_q$ of a loop momentum and an external one, or of the two loop momenta, each one raised to the power n_i, with $n_i \geq 1$. We will denote with $I_{t,r,s}$ integrals belonging to the same topology, with equal total degrees of the denominator $r = \Sigma_i m_i$ and of the numerator $s = \Sigma_i n_i$.

In the case of the calculation of NNLO mixed QCD-EW corrections to the Drell-Yan production of Z and W bosons two sets of corrections need to be considered. The first set includes the virtual corrections. In this part the most complex integral is of the class $I_{6,r,s}$, with six denominators and $r \geq 6$, $s \geq 0$ and with three external momenta, p_1, p_2 and $p = p_1 + p_2$: the planar triangle vertex with on-shell external legs. There are seven independent scalar products one can construct out of the two external momenta and two loop momenta, namely: $p_1 \cdot k_1$, $p_1 \cdot k_2$, $p_2 \cdot k_1$, $p_2 \cdot k_2$, $k_1 \cdot k_2$, k_1^2 and k_2^2. In fact, the t denominators D_i are linear combinations of the seven scalar products. The properties of dimensionally regularized Feynman integrals allow us to perform a formal simplification between a scalar product and a denominator in the loop integral. Therefore only $7 - t$ different scalar products can appear in $I_{t,r,s}$. The second set of corrections are the real corrections and the most complex integral that appears is of class $I_{7,r,s}$ after using the Cutkosky rules (which we will explain in the following section) with two external momenta, p_1, p_2: the planar and crossed box with on-shell external legs. The number of independent scalar products one can construct is equal to seven, as is the case of virtual corrections, but $t = 7$ and then we have $q = 0$. However, there are cases in the real radiation (cut diagrams) in which the number of the scalar products is bigger than the number of the propagators. This happens in some crossed topologies in which we can find more than seven independent propagators that contain the seven independent scalar products. In order to implement a computer program based on IBPs, the number of denominators should at most be equal to the number of scalar products. To overcome this problem, we write the forward scattering diagram back to a 4-point function with three independent momenta, p_1, p_2 and p_3 ($p_4 = p_1 + p_2 - p_3$), while we force in the Mandelstam invariants p_3 to be equal to p_2

(and $p_4 = p_1$), as it is the case for a forward scattering diagram, and therefore the Mandelstam invariant u to vanish, $u = 0$ (in the case of a planar cut diagram we have $t = 0$):

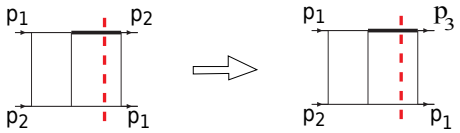

In so doing, the number of independent scalar products increases to 9 (as in the case of an actual 4-point function) and $q = 9 - t$ is again > 0. We recover the original forward scattering diagram imposing in the end $p_3 = p_2$.

We know from the principle of invariance that the amplitude is a function of three invariants. We can choose them to be the Mandelstam variable $p^2 = (p_1 + p_2)^2$ and the external momenta p_i^2, which we put on their mass shell ($p_1^2 = p_2^2 = 0$). In general, $I_{t,r,s} = I_{t,r,s}(p^2, a)$.

The evaluation of the integral, or, better, of the class of integrals $I_{t,r,s}$ is a rather complicated task if we want to perform integrations directly in D-dimensional space. However, we can use kinematics to elaborate an alternative computational method.

For the virtual part, we can split the approach to the calculation of the class $I_{6,r,s}$ in two steps:

The first one consists of the reduction of all the integrals to the MIs of the problem, *i.e.* the expression of all the integrals involved in the calculation in term of a small number of irreducible integrals.

The second step consists of the method for the calculation of these MIs. The direct integration is substituted by the establishment of a system of differential equations in the external kinematical invariants, in which the MIs are the unknown functions. Initial or boundary conditions can be extracted, in general, from the equations themselves, knowing the analyticity properties of the Feynman integrals.

For the real part, one first has to use the Cutkosky rules for the phase-space integrals. After this, the real contribution can be expressed as a forward scattering diagram and we can use the same technique as for the virtual corrections.

This method will be analysed in the following sections of this work. Let us remarke some among its features. The first merit is that the solution of the system of differential equation allows us to express amplitudes in a reasonably compact form, using known functions. In the case of equations solvable in a closed form, for an arbitrary number of dimensions D, these functions are hypergeometric functions. If we prefer, instead, a solution as a Laurent expansion in $(D - 4)$, around $D = 4$, we can express the result in terms of generalized harmonic polylogarithms. Finally, even if an analytic solution can not be found, the construction of the system of differential equations is a powerful tool for the numerical evaluation of the amplitude.

However, the biggest merit of the method may be the complete implementation, from a computational point of view, of the entire chain. Programs based on IBPs and

other symmetry identities can be written for the reduction to the MIs; other programs can be written for the construction and solution of the system of differential equations.

3.1 The reduction to master integrals

The first step of the method consists in the reduction of the class of integrals of the virtual $I_{6,r,s}$ and real $I_{7,r,s}$ parts to a small number of irreducible integrals, called Master Integrals (MIs). This reduction is made by using some properties belonging to the entire class, which can be translated in identity relations involving the integrals themselves. This kind of approach to the problem of the calculation of Feynman amplitudes is not new. It was first point out by F. V. Tkachov and K. G. Chetyrkin [54] for the evaluation at four loops of the beta function in QCD; from that time it constitutes the basis of multi-loop calculations.

The IBPs, derived in [54], were used in [55] for the systematic evaluation of the MIs for an entire class of integrals of a given topology $I_{t,r,s}$, and they were accompanied by other kind of identities. These new identities come from the symmetries of the problem. For example, identities derived from the Lorentz invariance of the scalar integrals, or derived from symmetries under transformations on the external and internal momenta.

3.1.1 Integration-by-parts identities

These identities are among the most remarkable properties of dimensionally regularized Feynman integrals [54]. They consist in the possibility of formal integrations by parts. In fact the following identity holds:

$$\int \frac{d^D k}{(2\pi)^{(D-2)}} \frac{\partial}{\partial k^\mu} J(k, \dot{[...]}) = 0. \tag{3.2}$$

This equation means that the integral over the total derivative with respect to any loop momentum vanishes because of the possibility of disregarding surface terms in the case of dimensionally regularized integrals. The integrand J can be a vector or a tensor of any rank. In our case we can write:

$$\int \frac{d^D k_1 d^D k_2}{(2\pi)^{(D-2)}} \frac{\partial}{\partial k_1^\mu} \nu^\mu \{ \frac{S_1^{n_1} \dot{[...]} S_q^{n_q}}{D_1^{m_1} \dot{[...]} D_t^{m_t}} \} = 0 \tag{3.3}$$

$$\int \frac{d^D k_1 d^D k_2}{(2\pi)^{(D-2)}} \frac{\partial}{\partial k_2^\mu} \nu^\mu \{ \frac{S_1^{n_1} \dot{[...]} S_q^{n_q}}{D_1^{m_1} \dot{[...]} D_t^{m_t}} \} = 0\,, \tag{3.4}$$

where $q = 7 - t$ and where the vector ν^μ can be any of the independent vectors of the problem, therefore $k_1, k_2, p_1, p_2,$. The explicit differentiation of the integrand in

the above equations generates up to 8 identities involving integrals of the topology t, with the degree of the numerator up to $s+1$ and the degree of the denominator up to $r+1$, and integrals of simpler topology, coming from the simplifications between the new scalar products produced by the differentiation of some denominators and corresponding denominator itself.

In general, if we have a class of integrals with n loops and m independent external momenta, we have a number N_{IBP} of IBPs given from the following relation:

$$N_{IBP} = n(m+n)\,. \tag{3.5}$$

3.2 Number of equations vs. number of unknown amplitudes

It is interesting now to understand how many equations we can use for the reduction of a certain class $I_{t,r,s}$ to the MIs, and how many unknown amplitudes are generated in these equations. If we fix t, r, and s the number of possible available amplitudes is [55]:

$$N[I_{t,r,s}] = \binom{r-1}{r-t}\binom{8-t+s}{s}. \tag{3.6}$$

For these amplitudes we can construct $N_{ID}N[I_{t,r,s}]$ identities, where N_{ID} is the number of identity relations that we use in the reduction (integration by part identities, Lorentz invariance identities, etc.). If we just use IBPs, we have for instance $N_{ID} = N_{IBP}$. These identities will contain not only amplitudes of degree r, s, but because of derivatives of IBP, also amplitudes with up to degree $r+1$ for the denominator and $s+1$ for the numerator. In general, therefore, we have $N_{ID}N[I_{t,r,s}]$ equations for $N[I_{t,r+1,s+1}]$ unknow amplitudes, where $N[I_{t,r+1,s+1}]$ is given by Eq.(3.6) replacing r and s with $r+1$ and $s+1$. It is clear, from the structure of the combinatorics, that, providing we fix t, it is possible to find a couple of r_0 and s_0 such that, for $r \geq r_0$ and $s \geq_0$, we have:

$$N_{Eqs} = N_{ID}N[I_{t,r,s}] \geq N[I_{t,r+1,s+1}] = N_{Unk}, \tag{3.7}$$

thus finding an apparently overconstrained linear system [56] of N_{Nqs} equations in N_{Unk} unknown amplitudes with which we can express the more complicated integrals in terms of simple ones. Let us point out that, obviously, not all the equations of the system are independent. Two cases can be encountered. The first one is when the number of independent equations is sufficient to express all the amplitudes of the topology t in terms of amplitudes of a simpler topology, $t-1$. In this case the problem is completely reducible. If we know the MIs of the simpler topologies we can calculate all the diagrams of the topology t without performing any additional calculation. The

r	s	$N\,[I_{7,r,s}]$	Cumul. Ampl.	N_{Eqs}		$N_{Unknowns}$
7+0	0	1	1	10	$<$	24
7+0	1	2	3	30	$<$	48
7+0	2	3	6	60	$<$	80
7+0	3	4	10	100	$<$	120
7+1	0	7	8	80	$<$	108
7+1	1	14	24	240	$>$	216
7+1	2	21	48	480	$>$	360
7+1	3	28	80	800	$>$	540
7+2	0	28	36	360	$=$	360
7+2	1	56	108	1080	$>$	720
7+2	2	84	216	2160	$>$	1200
7+2	3	112	360	3600	$>$	1800
7+3	0	84	120	1200	$>$	990
7+3	1	168	360	3600	$>$	1980
7+3	2	252	720	7200	$>$	3300
7+3	3	336	1200	12000	$>$	4950
7+4	0	210	330	3300	$>$	2376
7+4	1	420	990	9900	$>$	4752
7+4	2	630	1980	19800	$>$	7920
7+4	3	840	3300	33000	$>$	11880

Table 3.1: Number of equations as a function of the number of unknown amplitudes for a two-loop box (7 denominators, 3 independent external momenta). The first column of the table gives the degree of the denominator of the starting integral $I_{t,r,s}$, while the second one gives the degree of the numerator (we know that only two independent scalar products can remain in the numerator in this case). In the third column we have the number of amplitudes for given r and s and in the fourth column the cumulated number of amplitudes, i.e. the sum of all the amplitudes up to that specific r and s, for that topology. The last three columns are the most important. They show the number of equations (only IBPs, 10 per amplitude) compared to the number of unknown amplitudes involved. We see that N_{Eqs} grows rapidly and from the point where $r = 8$ and $s = 1$ in this table, it exceeds N_{Unk}.

second one is when the number of independent equations is not sufficient to make the system completely reducible, but all the amplitudes of the topology t can be expressed as a combination of a small number of MIs of that topology and of simpler ones. In this case we, therefore, have to calculate the MIs of the problem. Firstly, we can not say a priori if the system admits MIs or if it is completely reducible. We are talking about systems of hundreds of equation vs. hundreds of unknown amplitudes. Secondly, if we have a problem with a certain number of MIs, provided that this number is fixed, we can choose the set of MIs we prefer. It is sufficient to re-express the MIs that we want to keep out of the initial set in terms of another MI using the same identity relation as already found. This thing can be useful for later purposes. In fact, we can look for the set of MIs that makes the system of differential equations we construct for them as simple as possible.

All we said up to now constitutes a very suitable basis for a mechanical automatization of the procedure of the reduction to MIs. From a computational point of view, there is no limit to the size of the linear system to solve and we can think of constructing a system large enough for our goal.

3.3 Reduze

Reduze is a computer program written in C++ which generates the IBP and optionally the LI identities and then reduce the integrals to master integrals [62]. Reduze uses the GiNaC [46] library to perform the simplification of the prefactors.

The reduction algorithm is called the "Laporta algorithm". It is essentially the Gauss algorithm with additional rules to determine the next equation which should be solved and inserted into the others. To get the reduction of a certain Feynman diagram one first defines a set of integrals by restricting the exponents of the propagators. Reduze then generates the identities form the set and starts solving the system of equations.

For a reduction of several diagrams Reduze can treat different diagrams with the same number of propagators simultaneously. One defines how many cores or process are available and then Reduze will automatically launch some reductions simultaneously. Comparing to the other published reduction programs like AIR [47] and FIRE [48], the advantage of Reduze is that the more core are available the more diagrams one can reduce in parallel.

3.4 The calculation of the master integrals

Once we have obtained all the relations necessary to reduce the problem of the calculation of a certain class of integrals to the calculation of a small number of MIs, we have to consider how to solve this.

The way we proceed was first pointed out in [49, 50], and successively developed in [51]. It consists in the construction of a system of first-order linear differential equations in the external invariants where the unknown functions are the MIs themselves.

In the following sections we will explain how to construct the system and give two possible ways to its solution.

3.4.1 The differential equations method

Let us take, for simplicity, the case of a single MI (a three-point function):

$$\mathcal{F} = \int \frac{d^D k_1 d^D k_2}{(2\pi)^{2(D-2)}} \frac{s_1^{n_1} \cdots s_q^{n_q}}{D_1^{m_1} \cdots D_t^{m_t}} = \mathcal{F}(M_i), \tag{3.8}$$

function, in general, of three external kinematical invariants $M_1 = p^2 = (p_1 + p_2)^2$ and the square external momenta $M_{i+1} = p_i^2$, which will be put later on the mass shell.

Let us construct the following object:

$$O_{ij} = p_i^\mu \frac{\partial \mathcal{F}}{\partial p_j^\mu}. \tag{3.9}$$

By derivation of the function $\mathcal{F}$ with respect to the invariants M_i, we have:

$$O_{ij} = p_i^\mu \sum_\xi \Big[\frac{\partial \mathcal{F}}{\partial M_\xi} \frac{\partial M_\xi}{\partial p_j^\mu} \Big] = \sum_\xi a_\xi (p_i \cdot p_j) \frac{\partial \mathcal{F}}{\partial M_\xi} = \sum_\xi a_\xi (M_l) \frac{\partial \mathcal{F}}{\partial M_\xi}\,, \tag{3.10}$$

where $i, j = 1, 2, 3$ and where the functions $a_{\xi,ij}(M_l)$ are linear combinations of invariants.

On the other hand, because we are working with dimensionally regularized amplitudes, we can perform a direct derivation of the integrand in Eq. (3.9). This derivation gives a complicated combination of integrals: $\mathcal{F}$ itself; integrals that belong to the same topology class as $\mathcal{F}, I_{t,r,s}$, but can have a different degree of the numerator and the denominator(up to r+1 and s+1); other integrals belonging to lower topologies. Therefore, we also have:

$$O_{ij} = \sum_a h_{a,ij} I^a_{t,upto\,r+1,upto\,s+1} + h_{ij}\mathcal{F} + \Omega(M_l). \tag{3.11}$$

In $\Omega(M_l)$ we put integrals of the kind $I_{t-1,r,s}$. Putting the r.h.s. of Eq. (3.11) equal to that of Eq. (3.12), we find a linear system in the derivation $\frac{\partial \mathcal{F}}{\partial M_\xi}$, which can be solved to give:

$$\frac{\partial \mathcal{F}}{\partial M_\xi} = \sum_a h_a I^a_{t,upto\,r+1,upto\,s+1} + b_\xi(M_l)\mathcal{F} + \Omega'_\xi\,, \tag{3.12}$$

where $\xi = 1, 2, \cdots, 6$.

It is obvious that the system of Eq. (3.13) is not useful for our goals because it is not a true system of differential equations. It still involves integrals with different degrees of numerators and denominator.

We can recover a true system by using the relations we found for the reduction to MIs. They allow us to re-express the term $\sum_a h_a I^a_{t,up\,to\,r+1,up\,to\,s+1}$ in Eq. (3.13) as a combination of $\mathcal{F}$ itself and amplitudes of simpler topology, which we can absorb again in the last term, Ω. Putting the external momenta on the mass shell, we remain with a system of a linear partial differential equation in p^2 :

$$\frac{\partial \mathcal{F}}{\partial p^2} = h(p^2, a)\mathcal{F} + \Omega'_1(p^2, a), \tag{3.13}$$

The generalization to n MIs is straightforward:

$$\frac{\partial \mathcal{F}_n}{\partial p^2} = \sum_i h_{n,i}(p^2, a)\mathcal{F}_i + \Omega'_{n,1}(p^2, a), \tag{3.14}$$

We have an homogeneous part, which involves the functions $\mathcal{F}_i$ and gives the structure of the solution. The $\mathcal{F}_i$ now are to be considered as generic analytical functions of the complex variables p^2. The coefficient functions of the system, $h_{n,i}$ and $g_{n,i}$, determine the analytic behavior of $\mathcal{F}_i$, the possible singular point. However we know from analytical properties of Feynman integrals that not all the singular points occurring in the coefficient functions are really singular point for the amplitudes. The combination of knowledge of the analytical structure of the system and the general analytical properties of Feynman amplitudes gives us a powerful tool for the determination of boundary conditions.

The non-homogeneous part of the system determines the particular solution and then fixed the expression of the amplitudes $\mathcal{F}_i$. By construction, the function Ω_n are combinations of simpler topology amplitudes, which are to be considered as known. In effect we can proceed in the following way. Once we know all the MIs of the class $I_{t,r,s}$ to be calculated, we can note that they are in a pyramidal structure. At the basis there are the MIs with the minimum number of denominators and at top the MIs of the topology t. The analysis, because of the structure of the system of differential equations, must proceed from the bottom up; in fact each step of the pyramid enters in the non-homogeneous part of the following step. If we are able to calculate all the MIs of the first step, we can move to the second, and so on.

Where the boundary conditions are concerned, we have different cases to take into account. Sometimes we can extract them from the integral representation of the MIs, performing the suitable limit directly under the loop momenta integration; otherwise we can try to extract information directly from the system itself. There is no unique prescription and we have to find the right way time by time.

3.4.2 The exact D-dimensional solution and hypergeometric functions

Once we found the system of differential equations and boundary conditions that the MIs must verify, we can think of its solution.

We can distinguish two kinds of approaches. From one side we would like to express the final results in a form as compact as possible, in terms of known functions, directly in the D-dimensional space. We would also like a suitable analytical behavior of the functions used, in order to perform analytic continuations to the physical regions in which external invariants, our variables, are defined. On the opposite side, however, practical calculations force us to find a solution as Laurent expansion in $(D-4)$, because the renormalization procedure needs divergences (which occur as poles in $(D-4)$) to be removed and the finite part of the amplitude to be evaluated. Residues for given power of the poles are to be expressed anyhow in terms of known functions, in a way that is compact and non-redundant as well as suitable for numerical evaluations.

The two cases, obviously, must be connected, i.e. it must be possible to move from the exact D-dimensional expression to the expansion in Laurent series.

We know that an important role in mathematical physics is played by hypergeometric functions, since they are related to a wide class of special functions appearing in a large variety of fields. In particular the connection between multiloop calculations of Feynman amplitudes and generalized hypergeometric functions [57] has been known for a long time. A connection between hypergeometric functions and polylogarithms, which are in general used for the expression of residues in the expansion approach, is also well known. Therefore the following scenario is outlined. An exact D-dimensional solution is to be looked for in the class of generalized hypergeometric functions. Afterwards the Laurent expansion in $(D-4)$ can be performed from the exact solution. Practically, this step is not to be considered, and residues in the Laurent series have to be computed directly, without passing through hypergeometric representations.

Let us note that the connection between Feynman amplitudes and hypergeometric functions was established through their integral representations. In [51], however, solutions in term of hypergeometric functions were found for the two-loop MIs of the massless double box through the differential equations method.

In general, we have to deal with different kinds of structures, depending on how many scales the problem has.

In this work we are considering the case of on-shell amplitudes in which both W and Z bosons are present. Therefore, in the general case, the quantum corrections are characterized by three scales: s, m_Z and m_W. For some of the Feynman diagrams considered in the calculation of the perturbative corrections, only two scales are present at the same time. Nevertheless, there are corrections that involve all the three scales (see for instance the interference between the one-loop box diagram in

which the quark u and the anti-quark $\bar{d}$ produce a W and a gluon, exchanging a Z boson, and the corresponding tree-level). The presence of three scales makes the calculation more complicated. In particular, the functions involved in the expression of the analytic result should be function of two dimensionless variables (ratios of the scales under consideration). However, in the case at hand, the masses of the two bosons are not so different and a simplification can be made, considering few terms of a Taylor expansion in the parameter $\xi = \Delta m^2/m_W^2 \sim 0.26$, where $\Delta m^2 = m_Z^2 - m_W^2$. A propagator that depends on the Z mass in a scalar integral will be re-expressed as follows

$$\frac{1}{p^2 + m_Z^2} = \frac{1}{p^2 + m_W^2 + \Delta m^2} \sim \frac{1}{p^2 + m_W^2} - \frac{\Delta m^2}{m_W^2} \frac{m_W^2}{(p^2 + m_W^2)^2} + \dots \tag{3.15}$$

Order by order in the parameter ξ, we have to consider only integrals depending on one mass (for instance m_W) and, therefore, the results can be expressed in terms of a single dimensionless parameter $z = \frac{m_W^2}{s}$. Note that now, in the evaluation of the scalar integrals, we have to deal with integrals in which a propagator is squared. However, this does not cause any complication to the calculation of the cross section. In fact, these integrals are related to the MIs via IBPs identities. In the end, we will have a cross section expressed in a Taylor series of ξ, the first term being the cross section in which we use a degenerate mass for both the vector bosons Z and W equal to m_W:

$$\sigma \sim \sigma^{(0)}_{(m_Z=m_W)} + \xi\, \sigma^{(1)}_{(m_Z=m_W)} + \xi^2\, \sigma^{(2)}_{(m_Z=m_W)} + \dots \tag{3.16}$$

where $\sigma^{(1)}_{(m_Z=m_W)}$, $\sigma^{(2)}_{(m_Z=m_W)}$ are terms in which we have scalar integrals with propagators raised to power 2 and 4, and so on. Of course, the validity of the expansion relies in the fact that the coefficients $\sigma^{(1)}$, $\sigma^{(2)}$, etc., are all of order $\sigma^{(0)}$. This can be verified a posteriori once we computed the cross section.

Let us note that the solution of the differential equations, occurring for the MIs, in term of generalized hypergeometric function is very complicated. This is the case, for example, when the non-homogeneous part of the equation is constituted by a non-trivial combination of simpler topology MIs.

3.4.3 The $(D-4)$ expansion and harmonic polylogarithms

Because, in general, for renormalization purposes, we need to remove divergences in the amplitudes and to evaluate the finite part, we will solve the system of differential equations (3.15), directly expanding it in Laurent series, together with the amplitudes themselves. The reason is twofold. First of all, as we said in the previous section, it is not always possible to find a solution in terms of hypergeometric functions and consequently a $(D-4)$ expansion. Secondly, this kind of approach is the more powerful from a computational point of view. Computer programs were written for the symbolic

integration of the differential equations, based on the knowledge of the homogeneous part of the system at $D = 4$ and on the Euler's method of variation of constants.

We will write in general:

$$F_i = \sum_n \frac{A_{-n}^{(i)}}{(D-4)^n} + A_0^{(i)} + \mathcal{O}(D-4), \tag{3.17}$$

where n goes from 1 to an upper limit determined from the number of loops considered (in our case $n = 2$ for the virtual part, and $n = 3$ for the real part) and where the poles can be ultraviolet or infrared.

The structure derived from the Laurent expansion of the system is the following. We have the homogeneous system, which is common to all orders in the expansion and involves the amplitudes at that order. The triple pole in $(D-4)$ is the only order that involves only the function $A_{-3}^{(i)}$. Going ahead, we find a cascade structure in which the previous orders appear in the non-homogeneous part of the amplitude, it sometimes happens that first or second order in $(D-4)$ are needed. It is the case in which the amplitudes appear multiplied by power $(D-4)^{-n}$ in the non-homogeneous part of the amplitudes of an upper topology. We note that radiative corrections at the one-loop level suggest that a suitable basis to express result in the $D \to 4$ limit was constituted by Nielsen's generalized polylogarithm. An extension of this class of functions was introduced in [58], where harmonic polylogarithms (HPLs) of one variable are considered, and in [59], where a further extension to 2-dimensional harmonic polylogarithm(2dHPLs) was needed for the solution of the differential equations. The solution of our differential equations will be extracted, in general, in this particular case.

Chapter 4

IBPs reduction of the real part

Real radiative corrections at two-loop level for the W and Z production involve many Feynman diagrams. Some of them have been known for almost one decade. However, others have not been calculated yet. In particular, there are diagrams with more than one massive propagator, that appear specifically in the electroweak corrections and are not known. The purpose of this thesis is to present the calculation of these diagrams, using a technique that was introduced more than 10 years ago in [61] for the calculation of the total cross section of production of an Higgs boson at hadron colliders in NNLO QCD. This technique allows for the use of the "machinery" introduced in the previous Chapter in the case of calculation of virtual corrections, also in the case of phase-space integrals.

In order to do that, we use in a reversed way the Cutkosky rules.

The total cross section is related via the optical theorem to the imaginary part of the forward scattering amplitude, and then to the discontinuity across the physical branch cut. This discontinuity can be computed using the Cutkosky rules, cutting in all possible ways the corresponding diagrams and summing the contributions of all possible cuts. Here, we do the reverse process. The contributions of all the possible cuts (integrations over the phase-space) are re-written in terms of forward scattering two-loop integrals. These integrals are then evaluated using the reduction to the MIs via the Laporta algorithm and then the evaluation of the MIs with the differential equation method.

All the topologies will be classified by the number of cut propagators and the number of massive propagators.

4.1 The topologies of the real radiative corrections

4.1.1 Cutkosky rules

To illustrate the method, consider the following double-real contribution at NNLO:

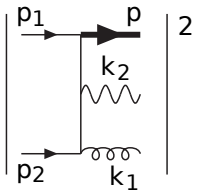

$$\sim \int \frac{d^d k_1 d^d k_2 \delta_+(p^2-m^2)\delta_+(k_1^2)\delta_+(k_2^2)\,[\ldots]}{(p-p_1)^4\,(k_1-p_2)^4}\,, \tag{4.1}$$

where we work in D dimensions, and δ^+ include the positive energy condition $E>0$. We can replace each delta function in the final state phase space with the difference of two propagators with opposite prescription for their imaginary parts [63]:

$$\delta(p^2-m^2)=\frac{1}{2\pi i}\left(\frac{1}{p^2-m^2-i0}-\frac{1}{p^2-m^2+i0}\right). \tag{4.2}$$

In so doing, the integral in Eq. (4.1) is now equal to a forward scattering diagram, as it is shown in Fig. 4.1. We have exchanged the square of a Born amplitude with

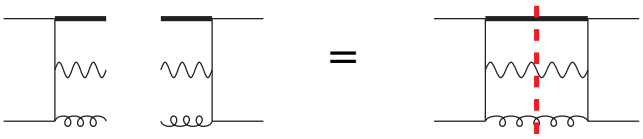

Figure 4.1: Forward scattering diagram.

a two-loop diagram, in contrast to the usual application of the Cutkosky rules. We do this in order to utilize IBPs and LI relations between multi-loop integrals. The phase-space integrals can then be evaluated in the same algorithmic fashion as the multi-loop integrals.

Note that this way to use Cutkosky rules can be applied also to differential quantities. In [36], the authors compute the rapidity distributions of Z and W bosons produced at Tevatron and LHC writing the distribution $d\sigma/dY$ as an integral over the phase space at fixed rapidity. This involves a delta function (that fixes the rapidity), that is then interpreted as the mass-shell condition of a fake particle and replaced by the difference of two "special" massive propagators, as in Eq. (4.2).

We begin our calculation by summing over the colors and spins of the external particles in the cut two-loop integral. These integrals are equal to the forward scattering diagram. Then these original diagrams are expressed in terms of a large number of scalar two-loop integrals to which the same cutting rules apply. We can use the IBPs

method to reduce the cut scalar integrals. This is a consequence of the fact that the delta-function in Eq. (4.3) is represented in a very simple manner by the difference of two propagators with opposite prescriptions for their imaginary parts. We derive the IBPs equations by integrating over derivatives which act on the propagators of the cut scalar integrals. The prescription for the imaginary part of the two propagators in the r.h.s of Eq. (4.3) is irrelevant for the differentiation. Therefore the IBP relations for the two descendants of these two terms have the same form as the IBP relations for the original integral without the cut. It is then allowed to commute the application of IBP reduction algorithms with the application of the Cutkosky rules.

4.1.2 Topologies for the real corrections

The modulus squared includes all the Feynman diagrams, we will combine all the possibilities in order to find the interference terms and replace the delta-functions by a difference of two propagators with opposite prescription. We consider all the light quarks, as well as gluons and photons, massless comparing to the W and Z bosons. From now on, the bold lines represent the massive W and Z bosons, and while massless gluon, photon and light quarks will be represented by the thin lines, the dashed (red) line cut the propagators that have been replaced by the δ function. A large number of combination has been found, but not all of them are independent. Symmetries help us to find the relation between diagrams and hopefully to reduce their number. For example, there are two diagrams we can find after the combination. These two diagrams can transform into each other by exchanging the two incoming momenta p_1 and p_2. This does not change the integration over the phase-space, which is a function of s:

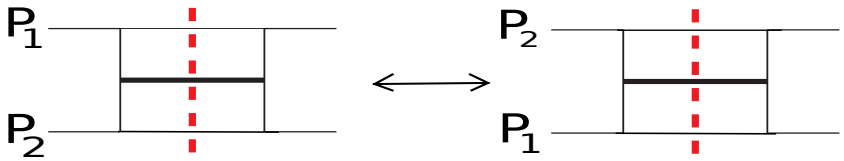

We choose the set of independent diagrams as they appear in Figs. 4.2, 4.3, 4.4, and 4.5[1]. To calculate them, we can distinguish two possible big sectors. In the first sector, there are 14 topologies with 3 cuts as show in Fig. 4.2. In the second sector, there are 20 topologies with 2 cuts (Figs. 4.3, 4.4, and 4.5). For the 3-cut diagrams, we have "planar" and "crossed" diagrams. In Fig. 4.2, for every planar diagram, there is a corresponding crossed digram; for example in the case of diagram (a) and (a'). The difference between the two is that the "final-state" momenta are exchanged.

[1]Note that in Fig. 4.2 the gluon and photon propagators are distinguished, while in Figs. 4.3–4.5 they are represented by plain thin lines.

Considering the virtual-real topologies, these include some massive boson propagator lines. Based on the number of the massive propagators of the 2-cut diagrams, we can classify them in three groups: *i)* the 2-cut diagrams with one massive propagator, shown in Fig. 4.3; *ii)* diagrams with two massive propagator lines, shown in Fig. 4.4, and diagrams with three massive propagators, shown in Fig. 4.5. In the first two groups, all the massive lines can be W-boson or Z-boson lines.

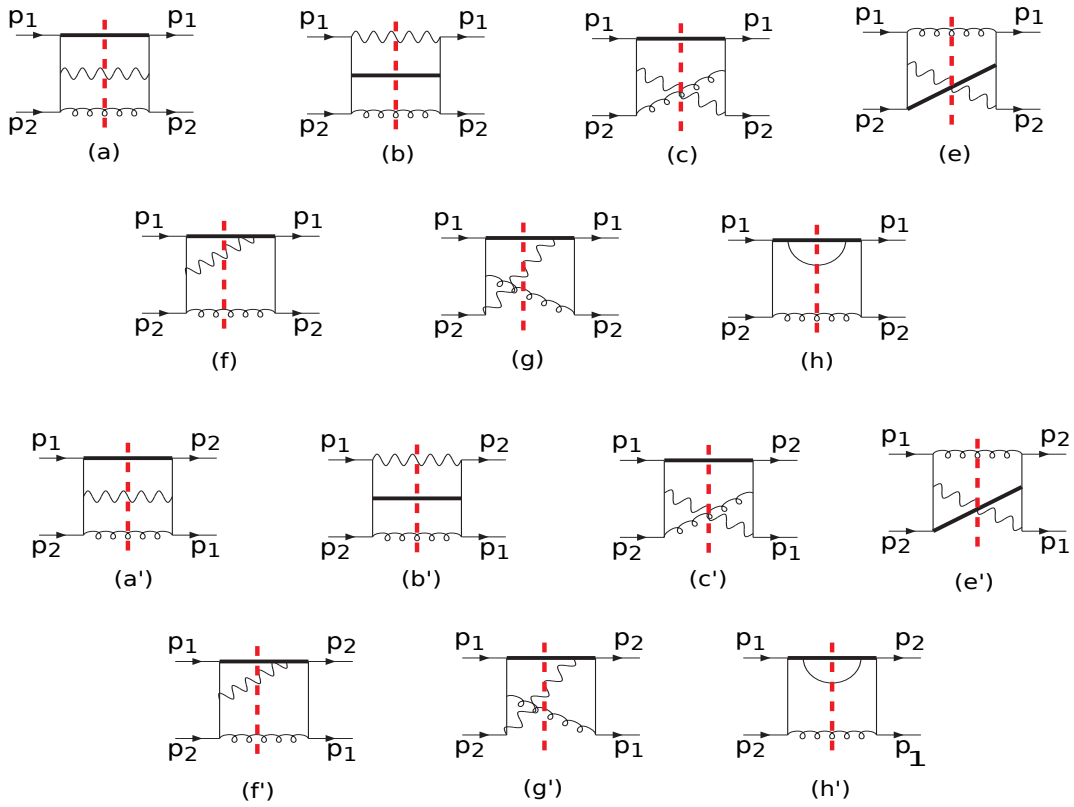

Figure 4.2: 3-cut diagrams: the first two lines include the planar diagrams, the last two lines include the corresponding crossed diagrams. Arrows do not indicate ferminic lines, but they label the flow of external momenta. On the left both p_1 and p_2 are incoming and on the right they are both outgoing.

4.1.3 Master integrals for the real corrections

When we perform the reduction of diagrams, we must pay attention to a point: the δ functions should be recovered using the inverse of Eq. (4.2). This means that a cut propagators cannot be shrinked in the reduction procedure. In other words, the original phase-space integral is expressed in terms of a small number of master

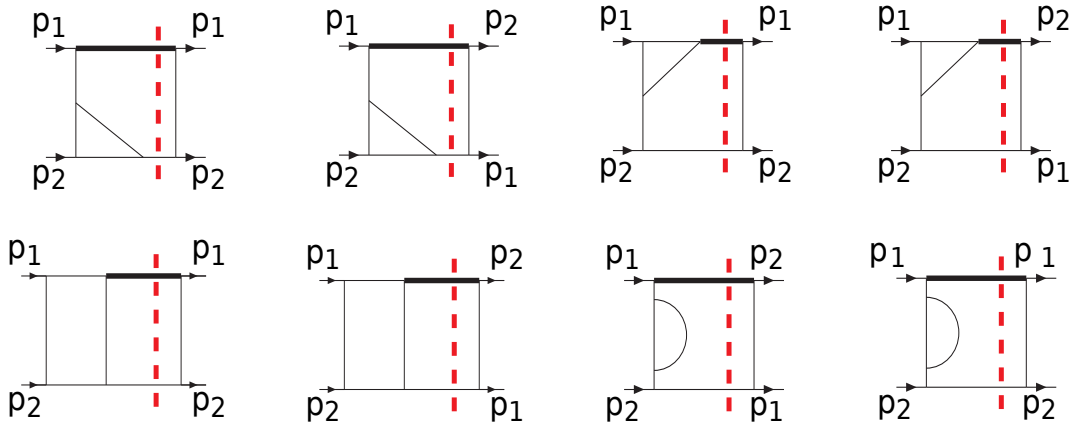

Figure 4.3: 2-cut diagrams with one massive propagator. Arrows do not indicate ferminic lines, but they label the flow of external momenta. On the left both p_1 and p_2 are incoming and on the right they are both outgoing.

integrals, which have the same cut propagators as the initial diagram. We process the reduction as mentioned in Chapter 2, by using the public program Reduze. The original phase-space integral is expressed in terms of a small number of irreducible and independent integrals, the MIs. Once we have the result of all the MIs, all the diagrams are solved immediately because all of them can be expressed by a combination of MIs.

Master integrals for the 3-cut diagrams

In Fig. 4.6, there is an example of 3-cut (double-real) diagram that can be reduced to a combination of MIs of the sub-topologies. G_i are functions that are known directly from the reduction. The last master integral in this formula is different from the second one, because it has one additional term on the numerator. After the reduction of all the 3-cut diagrams, all the MIs are presented in Fig. 4.7. First let us analyse these MIs. One thing to remarke is that in some cases more than one MI per topology is present. This is the case for instance of the first two masters or the fourth and fifth of Fig. 4.7. These entangled MIs will be, in general, more difficult to solve using the differential equations method. This is due to the fact that they give rise to systems of first-order linear differential equations instead of single equations.

Master integrals for the 2-cut diagrams

The reduction procedure can be applied to the 2-cut (virtual-real) diagrams. We have treated all the W and Z bosons as having the same mass, for the reduction. The first group is shown in Fig. 4.8 and it contains 5 MIs coming from the diagrams with one massive propagator. In Fig. 4.9 again entangled MIs show up. In particular, there

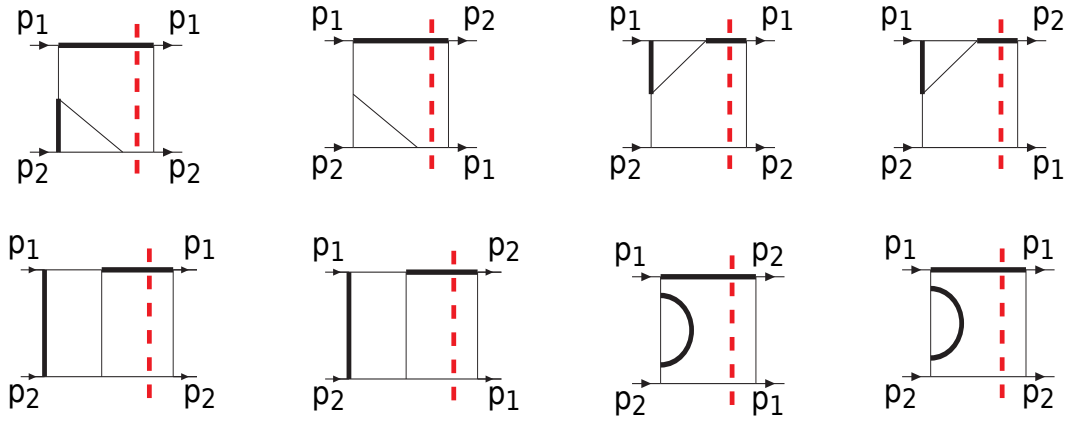

Figure 4.4: 2-cut diagrams with two massive propagators. Arrows do not indicate ferminic lines, but they label the flow of external momenta. On the left both p_1 and p_2 are incoming and on the right they are both outgoing.

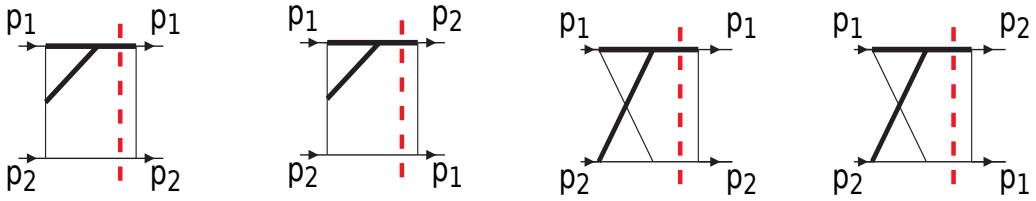

Figure 4.5: 2-cut diagrams with three massive propagators. Arrows do not indicate ferminic lines, but they label the flow of external momenta. On the left both p_1 and p_2 are incoming and on the right they are both outgoing.

are two entangled masters in the first line and three entangled MIs in the second line. In Fig. 4.10, we show the MIs with three massive propagators. The situation is even more complicated with respect to Fig. 4.8. In fact, in this case we find a topology with four entangled MIs.

4.2 Soft limits of the MIs

To find an analytic solution for the MIs presented above we apply the differential equations method. All the MIs depend on two invariants: the mass of boson squared, a^2, and the square of the sum of the incoming momenta, $s = -(p_1 + p_2)^2$. It is convenient to express the MIs in terms of the dimensionless ratio $z = \frac{a^2}{s}$.

In order to fully solve differential equations, we need to constrain the integration constants. This can be achieved by requiring the master integrals to take particular values, computed separately by other means, for special values of z. Since $0 < z < 1$,

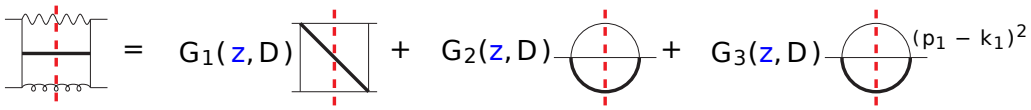

Figure 4.6: A 3-cut diagram which is reducible, i.e. it can be expressed as a combination of sub-topologies.

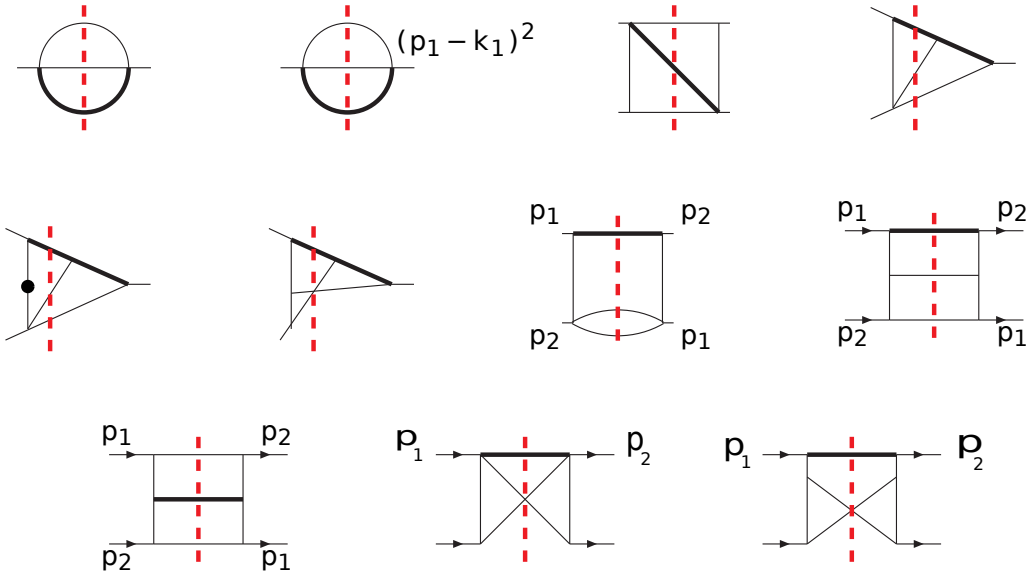

Figure 4.7: MIs for the 3-cut diagrams. A dot on the propagator line means that the propagator is rased to the power 2.

there are two natural choices for such special values. The case $z = 0$ physically corresponds to the situation where the produced particle is massless. The other limit, $z \to 1$ represents, instead, the threshold production of the gauge boson. This limit is in general not smooth, as the amplitude might develop new infrared poles in this region. For this reason we choose the point $z = 1$ as an initial condition to the differential equation. This corresponds to the "soft limit", where the momenta of all the final-state partons vanish simultanously. This limit is important not only as an initial condition for the differential equations, but also for the structure of the phase space integrals.

Following [64], we define the soft limit of a master integral, $\mathrm{F}(z,\epsilon)$ as

$$\mathrm{F}^S(z,\epsilon) = \sum^{n} \frac{F_n(z,\epsilon)}{(1-z)^{a+m\epsilon}}, \;\; a, n \geq 1, \tag{4.3}$$

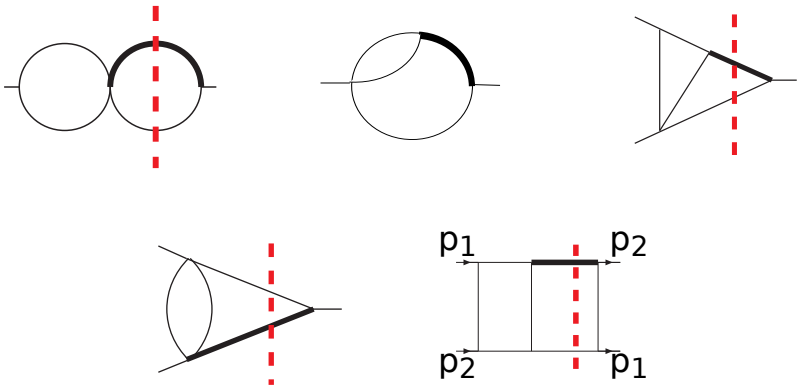

Figure 4.8: MIs for the 2-cut diagrams with one massive propagator.

The function $F_n(z,\epsilon)$ is finite at $z=1$. n is an integer, such that,

$$\lim_{z\to 1}\frac{\mathrm{F}^S(z,\epsilon)}{\mathrm{F}(z,\epsilon)}=1. \tag{4.4}$$

The right side is valid to all order in ϵ, so that the hard part $\mathrm{F}^H(z,\epsilon)$ of a master can be expressed by

$$\mathrm{F}^H(z,\epsilon)=\mathrm{F}(z,\epsilon)-\mathrm{F}^S(z,\epsilon) \tag{4.5}$$

From Eq. (4.6), we can see that the soft part will be the boundary condition to constrain the integral constants when we do the limit $z\to 1$. Moreover, let us study this behavior:

$$\begin{aligned}(1-z)^{-1+a\epsilon} &= \frac{\delta(1-z)}{a\epsilon}+a\epsilon\left[\frac{1}{1-z}\right]_+ +\frac{(a\epsilon)^2}{2!}\left[\frac{\log(1-z)}{1-z}\right]_+ \\ &\quad +\frac{(a\epsilon)^3}{3!}\left[\frac{\log(1-z)^2}{1-z}\right]_+ +\mathcal{O}\left((\epsilon^4)\right)\end{aligned} \tag{4.6}$$

and the + indicates the common plus-prescription,

$$\int_0^1 dz\left[\frac{(1-z)^k}{(1-z)}\right]_+ f(z)=\int_0^1 dz\frac{(1-z)^k}{(1-z)}\Big[f(z)-f(0)\Big]. \tag{4.7}$$

In general, measurement of the phase space volume for a massive particle X of mass m_X and $n-1$ massless particles can defined by

$$d\Phi_n=\frac{d^Dp_X}{(2\pi)^{D-1}}\delta_+(p_X^2-m_x^2)\Big(\prod_{i=3}^{n+1}\frac{d^Dp_i}{(2\pi)^{D-1}}\delta_+(p_i)^2\Big)(2\pi)^D\delta^(D)(p_1+\cdots+p_i-p_x)). \tag{4.8}$$

In following sections we will introduce a convenient parameterization to calculate the soft limit of the double-real and virtual-real MIs.

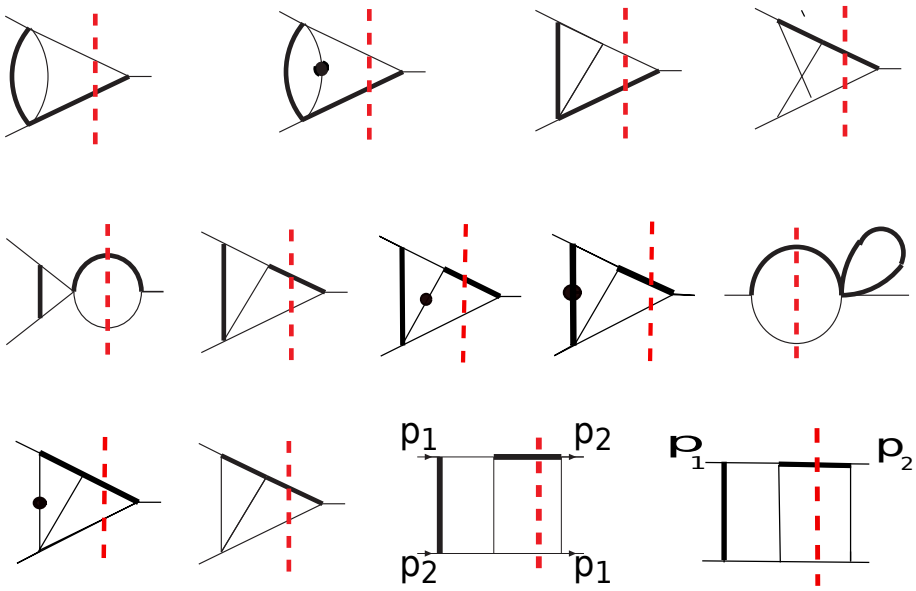

Figure 4.9: MIs for the 2-cut diagrams with two massive propagators. A dot on the propagator line means that the propagator is raised to power 2.

4.2.1 Soft limits of double-real MIs

To evaluate the soft limits of the double-real master integrals, we use the following exact parametrization for the $2 \to 3$ phase space [64], which allow for a more convenient evaluation of the different diagrams,

$$\int d\Phi_3 = \frac{(2\pi)^{-3+2\epsilon}}{16\Gamma(1-2\epsilon)} \int_0^1 dx_2 (\prod_{i=1}^{4} dy_i)\delta(\sum_{i=1}^{4} y_i - 1) \times (\frac{s\bar{z}^3\kappa^4}{2-\kappa})(s^2\bar{z}^4\kappa^4 \sin^2(\pi x_2) \prod_{i=1}^{4} y_i)^{-\epsilon} \tag{4.9}$$

with $\bar{z} = 1 - z$. We define,

$$\begin{aligned} s_{12} &= 2p_1p_2, \quad & s_{13} &= -2p_1p_3, \\ s_{23} &= -2p_2p_3, \quad & s_{14} &= -2p_1p_4, \\ s_{24} &= -2p_2p_4, \quad & s_{34} &= -2p_3p_4, \end{aligned} \tag{4.10}$$

In this parametrization the propagators of the massless parton read

$$\begin{aligned} s_{13} &= -s\bar{z}\kappa y_1, \quad & s_{23} &= -s\bar{z}\kappa y_2, \\ s_{14} &= -s\bar{z}\kappa y_3, \quad & s_{24} &= -s\bar{z}\kappa y_4, \\ s_{34} &= s\bar{z}\kappa^2\xi \end{aligned} \tag{4.11}$$

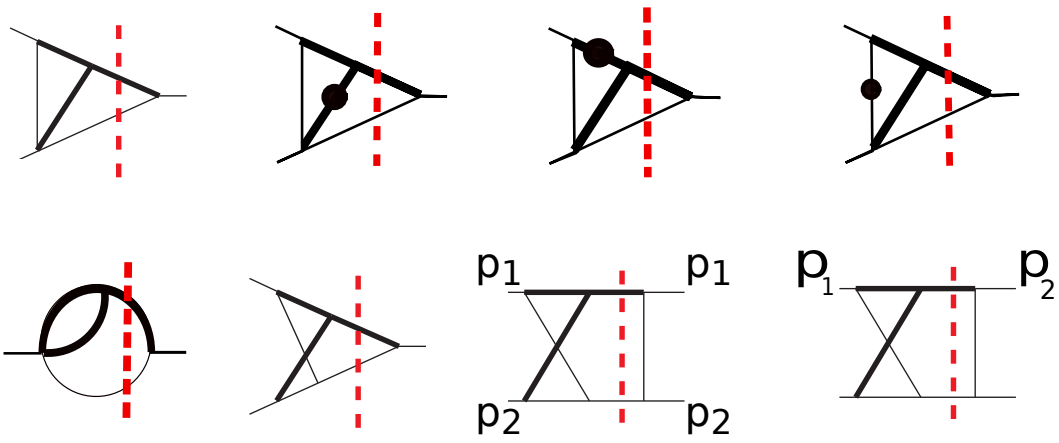

Figure 4.10: MIs for the 2-cut diagrams with three massive propagators.

where

$$\xi = \bar{z}(y_1 y_4 + y_2 y_3 + 2\cos(x_2\pi)\sqrt{y_1 y_4 y_2 y}), \tag{4.12}$$

and

$$\kappa = \frac{1-\sqrt{1-4\xi}}{2\xi} \in [1,2), \tag{4.13}$$

In addition, the MIs depend on the following denominators

$$\begin{aligned} &s_{134} = s_{13} + s_{14} + s_{34},\ s_{234} = s_{23} + s_{24} + s_{34}, \\ &s_{123} = s_{12} + s_{23} + s_{13}, s_{124} = s_{12} + s_{24} + s_{14}. \end{aligned} \tag{4.14}$$

If we now perform the change of variable [65]

$$y_1 = x_1 x_3 \quad y_2 = \bar{x}_3 x_1 \quad y_3 = x_4 \bar{x}_1 \quad y_4 = \bar{x}_1 \bar{x}_4 \tag{4.15}$$

One can obtain

$$\begin{aligned} \int \Phi_3 \;=\; & \frac{(2\pi)^{-3+2\epsilon}}{16\Gamma(1-2\epsilon)} \int_0^1 dx_1 dx_2 dx_3 dx_4 \left(\frac{s(1-z)^3\kappa^4 x_1(1-x_1)}{2-\kappa}\right) \\ & \times (s^2(1-z)^4\kappa^4 x_1^2(1-x_1)^2 x_3(1-x_3)x_4(1-x_4)\sin^2(\pi x_2))^{-\epsilon} \end{aligned} \tag{4.16}$$

The propagators of massless partons in this parameterization take the following form:

$$\begin{aligned} s_{13} &= -s(1-z)\kappa x_1 x_3 \\ s_{23} &= -s(1-z)\kappa x_1(1-x_3) \\ s_{14} &= -s(1-z)\kappa(1-x_1)x_4 \\ s_{24} &= -s(1-z)\kappa(1-x_1)(1-x_4) \end{aligned} \tag{4.17}$$

We now take the limit, $z \to 1$. It is easy to see that in the soft limit we have the relations

$$\lim_{z\to 1} s_{123} = \lim_{z\to 1} s_{124} = s_{12} = s, \quad \lim_{z\to 1} \kappa = 1,$$
$$\lim_{z\to 1} s_{134} = s_{13} + s_{14}, \quad \lim_{z\to 1} s_{234} = s_{23} + s_{24}. \tag{4.18}$$

This construction therefore allows one to derive the soft limits of almost all master integrals in terms of simple Beta-functions,

$$B(x,y) = \int_0^1 dt\, t^{x-1}(1-t)^{y-1} = \frac{\Gamma(x)\Gamma(y)}{\Gamma(x+y)} \tag{4.19}$$

Let us calculate the three-body phase space, using the Eq. (4.13) and taking the limit,

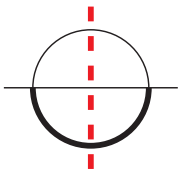

$$\overset{\lim z\to 1}{=} \frac{(2\pi)^{-3+2\epsilon} s^{1-2\epsilon}(1-z)^{3-4\epsilon}}{16\Gamma(1-2\epsilon)} \int_0^1 x_1(1-x_1)dx_1dx_2dx_3dx_4$$
$$\times (x_1^2(1-x_1)^2 x_3(1-x_3)x_4(1-x_4)\sin^2(\pi x_2))^{-\epsilon}$$
$$= \frac{(2\pi)^{-3+2\epsilon} s^{(1-2\epsilon)}(1-z)^{3-4\epsilon}}{16\Gamma(1-2\epsilon)} \int_0^1 dx_1 x_1^{1-2\epsilon}(1-x_1)^{1-2\epsilon} \int_0^1 dx_3 x_3^{-\epsilon}(1-x_3)^{-\epsilon}$$
$$\times \int_0^1 dx_4 x_4^{-\epsilon}(1-x_4)^{-\epsilon} \int_0^1 dx_2 (\sin^2(\pi x_2))^{-\epsilon}, \tag{4.20}$$

where we used the formula

$$\frac{\Gamma(x)}{\Gamma(2x)} = \frac{\sqrt{\pi}}{2^{2x-1}} \frac{1}{\Gamma(x+\frac{1}{2})} \tag{4.21}$$

and

$$n\Gamma(n) = \Gamma(n+1). \tag{4.22}$$

Then, we have

$$\int_0^1 dx_2 (\sin^2(\pi x_2))^{-\epsilon} = \frac{1}{\sqrt{\pi}} \frac{\Gamma(\frac{1}{2}-\epsilon)}{\Gamma(1-\epsilon)} = \frac{2^{2\epsilon}\Gamma(1-2\epsilon)}{\Gamma^2(1-\epsilon)}. \tag{4.23}$$

Using the Beta-function of Eq. (4.21), we find

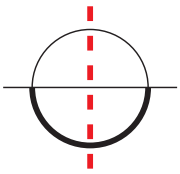

$$\overset{\lim z\to 1}{=} \frac{(2\pi)^{-3+2\epsilon} s^{(1-2\epsilon)}(1-z)^{3-4\epsilon}}{16\Gamma(1-2\epsilon)} \frac{\Gamma^3(1-\epsilon)}{\Gamma(4-4\epsilon)} \frac{\Gamma(\frac{1}{2}-\epsilon)}{\sqrt{\pi}}$$

$$= \frac{2^{-3+4\epsilon}\pi^{-3+2\epsilon}s^{(1-2\epsilon)}(1-z)^{3-4\epsilon}}{16}\frac{\Gamma(1-\epsilon)^2}{\Gamma(4-4\epsilon)}. \tag{4.24}$$

For the other MIs, with different propagators, we can perform the same steps, finding

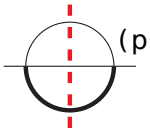

$$\begin{aligned}
&= \int d\Phi_3 \times (s_{23}+s_{24}) \\
&\overset{\lim z\to 1}{=} -\frac{2^{-3+2\epsilon}\pi^{-3+2\epsilon}s^{2-2\epsilon}(1-z)^{4-4\epsilon}}{16\Gamma(1-2\epsilon)}\int_0^1 dx_2(\sin^2(\pi x_2))^{-\epsilon} \\
&\quad\times\Bigg(\int_0^1 dx_1 x_1^{2-2\epsilon}(1-x_1)^{1-2\epsilon}\int_0^1 dx_3 x_3^{-\epsilon}(1-x_3)^{1-\epsilon} \\
&\qquad\times\int_0^1 dx_4 x_4^{-\epsilon}(1-x_4)^{-\epsilon} \\
&\quad+\int_0^1 dx_1 x_1^{1-2\epsilon}(1-x_1)^{2-2\epsilon}\int_0^1 dx_3 x_3^{-\epsilon}(1-x_3)^{-\epsilon} \\
&\qquad\times\int_0^1 dx_4 x_4^{-\epsilon}(1-x_4)^{1-\epsilon}\Bigg) \\
&= 2^{-6+4\epsilon}\pi^{-3+2\epsilon}s^{2-2\epsilon}(1-z)^{4-4\epsilon}\frac{\Gamma(1-\epsilon)\Gamma(2-\epsilon)}{\Gamma(5-4\epsilon)}.
\end{aligned} \tag{4.25}$$

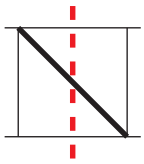

$$\begin{aligned}
&= \int \frac{d\Phi_3}{s_{14}s_{23}} \\
&\overset{\lim z\to 1}{=} \frac{2^{-7+2\epsilon}\pi^{-3+2\epsilon}s^{-1-2\epsilon}(1-z)^{1-4\epsilon}}{\Gamma(1-2\epsilon)}\int_0^1 dx_2(\sin^2(\pi x_2))^{-\epsilon} \\
&\quad\times\Bigg(\int_0^1 dx_1 x_1^{-2\epsilon}(1-x_1)^{-2\epsilon}\int_0^1 dx_3 x_3^{-\epsilon}(1-x_3)^{-1-\epsilon} \\
&\qquad\times\int_0^1 dx_4 x_4^{-1-\epsilon}(1-x_4)^{-\epsilon}\Bigg) \\
&= 2^{-7+4\epsilon}\pi^{-3+2\epsilon}s^{-1-2\epsilon}(1-z)^{1-4\epsilon}\frac{\Gamma^2(1-\epsilon)}{\Gamma(2-4\epsilon)}.
\end{aligned} \tag{4.26}$$

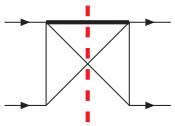

$$= \int \frac{d\Phi_3}{s_{24}s_{13}}$$

$$\overset{\lim z\to 1}{=} \frac{2^{-7+2\epsilon}\pi^{-3+2\epsilon}s^{-1-2\epsilon}(1-z)^{1-4\epsilon}}{\Gamma(1-2\epsilon)} \int_0^1 dx_2(\sin^2(\pi x_2))^{-\epsilon}$$

$$\times\Bigg(\int_0^1 dx_1 x_1^{-2\epsilon}(1-x_1)^{-2\epsilon} \int_0^1 dx_3 x_3^{-1-\epsilon}(1-x_3)^{-\epsilon}$$

$$\times \int_0^1 dx_4 x_4^{-\epsilon}(1-x_4)^{-1-\epsilon}\Bigg)$$

$$= 2^{-7+4\epsilon}\pi^{-3+2\epsilon}s^{-1-2\epsilon}(1-z)^{1-4\epsilon}\frac{\Gamma^2(1-\epsilon)}{\Gamma(2-4\epsilon)}. \tag{4.27}$$

We list all the results of soft limits of the MIs which have an infrared divergence when $z \to 1$. These will be used as boundary conditions to fix the integration constants in the solution of the differential equations.

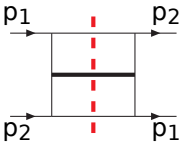

$$= \int \frac{d\Phi_3}{s_{13}s_{23}s_{14}s_{24}}$$

$$\overset{\lim z\to 1}{=} \frac{(2\pi)^{-3+2\epsilon}s^{(3-2\epsilon)}(1-z)^{-1-4\epsilon}}{16\Gamma(1-2\epsilon)} \int_0^1 dx_1 x_1^{-1-2\epsilon}(1-x_1)^{-1-2\epsilon}$$

$$\times \int_0^1 dt_3 x_3^{-1-\epsilon}(1-x_3)^{-1-\epsilon} \int_0^1 dx_4 x_4^{-1-\epsilon}(1-x_4)^{-1-\epsilon} \int_0^1 dx_2(\sin^2(\pi x_2))^{-\epsilon}$$

$$= 2^{-7+4\epsilon}\pi^{-3+4\epsilon}s^{-3-2\epsilon}(1-z)^{-1-4\epsilon}\frac{\Gamma(1-\epsilon)^2}{\Gamma(4-4\epsilon)}\frac{-8(1-2\epsilon)(1-4\epsilon)(3-4\epsilon)}{\epsilon^3}$$

$$= 2^{-7+4\epsilon}\pi^{-3+4\epsilon}s^{-3-2\epsilon}(1-z)^{-1-4\epsilon}(-\frac{4}{\epsilon^3}+\frac{32\xi(2)}{\epsilon}+80\xi(3)+\mathcal{O}(\epsilon)) \tag{4.28}$$

If we perform the change of variables

$$y_1 = t_1 t_3, \quad y_2 = \bar{t}_1 t_4, \quad y_3 = t_1 \bar{t}_3, \quad y_4 = \bar{t}_1 \bar{t}_4. \tag{4.29}$$

Then soft limit of the following two master integrals can be easier calculated. In particular the term of $s_{13}+s_{14}$ and $s_{23}+s_{24}$ effectively reduce to t_1 and $\bar{t}_1$ respectively

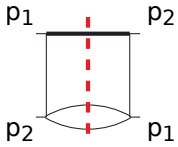

$$= \int \frac{d\Phi_3}{s_{234}s_{134}}$$

$$\lim_{z\to 1} \frac{2^{-7+2\epsilon}\pi^{-3+2\epsilon}s^{-1-2\epsilon}(1-z)^{1-4\epsilon}}{\Gamma(1-2\epsilon)} \int_0^1 dx_2(\sin^2(\pi x_2))^{-\epsilon}$$
$$\times\Bigg(\int_0^1 dt_1 t_1^{-2\epsilon}(1-t_1)^{-2\epsilon}\int_0^1 dt_3 t_3^{-\epsilon}(1-t_3)^{-\epsilon}$$
$$\times\int_0^1 dt_4 t_4^{-\epsilon}(1-t_4)^{-\epsilon}\Bigg)$$
$$= 2^{-7+4\epsilon}\pi^{-3+2\epsilon}s^{-1-2\epsilon}(1-z)^{1-4\epsilon}\frac{\Gamma^2(1-2\epsilon)\Gamma^2(1-\epsilon)}{\Gamma^2(2-2\epsilon)\Gamma(2-4\epsilon)}$$
$$= 2^{-7+4\epsilon}\pi^{-3+2\epsilon}s^{-1-2\epsilon}(1-z)^{1-4\epsilon}\frac{2(3-4\epsilon)\Gamma^2(1-\epsilon)}{(1-2\epsilon)\Gamma(4-4\epsilon)}. \tag{4.30}$$

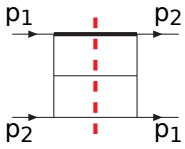

$$= \int \frac{d\Phi_3}{s_{234}s_{23}s_{13}s_{134}}$$
$$\lim_{z\to 1} \frac{(2\pi)^{-3+2\epsilon}s^{-3-2\epsilon}(1-z)^{-1-4\epsilon}}{16\Gamma(1-2\epsilon)} \int_0^1 dt_1 x_1^{-1-2\epsilon}(1-t_1)^{-1-2\epsilon}$$
$$\times\int_0^1 dt_3 t_3^{-1-\epsilon}(1-t_3)^{-\epsilon}\int_0^1 dt_4 t_4^{-1-\epsilon}(1-t_4)^{-\epsilon}\int_0^1 dx_2(\sin^2(\pi x_2))^{-\epsilon}$$
$$= 2^{-7+4\epsilon}\pi^{-3+4\epsilon}s^{(3-2\epsilon)}(1-z)^{-1-4\epsilon}\frac{\Gamma(1-\epsilon)^2}{\Gamma(4-4\epsilon)}\frac{-2(1-2\epsilon)(1-4\epsilon)(3-4\epsilon)}{\epsilon^3}$$
$$= 2^{-7+4\epsilon}\pi^{-3+4\epsilon}s^{(3-2\epsilon)}(1-z)^{-1-4\epsilon}(-\frac{1}{\epsilon^3}+\frac{8\xi(2)}{\epsilon}+20\xi(3)+\mathcal{O}(\epsilon)). \tag{4.31}$$

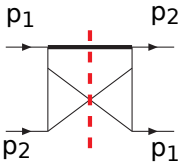

$$= \int \frac{d\Phi_3}{s_{234}s_{24}s_{13}s_{134}}$$
$$\lim_{z\to 1} \frac{(2\pi)^{-3+2\epsilon}s^{-3-2\epsilon}(1-z)^{-1-4\epsilon}}{16\Gamma(1-2\epsilon)} \int_0^1 dt_1 x_1^{-1-2\epsilon}(1-t_1)^{-1-2\epsilon}$$
$$\times\int_0^1 dt_3 t_3^{-1-\epsilon}(1-t_3)^{-\epsilon}\int_0^1 dt_4 t_4^{-\epsilon}(1-t_4)^{-1-\epsilon}\int_0^1 dx_2(\sin^2(\pi x_2))^{-\epsilon}$$
$$= 2^{-7+4\epsilon}\pi^{-3+4\epsilon}s^{(3-2\epsilon)}(1-z)^{-1-4\epsilon}\frac{\Gamma(1-\epsilon)^2}{\Gamma(4-4\epsilon)}\frac{-2(1-2\epsilon)(1-4\epsilon)(3-4\epsilon)}{\epsilon^3}$$

$$= 2^{-7+4\epsilon}\pi^{-3+4\epsilon}s^{(3-2\epsilon)}(1-z)^{-1-4\epsilon}(-\frac{1}{\epsilon^3}+\frac{8\xi(2)}{\epsilon}+20\xi(3)+\mathcal{O}(\epsilon). \quad (4.32)$$

4.2.2 Soft limits of virtual-real MIs

The virtual-real MIs with one massive propagator are shown in Fig. 4.8. A convenient phase space parametrization is given by

$$d\Phi_2 = \frac{1}{8\pi}\frac{(4\pi)^\epsilon}{\Gamma(1-\epsilon)}s^{-\epsilon}(1-z)^{1-2\epsilon}[\lambda(1-\lambda)]^{-\epsilon}d\lambda, \quad (4.33)$$

where $\lambda \in [0,1]$, with the Lorentz invariants taking the simple form

$$\begin{aligned} s_{13} &= (p_1-p_3)^2 = -s_{12}(1-z)\lambda, \\ s_{23} &= (p_2-p_3)^2 = -s_{12}(1-z)(1-\lambda). \end{aligned} \quad (4.34)$$

Note that the singularities of s_{13} and s_{23} are factorized in λ, $(1-\lambda)$ and $(1-z)$ which allows for a simple substraction of the poles. Now one can derive all the soft limits of master integrals using the Beta-function identity (4.21). The following three MIs include a massless bubble ($Bub(x)$ as a function of the invariant x). We can insert the result in the integration with the correspondent momentum:

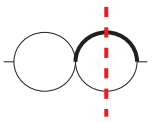

$$= \int d\Phi_2 \mathrm{Bub}(s_{12})$$

$$\begin{aligned} &\overset{\lim z\to 1}{=} \int_0^1 \frac{1}{8\pi}\frac{(4\pi)^\epsilon}{\Gamma(1-\epsilon)}(-s)^{-\epsilon}(1-z)^{1-2\epsilon}\frac{1}{4\pi^2}\frac{\Gamma(1+\epsilon)\Gamma^2(1-\epsilon)}{4\epsilon(4\pi)^{-\epsilon}\Gamma(2-2\epsilon)} \\ &\quad \times (s_{12})^{-\epsilon}[\lambda(1-\lambda)]^{-\epsilon}d\lambda \\ &= \frac{\mathrm{Re}(-1)^{-\epsilon}}{8\pi}\frac{(4\pi)^\epsilon}{\Gamma(1-\epsilon)}s^{-2\epsilon}(1-z)^{1-2\epsilon}\frac{1}{4\pi^2}\frac{\Gamma(1+\epsilon)\Gamma^4(1-\epsilon)}{4\epsilon(4\pi)^{-\epsilon}\Gamma^2(2-2\epsilon)} \\ &= 2^{-7+4\epsilon}\pi^{-3+2\epsilon}\cos(\pi\epsilon)s^{-2\epsilon}(1-z)^{1-2\epsilon}\frac{\Gamma(1+\epsilon)\Gamma^3(1-\epsilon)}{\epsilon\Gamma^2(2-2\epsilon)}; \end{aligned} \quad (4.35)$$

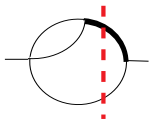

$$= \int d\Phi_2 \mathrm{Bub}(a^2)$$

$$\overset{\lim z\to 1}{=} \int_0^1 \frac{1}{8\pi}\frac{(4\pi)^\epsilon}{\Gamma(1-\epsilon)}(-s)^{-\epsilon}(1-z)^{1-2\epsilon}\frac{1}{4\pi^2}\frac{\Gamma(1+\epsilon)\Gamma^2(1-\epsilon)}{4\epsilon(4\pi)^{-\epsilon}\Gamma(2-2\epsilon)}$$

$$\times (s_{123})^{-\epsilon}[\lambda(1-\lambda)]^{-\epsilon} d\lambda$$

$$= \frac{\mathrm{Re}(-1)^{-\epsilon}}{8\pi} \frac{(4\pi)^{\epsilon}}{\Gamma(1-\epsilon)} s^{-\epsilon} m^{-2\epsilon} (1-z)^{1-2\epsilon} \frac{1}{4\pi^2} \frac{\Gamma(1+\epsilon)\Gamma^4(1-\epsilon)}{4\epsilon(4\pi)^{-\epsilon}\Gamma^2(2-2\epsilon)}$$

$$= 2^{-7+4\epsilon}\pi^{-1+2\epsilon}\cos(\pi\epsilon) s^{-\epsilon} a^{-2\epsilon} (1-z)^{1-2\epsilon} \frac{\Gamma(1+\epsilon)\Gamma^3(1-\epsilon)}{\epsilon\Gamma^2(2-2\epsilon)}; \qquad (4.36)$$

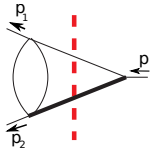

$$= \int d\Phi_2 \mathrm{Bub}(s_{13})$$

$$\overset{\lim z\to 1}{=} \int_0^1 \frac{1}{8\pi} \frac{(4\pi)^{\epsilon}}{\Gamma(1-\epsilon)} (-s_{12})^{-\epsilon} (-s)^{-\epsilon} (1-z)^{1-3\epsilon} \frac{1}{4\pi^2} \frac{\Gamma(1+\epsilon)\Gamma^2(1-\epsilon)}{4\epsilon(4\pi)^{-\epsilon}\Gamma(2-2\epsilon)}$$

$$\times \lambda^{-2\epsilon}(1-\lambda)^{-\epsilon} d\lambda$$

$$= \frac{1}{8\pi} \frac{(4\pi)^{\epsilon}}{\Gamma(1-\epsilon)} s^{-2\epsilon} (1-z)^{1-3\epsilon} \frac{1}{4\pi^2} \frac{\Gamma(1+\epsilon)\Gamma^3(1-\epsilon)\Gamma(1-2\epsilon)}{4\epsilon(4\pi)^{-\epsilon}\Gamma(2-2\epsilon)\Gamma(2-3\epsilon)}$$

$$= 2^{-7+4\epsilon}\pi^{-3+2\epsilon} s^{-2\epsilon} (1-z)^{1-3\epsilon} \frac{\Gamma(1+\epsilon)\Gamma^2(1-\epsilon)\Gamma(1-2\epsilon)}{\epsilon\Gamma(2-2\epsilon)\Gamma(2-3\epsilon)}. \qquad (4.37)$$

Before calculating the other MIs, let us first study the massless box with one off-shell leg. The four point-function (in the following we refer to it as Box) can be expressed as follows

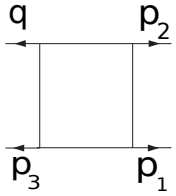

$$= \int \frac{d^D k}{(2\pi)^D} \frac{1}{k^2 (k-p_2)^2 (k-p_1-p_2)^2 (k-p_1-p_2-p_3)^2}. \qquad (4.38)$$

The three-point function (in the following we refer to it as Tri) can be obtained after reducing the box,

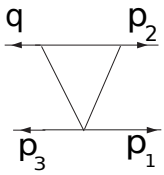

$$= \int \frac{d^D k}{(2\pi)^D} \frac{1}{k^2 (k-p_2)^2 (k-p_1-p_2-p_3)^2}. \qquad (4.39)$$

Using the IBPs, we find that this vertex is reducible:

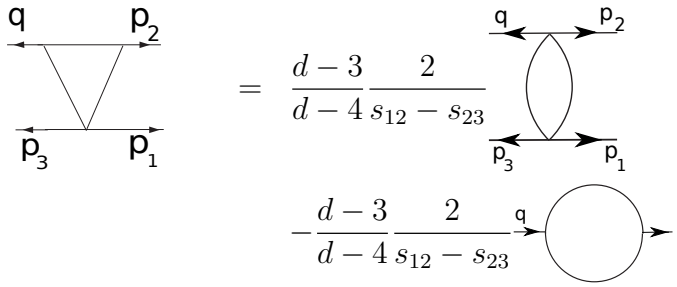

$$= \frac{d-3}{d-4}\frac{2}{s_{12}-s_{23}}$$

$$-\frac{d-3}{d-4}\frac{2}{s_{12}-s_{23}}$$

(4.40)

Then we have the relation

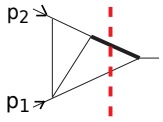

$$= \int d\Phi_2 \mathrm{Tri}(s_{13}, a^2)$$

$$= -\int d\Phi_2 \frac{1-2\epsilon}{\epsilon}\frac{1}{s_{12}-s_{23}}$$

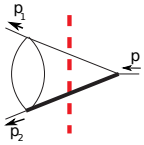

$$+\int d\Phi_2 \frac{1-2\epsilon}{\epsilon}\frac{1}{s_{12}-s_{23}}$$

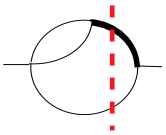

$$\stackrel{\lim z\to 1}{=} -2^{-7+4\epsilon}\pi^{-3+2\epsilon}s^{-1-2\epsilon}(1-z)^{1-3\epsilon}\frac{\Gamma(1+\epsilon)\Gamma^2(1-\epsilon)}{\epsilon^2\Gamma(2-3\epsilon)}$$

$$+2^{-7+4\epsilon}\pi^{-3+2\epsilon}\cos(\pi\epsilon)s^{-1-\epsilon}a^{-2\epsilon}(1-z)^{1-2\epsilon}\frac{(1-2\epsilon)\Gamma(1+\epsilon)\Gamma^3(1-\epsilon)}{\epsilon^2\Gamma^2(2-2\epsilon)}. \quad (4.41)$$

The virtual result of the massless box can be found in [66]:

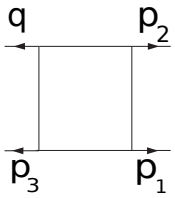

$$= \frac{4(1-2\epsilon)}{2\epsilon}\frac{1}{s_{13}s_{12}}$$

$$\times\left[\left(\frac{s_{13}s_{12}}{s_{12}+s_{23}}\right)^{-\epsilon}{}_2F_1\left(-\epsilon,-\epsilon,1-\epsilon,\frac{s_{23}}{s_{12}+s_{23}}\right)\right.$$

$$+\left(\frac{s_{13}s_{12}}{s_{13}+s_{23}}\right)^{-\epsilon}{}_2F_1\left(-\epsilon,-\epsilon,1-\epsilon,\frac{s_{23}}{s_{13}+s_{23}}\right)$$

$$-\left(\frac{s_{123}s_{12}s_{13}}{(s_{12}+s_{13})(s_{13}+s_{23})}\right)^{-\epsilon}$$

$$\left.\times\,{}_2F_1\left(-\epsilon,-\epsilon,1-\epsilon,\frac{s_{123}s_{23}}{(s_{12}+s_{13})(s_{23}+s_{13})}\right)\right], \quad (4.42)$$

where ${}_2F_1$ indicates the hypergeometric function. Then, we have

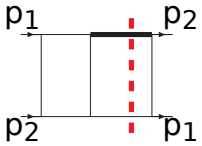

$$= \int d\Phi_2 \frac{\mathrm{Box}(\mathrm{s}_{13}, \mathrm{s}_{12}, \mathrm{a}^2)}{s_{23}}$$

$$\overset{\lim z\to 1}{=} \int_0^1 \frac{4(1-2\epsilon)}{2\epsilon} \frac{1}{s_{13}s_{12}s_{23}} s_{13}^{-\epsilon} \frac{(4\pi)^\epsilon}{4\pi^2} \frac{\Gamma(1+\epsilon)\Gamma^2(1-\epsilon)}{4\epsilon\Gamma(2-2\epsilon)} \frac{1}{8\pi} \frac{(4\pi)^\epsilon}{\Gamma(1-\epsilon)}$$
$$\times {}_2F_1(-\epsilon,-\epsilon,1-\epsilon,1) s^{-\epsilon}(1-z)^{1-2\epsilon}\lambda^{-\epsilon}(1-\lambda)^{-\epsilon}d\lambda$$

$$= 2^{-6+4\epsilon}\pi^{-3+2\epsilon}s^{-\epsilon}s_{12}^{-3-\epsilon}(1-z)^{-1-3\epsilon}\ {}_2F_1(-\epsilon,-\epsilon,1-\epsilon,0)$$
$$\times \int_0^1 \frac{(1-2\epsilon)}{\epsilon^2} \frac{\Gamma(1+\epsilon)\Gamma(1-\epsilon)}{\Gamma(2-2\epsilon)} \lambda^{-1-2\epsilon}(1-\lambda)^{-1-\epsilon}d\lambda$$
$$= 2^{-7+4\epsilon}\pi^{-3+2\epsilon}s^{-3-2\epsilon}(1-z)^{-1-3\epsilon} \frac{-3\Gamma^2(1-\epsilon)\Gamma(1+\epsilon)}{\epsilon^3\Gamma(1-3\epsilon)}. \tag{4.43}$$

Now let us consider a 2-cut MIs with two massive propagators. We use the same parameters and we find

$$= \int d\Phi_2 \mathrm{Tad}(a^2)$$

$$\overset{\lim z\to 1}{=} \int_0^1 \frac{1}{8\pi} \frac{(4\pi)^\epsilon}{\Gamma(1-\epsilon)} s^{-\epsilon}(1-z)^{1-2\epsilon}(m^2)^{1-\epsilon} \frac{1}{4\pi^2} \frac{\Gamma(1+\epsilon)}{4\epsilon(4\pi)^{-\epsilon}(1-\epsilon)} [\lambda(1-\lambda)]^{-\epsilon}d\lambda$$
$$= 2^{-7+4\epsilon}\pi^{-3+2\epsilon}s^{-\epsilon}(a^2)^{1-\epsilon}(1-z)^{1-2\epsilon} \frac{\Gamma(1-\epsilon)\Gamma(1+\epsilon)}{(1-\epsilon)\Gamma(2-2\epsilon)}, \tag{4.44}$$

where $Tad(a^2)$ is the tadpole of mass a, i.e. the integral

$$\int \frac{d^Dk}{(2\pi)^D} \frac{1}{k^2+a^2}\,. \tag{4.45}$$

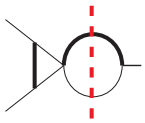

$$= \int d\Phi_2\, \mathrm{Tri}(\mathrm{s}_{12})$$

$$\overset{\lim z\to 1}{=} \int_0^1 \frac{1}{8\pi} \frac{(4\pi)^\epsilon}{\Gamma(1-\epsilon)} s^{-\epsilon}(1-z)^{1-2\epsilon}[\lambda(1-\lambda)]^{-\epsilon}d\lambda \times \frac{\Gamma(1+\epsilon)}{(2\pi)^2(4\pi)^{-\epsilon}}$$

$$\times(-\frac{1}{4}a^{-2}z(H(0,0,z)-H(1,0,z)-\frac{\pi^2}{4}+\mathcal{O}(\epsilon))$$

$$= \quad 2^{-7+4\epsilon}\pi^{-3+2\epsilon}s^{-\epsilon}(1-z)^{1-2\epsilon}a^{-2}z\frac{\Gamma(1-\epsilon)\Gamma(1+\epsilon)}{\Gamma(2-2\epsilon)}\times$$

$$\times(H(0,0,z)-H(1,0,z)-6\zeta(2)+\mathcal{O}(\epsilon)). \tag{4.46}$$

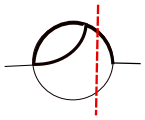

$$= \quad \int d\Phi_2\,\mathrm{Bub}(s_{12})$$

$$\overset{\lim z\to 1}{=} \int_0^1 \frac{1}{8\pi}\frac{(4\pi)^\epsilon}{\Gamma(1-\epsilon)}s^{-\epsilon}(1-z)^{1-2\epsilon}[\lambda(1-\lambda)]^{-\epsilon}d\lambda\times\frac{\Gamma(1+\epsilon)}{(2\pi)^2(4\pi)^{-\epsilon}}$$

$$\times(\frac{3}{4})^{\frac{1-2\epsilon}{2}}\,{}_2F_1(\frac{3-\epsilon}{2},\frac{1}{2},\frac{3}{2},-\frac{1}{4})$$

$$= \quad 2^{-7+4\epsilon}\pi^{-3+2\epsilon}s^{-\epsilon}(1-z)^{1-2\epsilon}\frac{\Gamma(1-\epsilon)\Gamma(1+\epsilon)}{4\Gamma(2-2\epsilon)}\times$$

$$\times(\frac{3}{4})^{\frac{1-2\epsilon}{2}}\,{}_2F_1(\frac{3-\epsilon}{2},\frac{1}{2},\frac{3}{2},-\frac{1}{4}). \tag{4.47}$$

Chapter 5

Differential Equations and Solution

In the last chapter we have shown all the MIs. The MIs with one massive propagator have been calculated in [61]. The MIs with more massive propagators are still unknown. In this chapter, we first present the MIs of every group, ordering them in a "pyramid" in which at the base there are the masters with the smallest number of denominators and on the top the ones with up to 7 denominators. We are free to choose them at our wish. The point that matters is the complexity of the system of differential equations derived. Moreover, when the linear differential equations are introduced to solve the MIs, one should start from the bottom to the top of the pyramid. Usually we call the MIs appearing in the bottom of the pyramid as "base" master integrals.

It is important to note that the entire reduction of diagrams to the independent topologies and finally to the MIs is done in a completely mechanical way. This is crucial, because of the number of equation involved. It would be impossible to perform the calculation by hand. Then next step is to calculate the MIs. The base MIs stay in the bottom of the pyramid and they have to be integrated firstly. Some of the base MIs should be integrated directly, since the corresponding differential equations are homogeneous. After we have the result of the base MIs, which are expressed in Laurent series of $(D-4)$ with the coefficients of the series expressed in terms of harmonic polylogarithms, we solve the MIs with more denominators, using the linear differential equations and the appropriate initial conditions. Higher-order differential equations can be created to handle the entangled MIs. However, a good strategy consists in finding a base of masters which triangularizes the system of first order linear differential equations in $(D-4)$. This strategy was considered during all the calculations.

Table 5.1: MIs for the 3-cut diagrams

Topology t	Master integrals
7	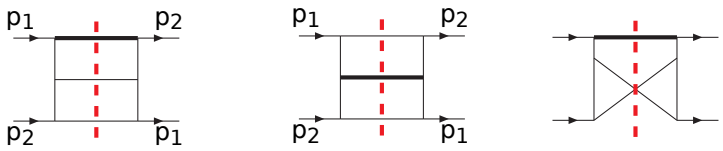
6	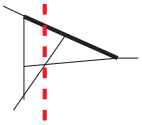
5	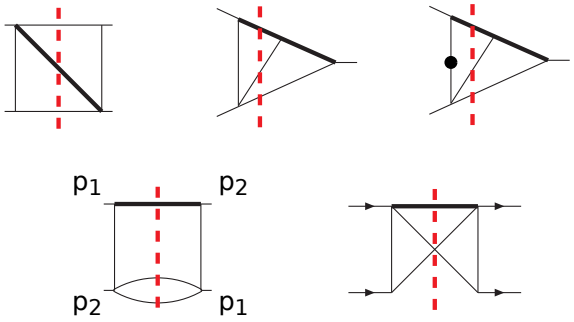
3	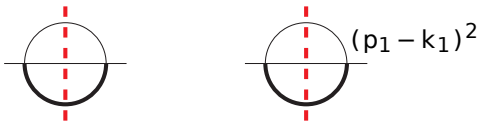

5.1 The calculation of Master integrals with 3 cuts

We present the MIs for the pyramid of the 3-cut diagrams in Table 5.1. The calculation will start from the bottom of the table: from the masters with three denominators. These base MIs appear as a sub-topology in the non-homogenous part of the linear differential equations of the MIs with four denominators, and so on.

5.1.1 The solution of the base Master integrals with 3 cuts

In order to integrate the base MIs we use the optical theorem. The optical theorem relates the imaginary part of a loop diagram to the sum over all its cuts in the form of a unitarity relation. For instance, for vacuum polarization diagrams, the following

unitarity relation holds:

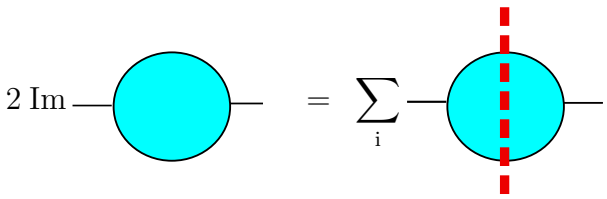

(5.1)

where the i enumerates all possible ways to cut this diagram into two connected amplitudes under the condition that the final state resulting from the cut lines belong to physical processes.

We illustrate the application of the method on the derivation of the base MI. The unitarity relation relevant to the base MIs reads pictorially:

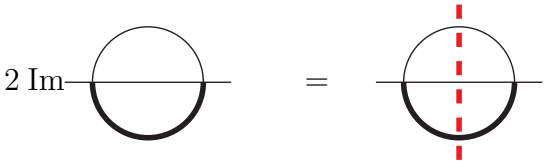

(5.2)

The full expression of MI in the left side of the Eq. (5.2) in D dimensions can be easily computed using Feynman parameters. We find:

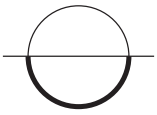

$$
\begin{aligned}
&= \mu^{2(4-D)} \int \frac{d^D k_1}{(2\pi)^D} \frac{d^D k_2}{(2\pi)^D} \frac{1}{(k_1^2+m^2) k_2^2 (p-k_1-k_2)^2} \\
&= (2\pi)^{-4} \frac{C^2(D) a^2}{4(D-4)^2} \left(\frac{a^2}{\mu^2}\right)^{D-4} \frac{\Gamma(3-D)\Gamma^2(\frac{D-2}{2})}{\Gamma(\frac{D}{2})\Gamma(\frac{4-D}{2})} \\
&\quad \times {}_2F_1(3-D, \frac{4-D}{2}; \frac{D}{2}; \frac{s}{a^2})
\end{aligned}
\tag{5.3}
$$

where a is the mass of the W or Z boson, and p the incoming momentum, $s = -(p_1+p_2)^2$. $C(D)$ is the following function of the dimension D :

$$
C(D) = (4\pi)^{\frac{(4-D)}{2}} \Gamma(3-\frac{D}{2}). \tag{5.4}
$$

The function $C(D)$ is an overall multiplicative term and it appears in each 1-loop diagram. Let us remember that, after the renormalization procedure, in the final physical quantities all singular terms in $\frac{1}{(D-4)}$ cancel out, so that one could take simply the $D \to 4$ limit of $C(D)$:

$$
\lim_{D\to 4} C(D) = 1. \tag{5.5}
$$

However, in intermediate states of the calculation it is better to keep the overall term, that has a non trivial D dependence.

Note that the integrals depend on a and s and we can express the master integrals in term of the dimensionless ratio $z = a^2/s$. We transformed the hypergeometric function of $1/z$ in a combination of hypergeometric functions of z:

$$\begin{aligned} {}_2F_1(A_1, A_2, B_1; z) &= \frac{\Gamma(B_1)\Gamma(A_2 - A_1)}{\Gamma(A_2)\Gamma(B_1 - A_1)}(-z)_2^{-A_1} F_1(A_1, A_1 + 1 - B_1; A_1 + 1 - A_2; \frac{1}{z}) \\ &+ \frac{\Gamma(B_1)\Gamma(A_1 - A_2)}{\Gamma(A_1)\Gamma(B_1 - A_2)}(-z)_2^{-A_2} F_1(A_2, A_2 + 1 - B_1; A_2 + 1 - A_1; \frac{1}{z}). \end{aligned} \tag{5.6}$$

Since in any case we will need to extract the behavior at the threshold of the different integrals (to cure the soft divergences), we start already with the example of the sunrise. Note that the behavior at $z \to 0$ (asymptotic behavior) is not important in this case, since the integration in z for the hadronic cross section will go from $z = 1$ to the (finite) collider energy. Using the relevant Kummer relation for the hypergeometric function

$${}_2F_1(A_1, A_2, B_1; z) = (1 - z)^{B_1 - A_1 - A_2}\, {}_2F_1(B_1 - A_1, B_1 - A_2, B_1, z), \tag{5.7}$$

we find:

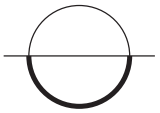

$$\begin{aligned} &= (2\pi)^{-4}\frac{(4\pi)^{2\epsilon}}{16\epsilon^2}a^2\left(\frac{a^2}{\mu^2}\right)(1 - z)^{3-4\epsilon}\Bigg\{ \\ &-\epsilon^2\frac{\Gamma(-1 + 2\epsilon)\Gamma(1 - \epsilon)^3}{\Gamma(3 - 3\epsilon)}z^{-1+2\epsilon}(-1 + i\lambda)^{2\epsilon}\, {}_2F_1(1 - \epsilon, 2 - 2\epsilon, \epsilon; z) \\ &+\epsilon\frac{\Gamma(1 + \epsilon)\Gamma(1 - \epsilon)^2\Gamma(-1 + \epsilon)}{\Gamma(2 - 2\epsilon)}z^{\epsilon}(-1 + \lambda)^{\epsilon}\times \\ &\times {}_2F_1(2 - 2\epsilon, 3 - 3\epsilon, 2 - \epsilon; z)\Bigg\} \end{aligned} \tag{5.8}$$

Using the following relations for the imaginary part,

$$\begin{aligned} Im\Big\{(-1 + i\lambda)^{-n\epsilon}\Gamma(1 + n\epsilon)\Gamma(1 - n\epsilon)\Big\} &= -\pi, \\ Im\Big\{(-1 + i\lambda)^{n\epsilon}\Gamma(1 + n\epsilon)\Gamma(1 - n\epsilon)\Big\} &= \pi, \\ Im\Big\{(-1 - i\lambda)^{-n\epsilon}\Gamma(1 + n\epsilon)\Gamma(1 - n\epsilon)\Big\} &= \pi, \\ Im\Big\{(-1 - i\lambda)^{n\epsilon}\Gamma(1 + n\epsilon)\Gamma(1 - n\epsilon)\Big\} &= -\pi, \end{aligned} \tag{5.9}$$

the base MI can be evaluated by extracting the imaginary part of the virtual loop integration

$$= \mu^{2(4-D)} \int \frac{d^D k_1 d^D k_2}{(2\pi)^{2D}} \delta((k_1-k_2)^2-a^2)\delta((k_2+p)^2)\delta(k_1^2)$$

$$= \mathcal{N} a^2 [z^{-1+2\epsilon} \frac{-2\Gamma^3(1-\epsilon)\Gamma(-1+2\epsilon)}{\epsilon\Gamma^2(\epsilon)\Gamma(3-3\epsilon)\Gamma(1+2\epsilon)\Gamma(1-2\epsilon)}$$

$$\times (1-z)^{3-4\epsilon}\, {}_2F_1(1-\epsilon, 2-2\epsilon; \epsilon; z)$$

$$+ z^{\epsilon} \frac{\Gamma(-1+\epsilon)\Gamma(1-\epsilon)}{\epsilon\Gamma(2-2\epsilon)\Gamma(1+\epsilon)\Gamma(\epsilon)} (1-z)^{3-4\epsilon}\, {}_2F_1(3-3\epsilon, 2-2\epsilon; 2-\epsilon; z)]$$

$$= \mathcal{N} a^2 [z^{-1+2\epsilon} \frac{\Gamma^3(1-\epsilon)}{\epsilon^2\Gamma^2(\epsilon)\Gamma(3-3\epsilon)\Gamma(2-2\epsilon)}$$

$$\times (1-z)^{3-4\epsilon}\, {}_2F_1(1-\epsilon, 2-2\epsilon; \epsilon; z)$$

$$+ z^{\epsilon} \frac{\Gamma(-1+\epsilon)\Gamma(1-\epsilon)}{\epsilon\Gamma(2-2\epsilon)\Gamma(1+\epsilon)\Gamma(\epsilon)} (1-z)^{3-4\epsilon}\, {}_2F_1(3-3\epsilon, 2-2\epsilon; 2-\epsilon; z)] \tag{5.10}$$

where the $\mathcal{N}$ is a normalization factor:

$$\mathcal{N} = C^2(D)(\frac{a^2}{\mu^2})^{D-4}(2\pi)^{-4} = 2^{-7+4\epsilon}\pi^{-3+2\epsilon}\Gamma^2(1+\epsilon)(\frac{a^2}{\mu^2})^{D-4}. \tag{5.11}$$

It is important to extract the $(1-z)^{3-4\epsilon}$ part, because when we consider the total cross section, the power of the $(1-z)$ can become negative which means this term will contribute to the infrared divergences. The hypergeometric function, instead, can be expanded in ϵ and the coefficients of such an expansion will be expressed in terms of Harmonic Polylogarithms (HPLs) .

To explain how the system of differential equation for the MIs is obtain, let us consider a two-loop scalar integral with a single W/Z boson propagator

$$\mathcal{F}_i(p^2, a^2) = \int \frac{d^D k}{(2\pi)^{(D-2)}} \frac{d^D l}{(2\pi)^{(D-2)}} \frac{1}{[k^2-a^2]^v D_1^{m_1} \cdots D_t^{m_t}}. \tag{5.12}$$

By differentiating with respect to a^2, we obtain:

$$\frac{\partial \mathcal{F}_i(p^2, a^2)}{\partial a^2} = -v \int \frac{d^D k}{(2\pi)^{(D-2)}} \frac{d^D l}{(2\pi)^{(D-2)}} \frac{1}{[k^2-a^2]^{v+1} D_1^{m_1} \cdots D_t^{m_t}}. \tag{5.13}$$

Using all the identity relations (IBPs, LI, Sym), we can construct the last equation in terms of the master intergrals $\mathcal{F}_i$,

$$\frac{\partial \mathcal{F}_i(p^2, a^2)}{\partial a^2} = \sum_j c_{ij} \mathcal{F}_j + \Omega_i, \tag{5.14}$$

where Ω_i contain the integrals of the sub-topologies to be considered known. These differential equation can be solved up to a constant in terms of logarithm and generalized Harmonic polylogarithms, order by order in $(D-4)$. This constant is obtained by evaluating the master integrals at a specific kinematic point. An example is shown below.

$$\frac{\partial}{\partial z}$$  $$= \mathcal{F}_1(z,D)$$  $$+ \mathcal{F}_2(z,D)$$  $$+ \mathcal{F}_3(z,D)$$ 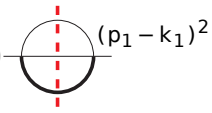

(5.15)

We compute the value of the integral at a specific kinematic point in order to determine the constant. A convenient choice is the threshold for W or Z boson, $z = 1$, where the hard part of the integral vanishes. When we do the limit $z \to 1$, if there is not infrared divergence in the soft limit, this MI will go to zero directly, for example:

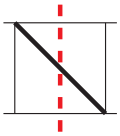 $$(z = 1) \quad = \quad 0\,.$$ (5.16)

5.2 The calculation of the MIs with 2 cuts

In this section, the pyramids for the 2-cut diagrams with a different number of massive propagators will be presented. The same technique was applied as the one for the 3-cut MIs. The greater difficulties come out from the MIs with 2 massive propagators, and in particular from the masters with 3 massive propagators. The solution of the fourfold entangled MIs with 3 massive propagators is a big challenge.

5.2.1 The calculation of the MIs with one massive propagator

The pyramid of 2-cut MIs with one massive propagator is shown in Table 5.2. There are three base MIs in the topology $t = 4$. All of them can be calculated directly using the optical theorem and the results of the virtual diagrams. The first two MIs are combinations of the one-loop massless bubble integral and the two-body phase-space integral. These two MIs can be evaluated directly by extracting the imaginary part from the cut-diagram and the real part from the remaining one-loop integral. The differential equation of virtual MI corresponding to the last real MI in topology $t = 4$ will be generated. After solving the differential equation, the result of real MI can be extracted with that technique. The result of virtual one-loop bubble with one massive propagator is as follows:

 $$= \mu^{2(4-D)} \int \frac{d^D k}{(2\pi)^D} \frac{1}{(k^2 - a^2)(k-p)^2}$$

Table 5.2: MIs for pyramid of 2-cut diagrams with one massive propagator

Topology t	Master integrals
7	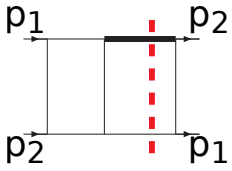
5	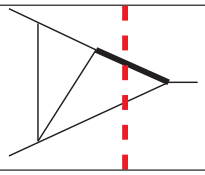
4	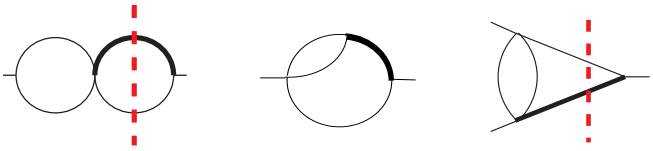

$$
\begin{aligned}
&= (2\pi)^{-2}\frac{C(D)}{(2\pi)^4}(\frac{a^2}{\mu^2})^{-\epsilon}(-z)^{-1+2\epsilon}(1-z)^{1-2\epsilon}\times \\
&\quad \times {}_2F_1(2-2\epsilon,1-\epsilon;2-\epsilon;\frac{1}{z}) \\
&= \frac{C(D)}{(2\pi)^2}(\frac{a^2}{\mu^2})^{-\epsilon}(1-z)^{1-2\epsilon}\Big\{z\frac{\Gamma(1+\epsilon)}{\epsilon(1-\epsilon)}{}_2F_1(2-2\epsilon,1-\epsilon,2-\epsilon;z)\times \\
&\quad \times\Big[(-1+i\lambda)^{\epsilon}\Gamma(1+\epsilon)\Gamma(1-\epsilon)\frac{1}{\epsilon}\Big]\frac{\Gamma(1-\epsilon)}{2-2\epsilon}z^{\epsilon}\Big\}. \qquad (5.17)
\end{aligned}
$$

Using the Eq. (5.9), we have:

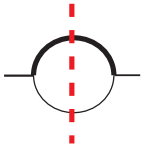

$$= \frac{C(D)}{(2\pi)^2}(\frac{a^2}{\mu^2})^{-\epsilon}[z^{\epsilon}(1-z)^{1-2\epsilon}\frac{\pi\Gamma(2-\epsilon)}{2(1-\epsilon)\Gamma(2-2\epsilon)\Gamma(1+\epsilon)}]. \qquad (5.18)$$

The result for the one-loop massless bubble is

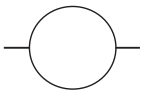

$$
\begin{aligned}
&= \mu^{2(4-D)}\int\frac{d^Dk}{(2\pi)^D}\frac{1}{k^2(k-p)^2} \\
&= -(2\pi)^{-2}\frac{C(D)}{2(D-4)}\frac{\Gamma^2(1-\epsilon)}{\Gamma(2-2\epsilon)}(-\frac{s}{\mu^2})^{-\epsilon}. \qquad (5.19)
\end{aligned}
$$

Taking the real part of the Eq. (5.19) and combining with Eq. (5.18), we have

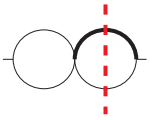

$$= \mu^{2(4-D)} \int \frac{d^D k_1 d^D k_2}{(2\pi)^{2D}} \frac{\delta(k_2^2 - a^2)\delta((k_2+p))^2}{k_1^2 (k_1+p)^2}$$

$$= \mathcal{N}[z^{2\epsilon}(1-z)^{1-2\epsilon} \frac{\Gamma^2(1-\epsilon)\Gamma(2-\epsilon)}{\epsilon(1-\epsilon)\Gamma^2(2-2\epsilon)\Gamma(1+\epsilon)} \mathrm{Re}(\mathrm{e}^{\mathrm{i}\pi\epsilon})]. \tag{5.20}$$

We found that the difference between the first two diagrams of topology $t = 4$ in Table 5.2 is the incoming momenta of the virtual part. So we can easily get the result of the second MI,

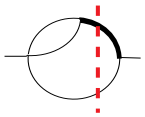

$$= \mu^{2(4-D)} \int \frac{d^D k_1 d^D k_2}{(2\pi)^{2D}} \frac{\delta(k_2^2 - a^2)\delta((k_2+p))^2}{k_1^2 (k_1+k_2)^2}$$

$$= \mathcal{N}[z^{\epsilon}(1-z)^{1-2\epsilon} \frac{\Gamma^2(1-\epsilon)\Gamma(2-\epsilon)}{\epsilon(1-\epsilon)\Gamma^2(2-2\epsilon)\Gamma(1+\epsilon)} \mathrm{Re}(\mathrm{e}^{\mathrm{i}\pi\epsilon})] \tag{5.21}$$

In order to use the same technique to calculate the last base MI extracting the imaginary part from the virtual diagram, we present the differential equation in Eq. (5.22). The result can be expressed in terms of an hypergeometric function.

$$\frac{\partial}{\partial p^2}$$ 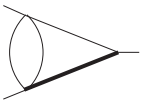

$$= (-\frac{D-2}{2p^2} + \frac{3D-10}{2(p^2-a^2)})$$ 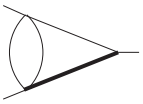

$$+\frac{1}{a^2}(-\frac{D-2}{2p^2} + \frac{D-2}{2(p^2-a^2)})$$ 

(5.22)

We choose $p^2 = 0$ as a regular point to constrain the integration constant:

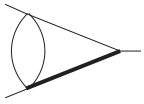

$$= -\frac{1}{a^2}(1-\frac{p^2}{a^2})^{1-3\epsilon}\, {}_2F_1(2-3\epsilon, 1-\epsilon; 2-\epsilon, \frac{p^2}{a^2})$$ 

(5.23)

The 2-loop tadpole with one massive propagator is known. Changing the variable to z, we find

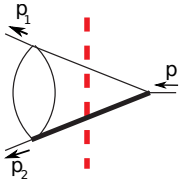

$$= \mu^{2(4-D)} \int \frac{d^D k_1 d^D k_2}{(2\pi)^{2D}} \frac{\delta(k_2^2 - a^2)\delta(k_2+p)^2}{k_1^2 (p_2+k_2-k_1)^2}$$

$$= \mathcal{N}[-z^{2\epsilon}(1-z)^{1-3\epsilon} \frac{2\Gamma(-1+2\epsilon)\Gamma^2(1-\epsilon)}{\epsilon\Gamma(2-3\epsilon)\Gamma(\epsilon)\Gamma(1+2\epsilon)}]. \tag{5.24}$$

$\mathcal{N}$ is the normalization factor defined in Eq. (5.11). Before starting to calculate the topologies with a bigger number of denominators, all the hypegeometric functions will be expanded in ϵ.

5.2.2 The calculation of the MIs with two massive propagators

Let us first have a look to the pyramid of the 2-cut MIs with two massive propagators. On the bottom of the pyramid, there is only one base diagram that will appear as sub-topology in the differential equation of other topologies. It should be taken into account first. It is easy to present the result of the following two MIs,

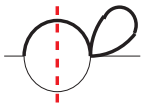

$$= \mu^{2(4-D)} \int \frac{d^D k_1 d^D k_2}{(2\pi)^{2D}} \frac{\delta(k_2^2-a^2)\delta(k_2+p)^2}{k_1^2-a^2}$$

$$= \mathcal{N} a^2 [-z^\epsilon (1-z)^{1-2\epsilon} \frac{\Gamma(2-\epsilon)}{\epsilon(1-\epsilon)^2\Gamma(2-2\epsilon)\Gamma(1+\epsilon)}], \tag{5.25}$$

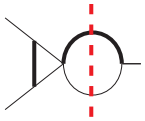

$$= \mu^{2(4-D)} \int \frac{d^D k_1 d^D k_2}{(2\pi)^{2D}} \frac{\delta(k_2^2-a^2)\delta(k_2+p)^2}{(k_1^2-a^2)(p_1-k_1)^2(p_2+k_1)^2}$$

$$= \mathcal{N} [z^\epsilon (1-z)^{1-2\epsilon} \frac{\Gamma(2-\epsilon)}{\epsilon(1-\epsilon)\Gamma(2-2\epsilon)\Gamma(1+\epsilon)}] \times$$

$$\times [-\frac{1}{4} a^{-2} z (H(0,0,z) - H(1,0,z) - \frac{3\zeta(2)}{2}) + \mathcal{O}(\epsilon)]. \tag{5.26}$$

5.2.3 The calculation of the MIs with three massive propagators

First we list the result of the one-loop bubble with two massive propagators:

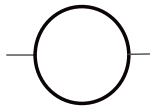

$$= \mu^{(4-D)} \int \frac{d^D k_1}{(2\pi)^D} \frac{1}{(k_1^2-a^2)((k_1+p)^2-a^2)}$$

$$= 2^{-4+2\epsilon} \pi^{-2+\epsilon} \frac{\Gamma(1+\epsilon)}{\epsilon} (1-\frac{s}{4a^2})^{\frac{1-2\epsilon}{2}} {}_2F_1(\frac{3-\epsilon}{2}, \frac{1}{2}, \frac{3}{2}, -\frac{s}{4a^2}). \tag{5.27}$$

Then we present the result of the base MI which has to be calculated directly,

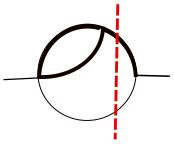

$$= \mu^{2(4-D)} \int \frac{d^D k_1 d^D k_2}{(2\pi)^{2D}} \frac{\delta((k_2^2-a^2)\delta(k_2+p)^2}{(k_1+k_2)^2-a^2)(k_1^2-a^2)}$$

$$= \mathcal{N} [z^\epsilon (1-z)^{1-2\epsilon} \frac{\Gamma(2-\epsilon)}{\epsilon(1-\epsilon)\Gamma(2-2\epsilon)\Gamma(1+\epsilon)}] \times$$

$$\times (\frac{3}{4})^{\frac{1-2\epsilon}{2}} {}_2F_1(\frac{3-\epsilon}{2}, \frac{1}{2}, \frac{3}{2}, -\frac{1}{4}). \tag{5.28}$$

5.3 Differential equation and solution of the MIs

In the last section the base MIs were calculated by extracting the imaginary part from the virtual result. We will illustrate, in this section, how to use the differential equations to solve the MIs with the results of base MIs and constrain the integral constants order by order in $(D-4)$.

First let us take a simple example as shown in Eq. (5.15). Since this master integral has no infrared divergences, when we use the initial conditions Eq. (5.16) this forces all the pieces to go to zero. Then the integral constants can be easily constrained. For more complicated MIs, which have an infrared soft divergence, the situation is more complicated. In particular, the behaviour of the integral in the limit $z \to 1$ has to be extracted in D dimensions. We consider the MI in Eq. (4.33). The differential equation is:

$$\frac{\partial}{\partial z}$$ 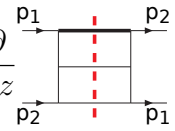

$$= \left[\frac{7-d}{z} + \frac{5-d}{1-z}\right]$$ 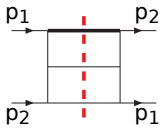

$$+ \left[\frac{2(3-d)}{1-z} + \frac{2(3-d)}{(1-z)^2}\right]\frac{1}{a^4}$$ 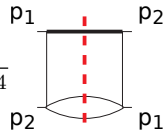

$$+ \left[(d-6) + \frac{48-72d}{(1-z)} + \frac{228d-132}{(1-z)^2} + \cdots\right]\frac{1}{a^{10}}$$ 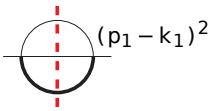

$$+ \left[4(d-1) + \frac{68-76d}{(1-z)} + \frac{268d-244}{(1-z)^2} + \cdots\right]\frac{1}{a^8}$$ 
(5.29)

Therefore, we have:

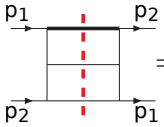

$$= z^3(1-z)^{-1-2\epsilon}\left(C + \int^z dt\; t^{-3}(1-t)^{1+2\epsilon}\times\right.$$
$$\times\left[\frac{2(3-d)}{1-t} + \frac{2(3-d)}{(1-t)^2}\right]\frac{1}{a^4}$$ 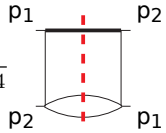

$$+ \int^z dt\; t^{-3}(1-t)^{1+2\epsilon}\times$$
$$\left.\times\left[4(d-1) + \frac{68-76d}{(1-t)} + \cdots + \frac{268d-244}{(1-t)^2} + \cdots\right]\frac{1}{a^8}\right.$$ 

$$+\int^z dt\; t^{-3}(1-t)^{1+2\epsilon}\times$$

$$\times\left[(d-6)+\frac{48-72d}{(1-t)}+\frac{228d-132}{(1-t)^2}+\cdots\right]\frac{1}{a^{10}}$$  $$\Big). \quad (5.30)$$

Inserting the result of the MIs of the sub-topologies into Eq. (5.30), the integrations will be calculated order by order, so everything will be expended in ϵ. Before doing the expansion in ϵ, we have to pay attention to some terms. For example, there is a term $\int^z (1-t)^{-1-2\epsilon} H(1,0,t)dt$ in the zeroth order. Integrating by part, we obtain:

$$\begin{aligned}\int^z (1-t)^{-1-2\epsilon} H(1,0,t)dt &= \frac{1}{2\epsilon}\Big((1-z)^{-2\epsilon}H(1,0,z)\\ &\quad -\int^z (1-t)^{-1-2\epsilon}H(0,z)dt\Big) \qquad (5.31)\end{aligned}$$

It can seem that this integration gives a pole which will be affect the previous order in ϵ. However, if we finish the integration and expand $(1-z)^{-2\epsilon}$ in ϵ, we find

$$\begin{aligned}\int^z (1-t)^{-1-2\epsilon} H(1,0,t)dt &= \frac{1}{2\epsilon}\Big((1-z)^{-2\epsilon}H(1,0,z) - H(1,0,z)\\ &\quad +2\epsilon(H(1,0,z)+H(0,1,z))+\mathcal{O}(\epsilon^2)\Big)\\ &= H(1,0,z)+H(0,1,z)+C+\mathcal{O}(\epsilon), \qquad (5.32)\end{aligned}$$

where C is the integral constant. We can treat in a similar way the terms $\int^z (1-t)^{-1-2\epsilon}H(1,1,0,t)dt$, $\int^z (1-t)^{-1-2\epsilon}H(1,1,1,0,t)dt$, etc. This kind of integrations has no contribution to the previous orders in ϵ, and therefore we can expand the terms $(1-t)^{-1-2\epsilon}$ directly from the beginning. A term like $\int^z (1-t)^{-1-2\epsilon}H(1,t)dt$, however, will affect the previous order in ϵ

$$\int^z (1-t)^{-1-2\epsilon}H(1,t)dt = \frac{1}{2\epsilon}\Big((1-z)^{-2\epsilon}H(1,z)-\frac{1}{2\epsilon}(1-z)^{-2\epsilon}+C\Big) \qquad (5.33)$$

This term belongs to the soft part and we can also expand it at the beginning, since the integration constants of the soft part can be constrained by the results of the soft limits.

Now we present the most complicated case with two massive propagators, the three entangled MIs. The system of differential equations is the following:

$$\frac{\partial}{\partial z}$$ 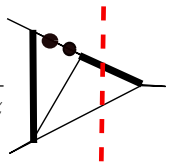 $$= \left[\frac{1}{z} + [d-4](\frac{1}{[1-z]^2} + \frac{7}{2[1-z]} + \frac{1}{[1+z]})\right]$$ 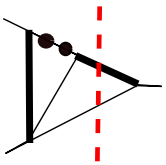

$$+\frac{[d-4]}{a^4}\left[-\frac{1}{2[1-z]^2} + \frac{7}{4[1-z]} - \frac{1}{4[1+z]}\right]$$ 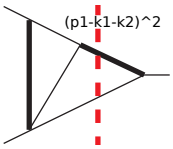

$$+\frac{[d-4]}{a^6}\left[-\frac{1}{2[1-z]^2} + \frac{7}{4[1-z]} - \frac{1}{4[1+z]}\right]$$ 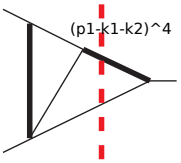

$$+a^{-4}\left[\frac{1}{[d-4]^2}\frac{16}{9z} + \frac{1}{[d-4]}(\frac{17}{9[1-z]} + \frac{19}{3[1+z]} + \cdots\right.$$
$$\left.-\frac{8}{9[1-z]^3} + \frac{3}{4(1-z)^2} + \cdots + \mathcal{O}(\epsilon)\right] \tag{5.34}$$

$$\frac{\partial}{\partial z}$$ 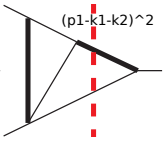

$$= \left[\frac{1}{z} - 2[d-4](\frac{1}{[1-z]^2} + \frac{9}{2[1-z]} - \frac{2}{[1+z]})\right]$$ 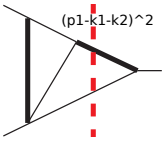

$$+a^{-2}\left[-\frac{2[d-4]}{[1-z]^2} - \frac{2}{[1-z]} + \frac{3[d-4]}{2[1+z]}\right]$$ 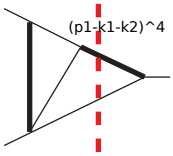

$$+a^4\left[\frac{4[d-4]}{[1-z]^2} + \frac{4}{[1-z]} - \frac{2[d-4]}{[1+z]}\right]$$ 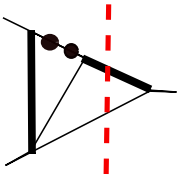

$$+\left[-\frac{1}{[d-4]^2}\frac{32}{3z} - \frac{4}{3[d-4]} + \frac{16}{[1+z]} + \frac{16H(0,z)}{3[1-z]^2} + \cdots\right.$$
$$\left.-\frac{15}{2} - \frac{4}{3[1-z]^2} + \frac{16}{3z^2} + \cdots + \mathcal{O}(\epsilon)\right] \tag{5.35}$$

$$\frac{\partial}{\partial z}$$ 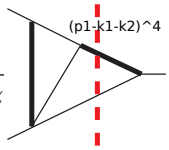

$$= \left[-\frac{2[d-4]}{[1-z]} - \frac{1}{z}\right]$$ 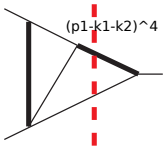

$$+a^2\Bigg[-\frac{2[d-4]}{[1-z]^2}-\frac{2}{[1-z]}+\frac{3[d-4]}{2[1+z]}\Bigg]$$

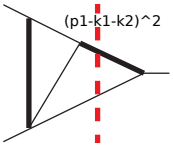

$$+a^6\Bigg[-\frac{2[d-4]}{[1-z]}-\frac{2}{z}-\frac{3[d-4]}{z}\Bigg]$$

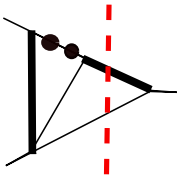

$$+a^2\Bigg[-\frac{1}{[d-4]^2}\frac{64}{3z}+\frac{32}{3[d-4]}\frac{1}{[1-z]}+\frac{16}{[1+z]}+\frac{32H(0,z)}{3[1-z]^2}+\cdots$$
$$+\frac{15}{2}+\frac{32}{3[1-z]^2}+\frac{67}{6z^2}+\cdots+\mathcal{O}(\epsilon)\Bigg], \tag{5.36}$$

where the dots in the equations stand for the remaining terms of zero oder in ϵ, the two dots on the propagator mean that the propagator is rased to power 3 and the two labels $(p_1-k_1-k_2)^2$ and $(p_1-k_1-k_2)^4$ appearing in the equations mean that the corresponding quantity is on the numerator of the scalar MI. The differential equation for the last MI is similar to Eq. (5.35). From Eq. (5.34), we can see that there is a coefficient $[d-4]$ for every entangled MIs which appear in the non-homogenous part. We choose these bases so that the MI with two dots decouples, order by order in ϵ, from the other two. The solution of the system can be therefore found order-by-order in ϵ solving a first-order linear differential equation and subsequently a second-order linear differential equation.

5.4 The calculation of the real corrections

We use the Laporta algorithm for the reduction of the dimensionally regularized scalar integrals to the set of MIs. Then the differential equations method [60] for their analytic evaluation. The integral constants are constrained by the initial condition and soft limit. In this section, we show the results of the MIs.

5.4.1 Results of the 3-cut MIs

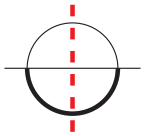

$$= \mu^{2(4-D)}\int\frac{d^Dk_1d^Dk_2}{(2\pi)^{2D}}\delta((k_1-k_2)^2-a^2)\delta(k_2+p)^2)\delta(k_1^2)$$
$$=\mathcal{N}a^2(1-z)^{-4\epsilon}\Bigg\{\Bigg(+\frac{1}{2z}-\frac{z}{2}+H(0,z)\Bigg)$$

$$
\begin{aligned}
&-2\epsilon\Bigg(-\frac{13}{8z}+\frac{13z}{8}-\frac{3H(0,z)}{2}-\frac{H(0,z)}{2z}+\frac{3zH(0,z)}{4}-\frac{3H(0,0,z)}{2}\\
&\qquad +2H(1,0,z)+2\zeta(2)\Bigg)\\
&+4\epsilon^2\Bigg(+\frac{115}{32z}-\frac{115z}{32}+\frac{3H(0,z)}{2}+\frac{13H(0,z)}{8z}-\frac{39zH(0,z)}{16}\\
&\qquad -\frac{5\zeta(2)H(0,z)}{2}+\frac{9H(0,0,z)}{4}+\frac{H(0,0,z)}{2z}-\frac{7zH(0,0,z)}{8}\\
&\qquad +\frac{7H(0,0,0,z)}{4}-\frac{H(0,1,0,z)}{2}+4\zeta(2)H(1,z)-3H(1,0,z)\\
&\qquad +\frac{H(1,0,z)}{4z}+\frac{zH(1,0,z)}{4}-3H(1,0,z)+4H(1,1,0,z)-3\zeta(2)\\
&\qquad -\frac{3\zeta(2)}{4z}+\frac{5\zeta(2)z}{4}-2\zeta(3)]+\mathcal{O}(\epsilon^3)\Bigg)\Bigg\}
\end{aligned}
\tag{5.37}
$$

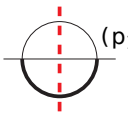

$$
\begin{aligned}
&= \mu^{2(4-D)}\int \frac{d^Dk_1d^Dk_2(p_1-k_1)^2\delta((k_1-k_2)^2-a^2)\delta(k_2+p)^2)\delta(k_1^2)}{(2\pi)^{2D}}\\
&=\mathcal{N}a^4(1-z)^{-4\epsilon}\Bigg\{ +\frac{1}{2}+\frac{1}{6z^2}-\frac{1}{z}+\frac{z}{3}-H(0,z)\\
&\qquad -2\epsilon\Bigg(-\frac{35}{24}-\frac{13}{24z^2}+\frac{37}{12z}-\frac{13z}{12}+\frac{3H(0,z)}{4}-\frac{H(0,z)}{6z^2}+\frac{H(0,z)}{z}-\frac{H(0,z)z}{2}\\
&\qquad\qquad +\frac{3H(0,0,z)}{2}-2H(1,0,z)-2\zeta(2)\Bigg)\\
&\qquad +4\epsilon^2\Bigg(+\frac{95}{32}+\frac{115}{96z^2}-\frac{105}{16z}+\frac{115z}{48}+\frac{29H(0,z)}{48}+\frac{13H(0,z)}{24z^2}-\frac{19H(0,z)}{6z}\\
&\qquad\qquad +\frac{13zH(0,z)}{8}+\frac{5H(0,z)\zeta(2)}{2}-\frac{11H(0,0,z)}{8}+\frac{H(0,0,z)}{6z^2}\\
&\qquad\qquad -\frac{H(0,0,z)}{z}+\frac{7zH(0,0,z)}{12}-\frac{7H(0,0,0,z)}{4}+\frac{H(0,1,0,z)}{2}\\
&\qquad\qquad -4\zeta(2)H(1,z)\Bigg)+\mathcal{O}(\epsilon^3)\Bigg\}
\end{aligned}
\tag{5.38}
$$

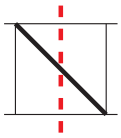

$$= \mu^{2(4-D)} \int \frac{d^D k_1 d^D k_2 \delta((k_1-k_2)^2-a^2)\delta(k_2+p)^2)\delta(k_1^2)}{(2\pi)^{2D}(p_1-k_1-k_2)^2(p_2-k_2)^2}$$

$$= \mathcal{N} a^{-2}\Bigg\{ -\frac{zH(0,z)}{4\epsilon^2} - \frac{1}{2\epsilon}\Big(4zH(0,0,z)+8zH(0,1,z)-8z\zeta(2)\Big) + 6z\zeta(2)H(0,z)$$
$$-4zH(0,0,0,z) - 8zH(0,0,1,z) - 10zH(0,1,0,z) - 16zH(0,1,1,z)$$
$$+4z\zeta(3) + \mathcal{O}(\epsilon)\Bigg\} \tag{5.39}$$

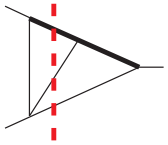

$$= \mu^{2(4-D)} \int \frac{d^D k_1 d^D k_2 \delta(k_1^2-a^2)\delta(p_1+p_2-k_1-k_2)^2)\delta(k_1^2)}{(2\pi)^{2D}(p_1-k_1)^2(k_1+k_2)^2}$$

$$= \mathcal{N} a^{-2} z\Bigg\{ \frac{zH(0,z)}{4\epsilon} - \frac{1}{2\epsilon}\Big(-\frac{H(0,0,z)}{2} - 2H(0,1,z) + 2\zeta(2)\Big)\Big)$$
$$-\frac{\zeta(2)H(0,z)}{2} + \frac{5H(0,0,0,z)}{4} + H(0,0,0,z)$$
$$+\frac{5H(0,1,0,z)}{2} + 4H(0,1,1,z)$$
$$-2\epsilon\Big(\frac{15\zeta(2)H(0,z)}{4} + \frac{9\zeta(2)H(0,0,z)}{4} - \frac{17H(0,0,0,0,z)}{8} - \frac{5H(0,0,0,1,z)}{2}$$
$$-\frac{5H(0,0,1,0,z)}{4} - 2H(0,0,1,1,z) + 4\zeta(2)H(0,1,z) - \frac{17H(0,1,0,0,z)}{4}$$
$$-5H(0,1,0,1,z) - 5H(0,1,1,0,z) - 8H(0,1,1,1,z) + 3\zeta(2)\Big) + \mathcal{O}(\epsilon^3)\Bigg\} \tag{5.40}$$

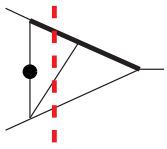

$$= \mu^{2(4-D)} \int \frac{d^D k_1 d^D k_2 \delta(k_1^2-a^2)\delta(p_1+p_2-k_1-k_2)^2)\delta(k_1^2)}{(2\pi)^{2D}(p_1-k_1)^4(k_1+k_2)^2}$$

$$= \mathcal{N} a^{-4} z(1-z)^{-4\epsilon}\Bigg\{ -\frac{H(0,z)}{2\epsilon} - \frac{H(0,0,z)}{2} + 2H(1,0,z) + 2\zeta(2)$$
$$-2\epsilon\Big(-\frac{\zeta(2)H(0,z)}{2} + \frac{H(0,0,0,z)}{4} + \frac{3H(0,1,0,z)}{2} + 4\zeta(2)H(1,z)$$

$$
\begin{aligned}
&-2H(1,0,0,z)+4H(1,1,0,z)+\zeta(3)\Big)\\
&+4\epsilon^2\Big(\frac{\zeta(3)H(0,z)}{4}+\frac{\zeta(2)H(0,0,z)}{4}-\frac{H(0,0,0,0,z)}{8}-\frac{3H(0,0,1,0,z)}{4}\\
&+3\zeta(2)H(0,1,z)-\frac{9H(0,1,0,0,z)}{4}+3H(0,1,1,0,z)-2\zeta(3)H(1,z)\\
&-3\zeta(2)H(1,0,z)+3H(1,0,0,0,z)+H(1,0,1,0,z)+8\zeta(2)H(1,1,z)\\
&-4H(1,1,0,0,z)+8H(1,1,1,0,z)+\frac{3\zeta(2)}{5}+\mathcal{O}(\epsilon^3)\Big\}
\end{aligned}
\tag{5.41}
$$

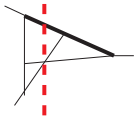

$$
\begin{aligned}
&=\mu^{2(4-D)}\int\frac{d^Dk_1d^Dk_2\delta(k_1^2-a^2)\delta(p_1+p_2-k_1-k_2)^2)\delta(k_1^2)}{(2\pi)^{2D}(p_1-k_1)^2(k_1+k_2)^2(p_2-k_2)^2}\\
&=\mathcal{N}a^{-4}z^2\Big\{+\frac{H(0,z)}{4\epsilon^2}-\frac{1}{2\epsilon}\Big(-9H(0,0,z)-12H(0,1,z)-5H(1,0,z)\Big)\\
&-8\zeta(2)H(0,z)+\frac{27H(0,0,0,z)}{2}+22H(0,0,1,z)+15H(0,1,0,z)+24H(0,1,1,z)\\
&+\frac{9H(1,0,1,z)}{2}+10H(1,0,1,z)+10H(1,1,0,z)+2\zeta(2)\\
&+\frac{C(6,[\,],-2)}{\epsilon^2}+\frac{C(6,[\,],-1)}{\epsilon}+C(6,[\,]0)+\mathcal{O}(\epsilon)\Big\}
\end{aligned}
\tag{5.42}
$$

The following results for the two entangled MIs will be fully determinated by their soft limits. Here we keep the integration constants $C_{(n,[\ ],m)}$, where n refers to the number of MI and m labels the order in ϵ.

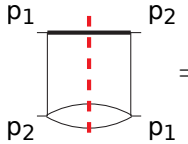

$$
\begin{aligned}
&=\mu^{2(4-D)}\int\frac{d^Dk_1d^Dk_2\delta((k_1-k_2)^2-a^2)\delta(k_2+p)^2)\delta(k_1^2)}{(2\pi)^{2D}(p_2-k_1-k_2)^2(p_1-k_1-k_2)^2}\\
&=\mathcal{N}a^{-2}(1-z)^{-2\epsilon}\Big\{zH(0,0,z)+zH(1,0,z)+z\zeta(2)-2\epsilon\Big(\frac{3zH(0,z)\zeta(2)}{2}\\
&-zH(0,0,z)-2zH(0,0,0,z)+\frac{3zH(0,1,0,z)}{2}+2zH(1,z)\zeta(2)-zH(1,0,z)
\end{aligned}
$$

$$-\frac{3H(1,0,0,z)}{2}+2zH(1,1,0,z)-z\zeta(2)+\frac{5z\zeta(3)}{2}\Bigg)+\mathcal{O}(\epsilon^2)\Bigg\} \tag{5.43}$$

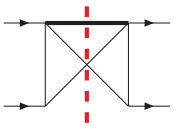

$$= \mu^{2(4-D)}\int\frac{d^Dk_1d^Dk_2\delta((k_1-k_2)^2-a^2)\delta(k_2+p)^2)\delta(k_1^2)}{(2\pi)^{2D}(p_2-k_1-k_2)^2(p_2-k_2)^2}$$

$$\begin{aligned}
&=\mathcal{N}a^{-2}\Bigg\{\frac{zH(0,z)}{\epsilon^2}-\frac{1}{2\epsilon}\Bigg(4zH(0,0,z)-8zH(1,0,z)-8z\zeta(2)\Bigg)\\
&\quad+6zH(0,z)\zeta(2)-4zH(0,0,0,z)-2zH(0,1,0,z)-16zH(1,z)\zeta(2)\\
&\quad+8zH(1,0,0,z)-16zH(1,1,0,z)+19z\zeta(3)\\
&\quad-2\epsilon\Bigg(-5zH(0,z)-6zH(0,0,z)\zeta(2)+4zH(0,0,0,0,z)\\
&\qquad+2zH(0,0,1,0,z)-4zH(0,1,z)\zeta(2)+3zH(0,1,0,0,z)\\
&\qquad-4zH(0,1,1,0,z)+38zH(1,z)\zeta(3)+12zH(1,0,z)\zeta(2)\\
&\qquad-8zH(1,0,0,0,z)-4zH(1,0,1,0,z)-32zH(1,1,z)\zeta(2)\\
&\qquad+16zH(1,1,0,0,z)-32H(1,1,1,0,z)+\frac{6z\zeta(2)}{5}\Bigg)+\mathcal{O}(\epsilon^2)\Bigg\}
\end{aligned} \tag{5.44}$$

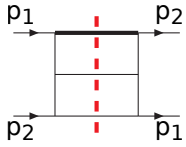

$$= \mu^{2(4-D)}\int\frac{d^Dk_1d^Dk_2\delta((k_1-k_2)^2-a^2)\delta(k_2+p)^2)\delta(k_1^2)}{(2\pi)^{2D}(p_2-k_1-k_2)^2(p_2-k_1)^2(p_1-k_1)^2(p_1-k_1-k_2)^2}$$

$$\begin{aligned}
&=\mathcal{N}z^3(1-z)^{-1-2\epsilon}a^{-6}\Bigg\{-\frac{1}{\epsilon^3}+\frac{8\zeta(2)}{4\epsilon}+20\zeta(3)+\mathcal{O}(\epsilon)\Bigg\}\\
&\quad+\mathcal{N}z^3(1-z)^{-1-2\epsilon}a^{-6}\Bigg\{-\frac{4H(0,z)}{\epsilon^2}-\frac{1}{2\epsilon}\Bigg(+24H(0,0,z)\\
&\qquad+16H(0,1,z)+8H(1,0,z)-8\zeta(2)\Bigg)\\
&\quad+38\zeta(2)H(0,z)-30H(0,0,0,z)-24H(0,0,1,z)-18H(0,1,0,z)
\end{aligned}$$

$$-16H(0,1,1,z)-2\zeta(2)H(0,z)-6H(1,0,0,z)-8H(1,0,1,z)$$

$$-10H(1,1,0,z)+4\zeta(3)+\mathcal{O}(\epsilon)\Big\} \tag{5.45}$$

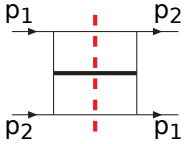

$$= \mu^{2(4-D)}\int\frac{d^Dk_1d^Dk_2\delta((k_1-k_2)^2-a^2)\delta(k_2+p)^2)\delta(k_1^2)}{(2\pi)^{2D}(p_1-k_1-k_2)^2(p_1-k_2)^2(p_2-k_1-k_2)^2(p_2-k_2)^2}$$

$$=\mathcal{N}z^3(1-z)^{-1-2\epsilon}a^{-6}\Big\{-\frac{4}{\epsilon^3}+\frac{32\zeta(2)}{\epsilon}+80\zeta(3)+\mathcal{O}(\epsilon)\Big\}$$

$$+\mathcal{N}z^3(1-z)^{-1-2\epsilon}a^{-6}\Big\{-\frac{10H(0,z)}{\epsilon^2}-\frac{1}{2\epsilon}\Big(40H(0,0,z)$$

$$+40H(0,1,z)+40H(1,0,z)\Big)$$

$$+60\zeta(2)H(0,z)-40H(0,0,0,z)-32H(0,0,1,z)$$

$$-52H(0,1,0,z)-40H(0,1,1,z)-44H(1,0,0,z)$$

$$-40H(1,0,1,z)-40H(1,1,0,z)-28\zeta(3)+\mathcal{O}(\epsilon)\Big\} \tag{5.46}$$

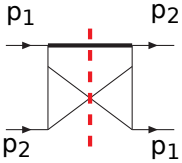

$$= \mu^{2(4-D)}\int\frac{d^Dk_1d^Dk_2\delta((k_1-k_2)^2-a^2)\delta(k_2^2)\delta(k_1^2)}{(2\pi)^{2D}(p_2-k_1)^2(p_2-k_1-k_2)^2(p_1-k_1)^2(p_2-k_2)^2}$$

$$=\mathcal{N}z^3(1-z)^{-1-2\epsilon}a^{-6}\Big\{-\frac{1}{\epsilon^3}+\frac{8\zeta(2)}{\epsilon}+20\zeta(3)+\mathcal{O}(\epsilon)\Big\}$$

$$+\mathcal{N}z^2(1-z)^{-1-2\epsilon}a^{-6}\Big\{-\frac{H(0,z)}{\epsilon^2}-\frac{1}{2}\Big(4H(0,1,z)$$

$$+12H(1,0,z)-8\zeta(2)\Big)$$

$$-2H(0,z)\zeta(2)-10H(0,1,0,z)-4H(0,1,1,z)+2H(1,z)\zeta(2)$$

$$-16H(1,0,0,z)-12H(1,0,1,z)-10H(1,1,0,z)$$

$$+14\zeta(3)+\mathcal{O}(\epsilon)\Big\} \tag{5.47}$$

5.4.2 Results of the 2-cut MIs with one massive propagator

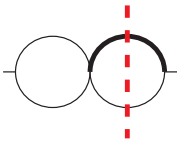

$$= \mu^{2(4-D)}\int \frac{d^Dk_1d^Dk_2}{(2\pi)^{2D}}\frac{\delta(k_2^2-a^2)\delta(k_2+p)^2}{k_1^2(k_1+p)^2}$$

$$\begin{aligned}
&= \mathcal{N}(1-z)^{1-2\epsilon}\Big\{\frac{1}{\epsilon}+4+2H(0,z)\\
&\quad -2\epsilon\Big(-6-4H(0,z)-2H(0,0,z)+3\zeta(2)\Big)\\
&\quad +4\epsilon^2\Big(8+6H(0,z)-3\zeta(2)H(0,z)+4H(0,0,z)+2H(0,0,0,z)\\
&\qquad -6\zeta(2)-\zeta(3)\Big)\\
&\quad -8\epsilon^3\Big(-10-8H(0,z)+6\zeta(2)H(0,z)+\zeta(3)H(0,z)-6H(0,0,z)\\
&\qquad +3\zeta(2)H(0,0,z)-4H(0,0,0,z)-2H(0,0,0,0,z)\\
&\qquad +9\zeta(2)-\frac{3\zeta(2)^2}{2}+2\zeta(3)\Big)+\mathcal{O}(\epsilon^4)\Big\}
\end{aligned} \tag{5.48}$$

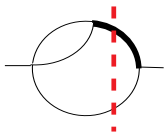

$$= \mu^{2(4-D)}\int \frac{d^Dk_1d^Dk_2}{(2\pi)^{2D}}\frac{\delta(k_2^2-a^2)\delta(k_2+p)^2}{k_1^2(k_1+p)^2}$$

$$\begin{aligned}
&= \mathcal{N}(1-z)^{1-2\epsilon}\Big\{\frac{1}{\epsilon}+4+H(0,z)\\
&\quad -2\epsilon\Big(-6-2H(0,z)-\frac{H(0,0,z)}{2}+3\zeta(2)\Big)\\
&\quad +4\epsilon^2\Big(8+3H(0,z)-\frac{3\zeta(2)H(0,z)}{2}+H(0,0,z)+\frac{H(0,0,0,z)}{4}\\
&\qquad -6\zeta(2)-\zeta(3)\Big)
\end{aligned}$$

$$
\begin{aligned}
&-8\epsilon^3\Bigg(-10 - 4H(0,z) + 3\zeta(2)H(0,z) + \frac{\zeta(3)H(0,z)}{2} - \frac{3H(0,0,z)}{2} \\
&\quad + \frac{3\zeta(2)H(0,0,z)}{4} - \frac{H(0,0,0,z)}{2} - \frac{H(0,0,0,0,z)}{8} \\
&\quad + 9\zeta(2) - \frac{3\zeta(2)^2}{2} + 2\zeta(3)\Bigg) + \mathcal{O}(\epsilon^4)\Bigg\}
\end{aligned} \tag{5.49}
$$

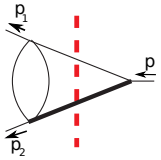

$$
\begin{aligned}
&= \mu^{2(4-D)} \int \frac{d^Dk_1 d^Dk_2}{(2\pi)^{2D}} \frac{\delta(k_2^2 - a^2)\delta(k_2 + p)^2}{k_1^2(p_2 + k_2 - k_1)^2} \\
&= \mathcal{N}(1-z)^{1-3\epsilon}\Bigg\{ \frac{1}{\epsilon} + 4 + H(0,z) \\
&\quad -16\epsilon\Bigg(-\frac{3}{4} - \frac{H(0,z)}{4} - \frac{H(0,0,z)}{16} + \frac{3\zeta(2)}{8}\Bigg) \\
&\quad +32\epsilon^2\Bigg(1 + \frac{3H(0,z)}{8} - \frac{3\zeta(2)H(0,z)}{16} + \frac{H(0,0,z)}{8} + \frac{H(0,0,0,z)}{32} \\
&\qquad -\frac{3\zeta(2)}{4} - \frac{\zeta(3)}{8}\Bigg) \\
&\quad -64\epsilon^3\Bigg(-\frac{5}{4} + \frac{h(0,z)}{2} + \frac{3\zeta(2)H(0,z)}{8} + \frac{\zeta(3)H(0,z)}{16} - \frac{3H(0,0,z)}{16} \\
&\qquad + \frac{3\zeta(2)H(0,0,z)}{32} - \frac{H(0,0,0,z)}{16} - \frac{H(0,0,0,0,z)}{64} \\
&\qquad + \frac{9\zeta(2)}{8} - \frac{3\zeta(2)^2}{16} + \frac{\zeta(3)}{4}\Bigg) + \mathcal{O}(\epsilon^4)\Bigg\}
\end{aligned} \tag{5.50}
$$

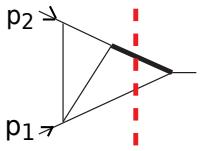

$$
\begin{aligned}
&= \mu^{2(4-D)} \int \frac{d^Dk_1 d^Dk_2}{(2\pi)^{2D}} \frac{\delta(k_2^2 - a^2)\delta(k_2 + p)^2}{k_1^2 k_2^2 (p_1 - k_1)^2} \\
&= \mathcal{N} z a^{-2}\Bigg\{ -\frac{1}{8\epsilon}\Bigg(H(0,0,z) + H(0,1,z) - \zeta(2)\Bigg) \\
&\quad -\frac{\zeta(2)H(0,z)}{4} - \frac{3H(0,0,0,z)}{8} - \frac{H(0,0,1,z)}{2}
\end{aligned}
$$

$$
\begin{aligned}
&-\frac{H(0,1,0,z)}{2}-\frac{5H(0,1,1,z)}{8}+\frac{\zeta(3)}{8}\\
&-2\epsilon\Bigg(\frac{\zeta(3)H(0,z)}{4}-\frac{\zeta(2)H(0,0,z)}{8}+\frac{7H(0,0,0,0,z)}{16}\\
&+\frac{5H(0,0,0,1,z)}{8}+\frac{5H(0,0,1,0,z)}{8}+\frac{7H(0,0,1,1,z)}{8}\\
&+\frac{5H(0,1,0,0,z)}{8}+\frac{7H(0,1,0,1,z)}{8}+\frac{7H(0,1,1,0,z)}{8}\\
&-\frac{13\zeta^2(2)}{80}\Bigg)+\mathcal{O}(\epsilon^2)\Bigg\}
\end{aligned}
\tag{5.51}
$$

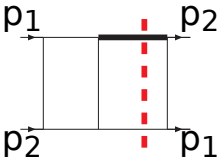

$$
= \mu^{2(4-D)}\int\frac{d^Dk_1d^Dk_2}{(2\pi)^{2D}}\frac{\delta((p_1-k_1-k_2)^2-a^2)\delta((k_1+k_2+p_2)^2)}{k_1^2k_2^2(p_1-k_1)^2(p_1+p_2-k_1-k_2)^2}
$$

$$
\begin{aligned}
&= 3\mathcal{N}a^{-6}z^3(1-z)^{-1-3\epsilon}\Bigg\{\frac{1}{\epsilon^3}-\frac{\pi^2}{2\epsilon}-8\zeta(3)+\mathcal{O}(\epsilon)\Bigg\}\\
&+\frac{\mathcal{N}a^{-6}z^3}{1-z}\Bigg\{\frac{9H(0,z)}{8\epsilon^2}-\frac{1}{2\epsilon}\Bigg(-\frac{11}{2}H(0,0,z)-\frac{25H(0,1,z)}{4}-6H(1,0,z)+\frac{\zeta(2)}{4}\Bigg)\\
&\qquad -5\zeta(2)H(0,z)+6H(0,0,0,z)+\frac{29H(0,0,1,z)}{4}+\frac{29H(0,1,0,z)}{4}\\
&\qquad +\frac{71H(0,1,1,z)}{8}-\frac{\zeta(2)H(1,z)}{4}+7H(1,0,0,z)+\frac{17H(1,0,1,z)}{2}\\
&\qquad +\frac{33H(1,1,0,z)}{4}+\frac{\zeta(3)}{8}+\mathcal{O}(\epsilon)\Bigg\}
\end{aligned}
\tag{5.52}
$$

5.4.3 Results for the 2-cut MIs with two massive propagators

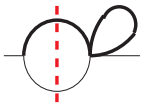

$$
\begin{aligned}
&= \mu^{2(4-D)}\int\frac{d^Dk_1d^Dk_2}{(2\pi)^{2D}}\frac{\delta(k_2^2-a^2)\delta(k_2+p)^2}{k_1^2(k_1+p)^2}\\
&= \mathcal{N}a^2(1-z)^{1-2\epsilon}\Bigg\{-\frac{1}{\epsilon}-3-2H(0,z)+
\end{aligned}
$$

$$
\begin{aligned}
&(-2\epsilon)\bigg(\frac{7}{2}+3H(0,z)+2H(0,0,z)-2\zeta(2)\bigg)\\
&+4\epsilon^2\bigg(-\frac{15}{4}-\frac{7H(0,z)}{2}+\zeta(2)H(0,z)-3H(0,0,z)\\
&-2H(0,0,0,z)+\frac{3\zeta(2)}{2}+\frac{\zeta(3)}{2}\bigg)+\mathcal{O}(\epsilon^3)\bigg\}
\end{aligned}
\tag{5.53}
$$

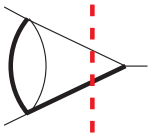

$$
\begin{aligned}
&= \mu^{2(4-D)}\int\frac{d^Dk_1d^Dk_2}{(2\pi)^{2D}}\frac{\delta((k_1+k_2)^2-a^2)\delta((k_1+k_2-p_1-p_2)^2)}{k_2^2((p_1-k_1)^2+a^2)}\\
&= \mathcal{N}\bigg\{-\frac{1}{2\epsilon}\bigg(-\frac{1}{4}+\frac{z}{4}\bigg)+\frac{9}{16}-\frac{9z}{16}+\frac{H(0,z)}{4}-\frac{zH(0,z)}{8}\\
&\quad-\frac{H(0,0,z)}{16}+\frac{H(1,z)}{4}-\frac{zH(1,z)}{4}\\
&\quad-\frac{H(1,0,z)}{16}-\frac{zH(1,0,z)}{16}-\frac{z\zeta(2)}{16}\\
&\quad-(2\epsilon)\bigg(-\frac{1}{675z^2}+\frac{1}{256z}-\frac{2125z}{2304}-\frac{33H(0,z)}{64}+\frac{9H(0,z)}{32}\\
&\quad-\frac{5\zeta(2)z}{64}-\frac{H(0,0,z)}{4}+\frac{5H(0,0,0,z)z}{64}\\
&\quad+\frac{5zH(0,0,0,z)}{64}+\frac{zH(0,0,0,1)}{16}-\frac{H(0,1,z)}{4}\\
&\quad+\frac{zH(0,1,z)}{8}-\frac{3\zeta(2)zH(1,z)}{64}-\frac{H(1,0,z)}{8}\\
&\quad+\frac{\zeta(2)}{4}-\frac{7z}{64}+\frac{3z}{32}\bigg)+\mathcal{O}(\epsilon^2)\bigg\}
\end{aligned}
\tag{5.54}
$$

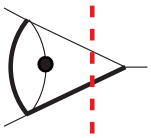

$$
\begin{aligned}
&= \mu^{2(4-D)}\int\frac{d^Dk_1d^Dk_2}{(2\pi)^{2D}}\frac{\delta((k_1+k_2)^2-a^2)\delta((k_1+k_2-p_1-p_2)^2)}{k_2^4((p_1-k_1)^2+a^2)}\\
&= \mathcal{N}a^2\bigg\{-\frac{1}{2\epsilon}\bigg(\frac{1}{16z}+\frac{1}{4}-\frac{5z}{16}\bigg)\\
&\quad-\frac{\zeta(9)}{64}-\frac{17}{32}+\frac{39z}{64}-\frac{H(0,z)}{16}-\frac{3H(0,z)}{16z}+\frac{5zH(0,z)}{32}
\end{aligned}
$$

$$+\frac{5zH(0,z)}{32}+\frac{zH(0,0,z)}{32}-\frac{H(0,z)}{16z}-\frac{H(1,z)}{4}+\frac{5zH(1,z)}{16}$$
$$+\frac{zH(1,0,z)}{32}+\frac{z\zeta(2)}{32}+\mathcal{O}(\epsilon)\Big\} \tag{5.55}$$

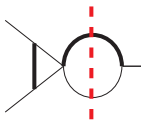

$$= \mu^{2(4-D)}\int\frac{d^Dk_1d^Dk_2}{(2\pi)^{2D}}\frac{\delta(k_2^2-a^2)\delta(k_2+p)^2}{(k_1^2-a^2)(p_1-k_1)^2(p_2+k_1)^2}$$
$$= \mathcal{N}a^{-2}[z^\epsilon(1-z)^{1-2\epsilon}\frac{\Gamma(2-\epsilon)}{\epsilon(1-\epsilon)\Gamma(2-2\epsilon)\Gamma(1+\epsilon)}]\times$$
$$\times(-\frac{1}{4}a^{-2}z(H(0,0,z)-H(1,0,z)-\frac{\pi^2}{4})+\mathcal{O}(\epsilon))$$
$$= \mathcal{N}a^{-2}z^{1+\epsilon}(1-z)^{1-2\epsilon}\Big(-\frac{1}{4\epsilon}(H(0,0,z)-H(1,0,z)-\frac{3\zeta(2)}{2})+C([\,],0)+$$
$$+\mathcal{O}(\epsilon)\Big) \tag{5.56}$$

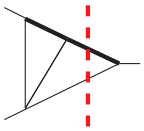

$$= \mu^{2(4-D)}\int\frac{d^Dk_1d^Dk_2}{(2\pi)^{2D}}\frac{\delta((k_1+k_2)^2-a^2)\delta(k_1+k_2-p_1-p_2)^2}{(k_1^2-a^2)(p_1-k_1)^2k_2^2}$$
$$= \mathcal{N}a^{-2}z\Big\{\frac{1}{4\epsilon^2}\Big(\frac{3H(0,z)a^4}{2}C_{(11,[\ ],-2)}-2H(0,z)\Big)$$
$$-\frac{1}{2\epsilon}\Big(C_{(10,[\ ],-2)}-\frac{3za^4H(0,0,z)}{4}C_{(11,[\ ],-2)}$$
$$-\frac{3za^4H(0,1,z)}{4}C_{(11,[\ ],-1)}+\frac{3za^4H(0,z)}{2}C_{(11,[\ ],-2)}\Big)$$
$$-\frac{1}{2}H(0,z)C_{(10,[\ ],-2)}+C_{(10,[\ ],0)}+\frac{3H(0,0,0,z)}{8}C_{(11,[\ ],-2)}$$
$$+\frac{3H(0,0,1,z)}{2}C_{(11,[\ ],-2)}+\frac{9H(0,1,0,z)}{4}C_{(11,[\ ],-2)}$$
$$-\frac{3H(0,0,z)}{4}C_{(11,[\ ],-1)}-3H(0,1,z)C_{(11,[\ ],-1)}$$
$$-\frac{3H(0,z)}{2}C_{(11,[\ ],0)}+\zeta(2)H(0,z)+H(0,0,0,z)$$

$$-\frac{3}{16}H(0,0,1,z)+\frac{9}{16}H(0,1,z)+\frac{5H(0,1,0,z)}{8}$$
$$-\frac{53H(0,1,1,z)}{16}+\mathcal{O}(\epsilon)\Big\} \tag{5.57}$$

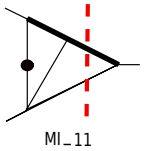

$$= \mu^{2(4-D)}\int\frac{d^Dk_1d^Dk_2}{(2\pi)^{2D}}\frac{\delta((k_1+k_2)^2-a^2)\delta(k_1+k_2-p_1-p_2)^2}{(k_1^2-a^2)(p_1-k_1)^4k_2^2}$$

$$= \mathcal{N}z\Big\{\frac{1}{4\epsilon^2}C_{(11,[\ ],-2)}-\frac{1}{2\epsilon}\Big(-2H(1,z)C_{(11,[\ ],-2)}+C_{(11,[\ ],-1)}$$
$$-2H(0,z)C_{(11,[\ ],-1)}+\frac{H(1,z)}{4}\Big)$$
$$+\frac{3H(1,0,z)}{2}C_{(10,[\ ],-2)}+4H(1,1,z)C_{(10,[\ ],0)}$$
$$-2H(1,z)C_{(11,[\ ],-1)}+C_{(11,[\ ],0)}$$
$$+2H(0,0,z)+2H(0,1,z)+-\frac{3H(1,z)}{8}$$
$$+\frac{7H(1,0,z)}{4}-\frac{7H(1,1,z)}{8}+\mathcal{O}(\epsilon)\Big\}. \tag{5.58}$$

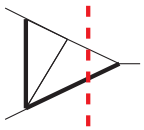

$$= \mu^{2(4-D)}\int\frac{d^Dk_1d^Dk_2}{(2\pi)^{2D}}\frac{\delta((k_1+k_2)^2-a^2)\delta(k_1+k_2-p_1-p_2)^2}{((p_1-k_1)^2-a^2)k_2^2}$$

$$= \mathcal{N}a^{-2}z\Big\{-\frac{1}{\epsilon}\Big(H(0,0,z)+H(1,0,z)+\zeta(2)\Big)$$
$$+\frac{5}{z}-5+\frac{3H(0,z)}{z}+2H(0,z)+2H(0,z)\zeta(2)$$
$$+H(0,0,z)-4H(0,0,0,z)-2H(0,0,1,z)+\zeta(2)H(1,z)$$
$$-5H(1,0,0,z)-2H(1,0,1,z)-H(1,1,0,z)-\frac{7\zeta(3)}{2}+\mathcal{O}(\epsilon)\Big\} \tag{5.59}$$

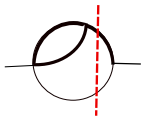

$$= \mu^{2(4-D)} \int \frac{d^D k_1 d^D k_2}{(2\pi)^{2D}} \frac{\delta((k_2^2 - a^2)\delta(k_2 + p)^2}{(k_1 + k_2)^2 - a^2)(k_1^2 - a^2)}$$

$$= \mathcal{N}[z^\epsilon (1-z)^{1-2\epsilon} \frac{\Gamma(2-\epsilon)}{\epsilon(1-\epsilon)\Gamma(2-2\epsilon)\Gamma(1+\epsilon)}] \times$$

$$\times (\frac{3}{4})^{\frac{1-2\epsilon}{2}} \, {}_2F_1(\frac{3-\epsilon}{2}, \frac{1}{2}, \frac{3}{2}, -\frac{1}{4}). \tag{5.60}$$

Table 5.3: MIs for the 2-cut diagrams with two massive propagators

Topology t	Master integrals
7	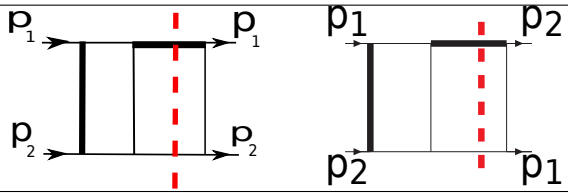
6	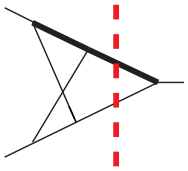
5	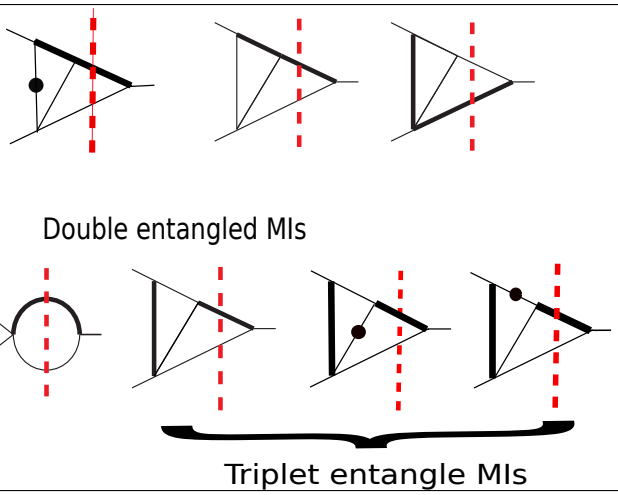
4	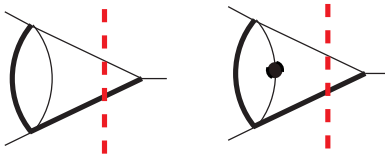
3	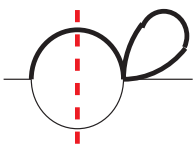

Table 5.4: MIs for the 2-cut diagrams with three massive propagators

Topology t	Master integrals
7	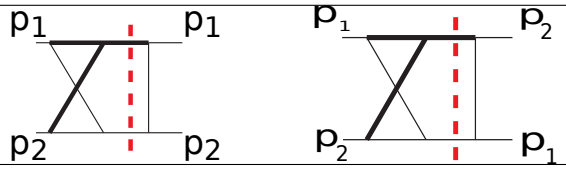
6	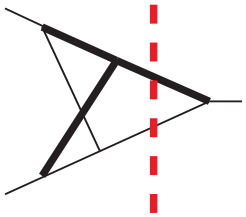
5	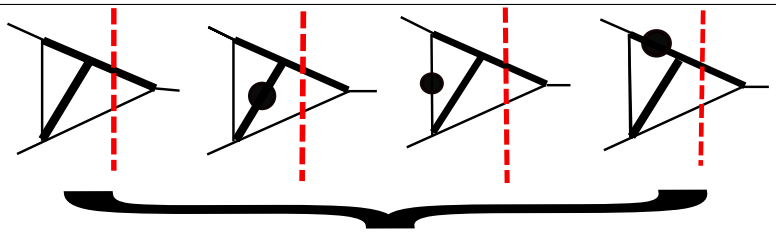
4	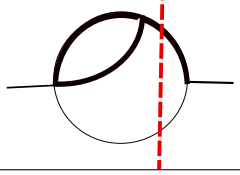

Chapter 6

Conclusions and outlook

Drell-Yan production of Z and W bosons is a fundamental process for an accurate check of the SM at hadron colliders. Fermion-pair production above the Z and W boson poles is a rich field for the search of new phenomena at present and future high energy colliders. The experimental measurements of observables related to the Drell-Yan mechanism will reach very high accuracy in the near future. Hence, it is very important to provide for the latter a reliable and equally accurate theoretical prediction. This means that a good control on the higher-order perturbative corrections is required for the physics studies at hadron colliders. Even though NNLO QCD corrections and NLO EW perturbative corrections to the total cross section of production of a lepton (or lepton-neutrino) pairs are known (including also the corrections to more exclusive quantities like the invariant mass distribution, the rapidity distribution, etc.), the NNLO mixed QCD-EW corrections are still missing. This constitutes the topic of the present thesis.

Using the narrow-width approximation, we decoupled the production of the on-shell gauge boson from its subsequent decay. We concentrated our attention, then, on the production process and in particular on the real part of the NNLO mixed QCD-EW corrections to the Drell-Yan production of an on-shell Z (or W) boson.

All the Feynman diagrams, needed for the calculation of the corrections at $\mathcal{O}(\alpha\alpha_S)$, were generated by `FeynArts`. The integration over the phase-space of the interference terms were re-written using the Cutkosky rules in terms of a combination of diagrams with propagators having the correct causality prescription and propagators with the opposite one. Then, these integrals were reduced using Integration-By-Parts Identities, to a small set of independent integrals, called Master Integrals. The reduction was done using the `C++` program called `Reduze`, which is publicly available. The calculation of the MIs is performed using the differential equations method. In order to constrain the integral constants, we calculated the soft-limits of the MIs.

The result of the basic MIs with one massive propagator can be extracted directly, since we know the results of the corresponding virtual MIs. For the rest, we found the

method of differential equations to be adequate to solve the MIs. We re-calculated all the results of the MIs with one massive propagator, which were already present in the literature for the calculation of the NNLO QCD corrections to Higgs boson hadro-production. They amount to 8 masters with three cuts and 5 masters with two cuts. After accounting for the different normalization, our results are in perfect agreement with the ones already existing in the literature [61] .

For the MIs with two massive propagators, the situation becomes trickier. The presence of the additional massive propagator makes in such a way that there are topologies with more than one MI. Consequently, the corresponding system of first-order linear differential equations is more complicated to solve. Moreover, the analytic structure of the result is richer and some of the masters exhibit the presence of additional denominators in the differential equations. This fact in turn translates into the need of an extended set of generalized polylogarithms, in order to express the final results. The basic MIs are calculated in the same way as the basic MIs with one massive propagator. The system of coupled linear differential equations can be dis-entangled if we chose the base of masters properly. In our case, the main difficulty is done by three entangled MIs. It is not easy to disentangle completely their differential equations. However, we can choose a base in which one of the masters can be disentangled in ϵ. In this way, the system can be solved in two steps: firstly we solve the first-order linear differential equation and then the second-order one. Once these difficulties are overcome, one is able to perform analytically all phase space integrals with two massive propagators. In the thesis, we collected the result for the 3 new MIs with three cuts and 7 new MIs with two cuts.

In the case of MIs with three massive propagators, the system of four entangled MIs constitutes the biggest challenge. At the moment, we are not able to disentangle the masters. This means that one should solve a fourth order linear differential equation, and no general algorithm is known for this goal. The hope is that, once the "correct" base of MIs will be found, the system will decouple at least in two second order linear differential equations. Since these masters enter in the non-homogeneous part of the three MIs with a bigger number of denominators, we were not able to perform the calculation of the latters. We have their differential equations and they do not present particular difficulties. The base MI with three massive denominators is calculated and its result presented in the thesis.

The soft limit of the boxes with two and three massive propagators also needs further studies.

Appendix A

Notations

For what concerns the relativistic notations, we use the "Pauli-Veltman" definitions of vector p^μ and scalar product:

$$p^\mu \,=\, (\mathbf{p}, ip^4)\,, \quad p_1 \cdot p_2 \,=\, p^\mu p^\nu\, \delta_{\mu\nu} \,=\, \mathbf{p}_1 \cdot \mathbf{p}_2 - p_1^4 p_2^4\,, \tag{A.1}$$

such that:

$$p^2 \,=\, \|\mathbf{p}\|^2 - p_4^2\,. \tag{A.2}$$

The vector p^μ will be said *time-like*, *light-like* or *space-like* if $p^2 < 0$, $p^2 = 0$ or $p^2 > 0$, respectively.

With this notation the mass-shell relation for a massive particle becomes:

$$p^2 \,=\, -m^2\,, \tag{A.3}$$

from which the energy can be extracted:

$$E \,=\, p_4^2 \,=\, \|\mathbf{p}\|^2 + m^2\,. \tag{A.4}$$

The metric tensor is the identity in four dimensions:

$$g_{\mu\nu} \to \delta_{\mu\nu} \,=\, \begin{pmatrix} 1 & 0 & 0 & 0 \\ 0 & 1 & 0 & 0 \\ 0 & 0 & 1 & 0 \\ 0 & 0 & 0 & 1 \end{pmatrix}$$

The notation adopted for the vectors brings to the following Feynman rules of the

propagator:

$$\frac{\delta_{\mu\nu}}{(k^2 - i\epsilon)} \quad \text{Photonic Propagator}\,, \tag{A.5}$$

$$\frac{(-i\ \not{p} + m)}{(p^2 + m^2 - i\epsilon)} \quad \text{Fermionic Propagator}\,, \tag{A.6}$$

$$\frac{\delta_{\mu\nu}}{(k^2 + m_W^2 - i\epsilon)} \quad \text{W Propagator}\,, \tag{A.7}$$

$$\frac{\delta_{\mu\nu}}{(k^2 + m_Z^2 - i\epsilon)} \quad \text{Z Propagator}\,, \tag{A.8}$$

$$\frac{\delta_{\mu\nu}\delta_{ab}}{(k^2 - i\epsilon)} \quad \text{Gloun Propagator}\,, \tag{A.9}$$

The Feynman rules for the vertices are:

$$i\, e\gamma^\mu \quad e\gamma\bar{e} \text{ Vertex}\,, \tag{A.10}$$

$$i\,\frac{1}{2} g_s \gamma^\mu \lambda_{ij}^a \quad qg^a\bar{q} \text{ Vertex}\,, \tag{A.11}$$

$$i\, g\frac{1}{4c_w}\gamma^\mu[1 - \frac{8}{3}s_w^2 + \gamma^5] \quad \bar{\mu}Z^0\mu \text{ Vertex}\,, \tag{A.12}$$

$$i\, g\frac{1}{4c_w}\gamma^\mu[4s_w^2 - 1 - \gamma^5] \quad \bar{e}Z^0 e \text{ Vertex}\,, \tag{A.13}$$

$$i\, g\frac{1}{2\sqrt{2}}\gamma^\mu(1 + \gamma^5)V_{ud}^* \quad \bar{d}W^- V_{ud}^*\mu \text{ Vertex}\,, \tag{A.14}$$

$$i\, g\frac{1}{2\sqrt{2}}\gamma^\mu(1 + \gamma^5)V_{ud} \quad \bar{\mu}W^+ V_{ud} d \text{ Vertex}\,, \tag{A.15}$$

$$i\, g\frac{1}{2\sqrt{2}}\gamma^\mu(1 + \gamma^5) \quad \bar{e}W^-\nu \text{ Vertex} \tag{A.16}$$

$$i\, g\frac{1}{2\sqrt{2}}\gamma^\mu(1 + \gamma^5) \quad \bar{\nu}W^+ e \text{ Vertex} \tag{A.17}$$

with the following expressions for the energy projectors:

$$\sum_s u(p)\,\overline{u}(p) \;=\; \frac{-i\ \not{p} + m}{2m}\,, \tag{A.18}$$

$$\sum_s v(p)\,\overline{v}(p) \;=\; -\frac{i\ \not{p} + m}{2m}\,. \tag{A.19}$$

The Mandelstam variables for a $2 \to 2$ particles process ($p_1 + p_2 \to p_3 + p_4$) are:

$$s \;=\; (p_1 + p_2)^2 \;=\; (p_3 + p_4)^2\,, \tag{A.20}$$

$$t \;=\; (p_1 - p_3)^2 \;=\; (p_4 - p_2)^2\,, \tag{A.21}$$

$$u \;=\; (p_1 + p_4)^2 \;=\; (p_3 - p_2)^2\,. \tag{A.22}$$

Finally, the causality prescription forces the squared center-of-mass energy, s, to get an infinitesimal positive imaginary part $s + i0^+$. This is important to correctly define the imaginary part of the integrals, when their value lie in the physical region, above the threshold of production of the final state particles. In particular, we usually solve the differential equations for "Euclidean" integrals (in which all the denominators are positive definite expressions and the integrals are real quantities). We recover the Minkowski region using the Wick rotation and the substitution

$$p^2 \to -(s + i0^+) \tag{A.23}$$

in the analytic formulas. This produces the imaginary part of the integral. For the differential equations that involve directly the cut diagrams (or equivalently the imaginary parts), we solve the equation directly in the physical s.

Appendix B

Harmonic Polylogarithms

In this appendix we review some well known results about Harmonic Polylogarithms of one variable (HPL).

We define the following set of functions:

$$f(-1,x) = \frac{1}{x}\,, \tag{B.1}$$

$$f(0,x) = \frac{1}{(1+x)}\,, \tag{B.2}$$

$$f(1,x) = \frac{1}{(1-x)}\,. \tag{B.3}$$

Then, one-dimensional HPL, $H(\mathbf{m}_\omega, x)$, are defined as the functions which form a closed and linearly independent set under the class of integrations

$$\int_0^x dt\,\{f(-1,t); f(0,t); f(1,t)\}\; H(\mathbf{m}_\omega, t)\,, \tag{B.4}$$

where we put

$$H(-1,x) = \int_0^x \frac{dt}{(1+t)} = \ln(1+x)\,, \tag{B.5}$$

$$H(0,x) = \ln x\,, \tag{B.6}$$

$$H(1,x) = \int_0^x \frac{dt}{(1-t)} = -\ln(1-x)\,, \tag{B.7}$$

and where $\mathbf{m}_\omega$ is an ω-dimensional vector with components 1, 0 or -1.

We have:

$$H(\mathbf{0}_\omega, x) = \frac{1}{\omega!}\ln^\omega x\,, \tag{B.8}$$

$$H(a, \mathbf{m}_{\omega-1}, x) = \int_0^x dt f(a,t) H(\mathbf{m}_{\omega-1}, t)\,, \tag{B.9}$$

$$\frac{d}{dx} H(a, \mathbf{m}_{\omega-1}, x) = f(a,x) H(\mathbf{m}_{\omega-1}, x)\,. \tag{B.10}$$

The following identities between HPL are widly used:

$$H(m_1,\cdots,m_q,x) = H(m_1,x)H(m_2,\cdots,m_q,x) - H(m_2,m_1,x)H(m_3,\cdots,m_q,x) + \\ +H(m_3,m_2,m_1,x)H(m_4,\cdots,m_q,x) - \cdots - (-1)^q H(m_q,\cdots,m_1,x) \quad \text{(B.11)}$$

which holds by subsequently integrating by parts, and

$$H(\mathbf{p},x)H(\mathbf{q},x) = \sum_{\mathbf{r}=\mathbf{p}+\mathbf{q}} H(\mathbf{r},x)\,, \quad \text{(B.12)}$$

where $\mathbf{r}$ is a $(\omega_p+\omega_q)$-dimensional vector constituted by all mergers of $\mathbf{p}$ and $\mathbf{q}$ in wich the relative orders of the elements of $\mathbf{p}$ and $\mathbf{q}$ are preserved. In the case $\omega_p = 1$, we have:

$$\begin{aligned} H(a,x)H(m_1,\cdots,m_q,x) &= H(a,m_1,\cdots,m_q,x) + H(m_1,a,m_2,\cdots,m_q,x) + \\ &\quad + \cdots + H(m_1,\cdots,m_q,a,x)\,. \end{aligned} \quad \text{(B.13)}$$

Relation Eq. (B.12) tells us that HPL fulfil an algebra; the product of two HPL of weights ω_1 and ω_2 of argument x is a combination of HPL of the same argument and weight $\omega = \omega_1 + \omega_2$.

Bibliography

[1] J. H. Christenson, G. S. Hicks, L. M. Lederman, P. J. Limon, B. G. Pope and E. Zavattini, Phys. Rev. Lett. **25**, 1523 (1970).

[2] R. P. Feynman, Phys. Rev. Lett. **23**, 1415 (1969). R. P. Feynman, Reading 1972, 282p

[3] T. Affolder *et al.* [CDF Collaboration], Phys. Rev. Lett. **87** (2001) 131802 [hep-ex/0106047].

[4] G. Altarelli and G. Parisi, Nucl. Phys. B **126**, 298 (1977).

[5] CMS Collaboration, CMS-PAS-SMP-12-011(2012).

[6] CMS Collaboration, JHEP **10** (2011) 132.

[7] ATLAS Collaboration, Phys. Rev. **D85**(2012) 072004

[8] LHCb Collaboration, LHCb-CONF-2012-013 (2012)

[9] A. A. Savin, arXiv:1212.3695 [hep-ex].

[10] K. Melnikov and F. Petriello, Phys. Rev. Lett. **96**, 231803 (2006). Phys. Rev. D **74**, 114017 (2006).

[11] M. Botje, J. Butterworth, A. Cooper-Sarkar, A. de Roeck, J. Feltesse, S. Forte, A. Glazov and J. Huston *et al.*, arXiv:1101.0538 [hep-ph].

[12] V. Buge, Ch. Jung, G. Quast, A. Ghezzi, M. Malberti, and T. Tabarelli de Fatis, Prospects for the precision measurement of the W mass with the CMS detector at the LHC CMS AN 20006/033

[13] N. Besson, M. Boonekamp, E. Klinkby, T. Petersen, and S. Mehlhase, for (ALTAS Collaboration), Eur. Phys. J . C **57**627(2008).

[14] G. Bozzi, J. Rojo and A. Vicini, Phys. Rev. D **83**, 113008(2011)

[15] G. Altarelli, *et al.*, Nucl. Phys. B**157**(1979)461. G. Altarelli, *et al.*, Nucl. Phys. B **246**(1984)12.

[16] R. K. Ellis, *et al.*, Nucl. Phys. B **211**(1983)106. P. B. Arnold, M. H. Reno, Nucl. Phys. B**319**(1989)37[Erratum-ibid. B **330**(1990)284]. R. J. Gonsalves, *et al.*, Phys. Rev. D **40**(1989)2245. F. T. Brandt, *et al.*, Int. J. Mod. Phys. A **6**(1991)3973. W. T. Giele, *et al.*, Nucl. Phys. B **403**(1993)633. L. J. Dion,*et al.*, Nucl. Phys. B **531**(1998)3.

[17] J. H. Kuhn, *et al.*, Phys. Lett. B **609**(2005)277; Nucl. Phys. B **727**(2005)368. Phys. Lett. B **651**(2007)160; Nucl. Phys. B **797**(2008)27; W. Hollik, *et al.*, Nucl. Phys. B **790**, 138(2008).

[18] P. B. Arnold and R. P. Kauffman, Nucl. Phys. B **349**, 381 (1991) C. Balazs, J. -w. Qiu and C. P. Yuan, Phys. Lett. B **355**, 548 (1995). R. K. Ellis, D. A. Ross and S. Veseli, Nucl. Phys. B **503**, 309 (1997). R. K. Ellis and S. Veseli, Nucl. Phys. B **511**, 649 (1998). J. -w. Qiu and X. -f. Zhang, Phys. Rev. Lett. **86**, 2724 (2001). Phys. Rev. D **66**(2001)114011. A. Kulesza and W. J. Stirling, Eur. Phys. J. C **20**, 349 (2001). A. Kulesza, G. F. Sterman and W. Vogelsang, Phys. Rev. D **66**, 014011 (2002). F. Landry, R. Brock, P. M. Nadolsky and C. P. Yuan, Phys. Rev. D **67**, 073016 (2003). G. Bozzi, S. Catani, G. Ferrera, D. de Florian and M. Grazzini, Phys. Lett. B **696**, 207 (2011).

[19] C. Balazs and C. P. Yuan, Phys. Rev. D **56**, 5558 (1997).

[20] S. D. Drell, T. -M. Yan, Phys. Rev. Lett. **25** (1970) 316 [Erratum-ibid. **25** (1970) 902].

[21] D. J. Gross and C. H. Llewellyn Smith, Nucl. Phys. B **14**, 337 (1969).

[22] S. L. Adler, Phys. Rev. **143**, 1144 (1966).

[23] V. M. Outschoorn *et al.* [ATLAS Collaboration], arXiv:1110.2054 [hep-ex].

[24] G. F. Sterman, Nucl. Phys. B **281**, 310 (1987).

[25] S. Catani and L. Trentadue, Nucl. Phys. B **327**, 323 (1989). S. Catani and L. Trentadue, Nucl. Phys. B **353**, 183 (1991).

[26] G. Sterman, Nucl. Phys. B **281**(1981). S. Catani, L. Trentadue, Nucl. Phys. B **327**323(1989); Nucl. Phys. B **353** 183(1991). S. Moch, A. Vogt, Phys. Lett. B **631**(2005)48. T. Becher, M. Neubert and G. Xu, JHEP **0807**, 030 (2008) [arXiv:0710.0680 [hep-ph]].

[27] T. Matsuura, *et al.*, Nucl. Phys. B **319**(1989)570. R. Hamberg, *et al.*, Nucl. Phys. B **359**(1991)343[Erratum-ibid.B**644**(2002)403].

[28] S. Catani and M. Grazzini, Phys. Rev. Lett. **98**, 222002 (2007). Phys. Rev. Lett. **103**, 082001 (2009).

[29] C. M. Carloni Calame, G. Montagna, O. Nicrosini and A. Vicini, JHEP **0612**, 016 (2006) [hep-ph/0609170].

[30] L. Barze', G. Montagna, P. Nason, O. Nicrosini, F. Piccinini and A. Vicini, Eur. Phys. J. C **73**, 2474 (2013) [arXiv:1302.4606 [hep-ph]].

[31] D. Wackeroth, W. Hollik, Phys. Rev. D **55**(1997)6788. U. Baur, *et al.*, Phys. Rev. D**59**(1999) 013002. S. Dittmaier, M. Kramer, Phys. Rev. D**65**(2002)073007. U. Baur, D. Wackeroth, Phys. Rev. D**70**(2004)073015. V. A. Zykunov, Phys. Atom. Nucl. **69**(2006)1522[Yad. Fiz. **69**(2006)1557].
A. Arbuzov, *et al.*, Eur. Phys. J. C. **46**(2006)407[Erratum-ibid. C **50**(2007)505].
C. M. Carloni Calame, *at el.*, JHEP**0612**(2006)016.

[32] U. Baur, *et al.*, Phys. Rev. D**57**(1998)199. U. Baur, *et al.*, Phys. Rev. D**65**(2002)033007. V. A. Zykunov,Phys. Rev. D**75**(2007)073019. C. M. Carloni Calame, G. Montagna, O. Nicrosini and A. Vicini, JHEP **0710**(2007)109. A. Arbuzov, *et al.*, Eur. Phys. J. C **54**(2008)451.

[33] S. Dittmaier and M. Kramer, Phys. Rev. D **65**, 073007 (2002).

[34] U. Baur and D. Wackeroth, Phys. Rev. D **70**, 073015 (2004).

[35] T. Gehrmann and L. Tancredi, JHEP **1202**, 004 (2012).

[36] C. Anastasiou, L. J. Dixon, K. Melnikov and F. Petriello, Phys. Rev. D **69**, 094008 (2004) [hep-ph/0312266].

[37] S. Frixione, B. R. Webber, JHEP**0206**(2002)029

[38] S. Frixione, *et al.*, JHEP**0711**(2007)070

[39] W. B. Kilgore and C. Sturm, Phys. Rev. D **85** (2012) 033005 [arXiv:1107.4798 [hep-ph]].

[40] N. Kauer, Phys. lett. B **649**, 413 (2007)

[41] T. Hahn, Comput. Phys. Commun. **140**, 418 (2001) [hep-ph/0012260].

[42] J. Beringer et al. (Particle Data Group), Phys. Rev. D **86** (2012) 010001.

[43] P. Nogueira, *Automatic Feynman graph generation*, J. Comput. Phys. **105** (1993) 279.

[44] A. Kotikov, J. H. Kuhn and O. Veretin, Nucl. Phys. B **788** (2008) 47 [arXiv:hep-ph/0703013].

[45] R. Bonciani, G. Degrassi and A. Vicini, in preparation.

[46] C. W. Bauer, A. Frink and R. Kreckel, cs/0004015 [cs-sc].

[47] C. Anastasiou and A. Lazopoulos, JHEP **0407**, 046 (2004) [hep-ph/0404258].

[48] A. V. Smirnov, JHEP **0810**, 107 (2008) [arXiv:0807.3243 [hep-ph]].

[49] E. Remiddi, Nuovo Cim. A **110**, 1435 (1997) [hep-th/9711188].

[50] M. Caffo, H. Czyz, S. Laporta and E. Remiddi, Acta Phys. Polon. B **29**, 2627 (1998) [hep-th/9807119]. M. Caffo, H. Czyz, S. Laporta and E. Remiddi, Nuovo Cim. A **111**, 365 (1998) [hep-th/9805118].

[51] T. Gehrmann and E. Remiddi, Nucl. Phys. B **580**, 485 (2000) [hep-ph/9912329].

[52] G. 't Hooft and M. Veltman, *Nucl. Phys.***B44**(1972)189.
C. G. Bollini and J. J. Giambiagi, Phys. Lett. **40B**(1972)566; Nuovo Cim. **12B**(1972)20.
J. Ashmore, Lett. Nuovo Cimento **4**(1972)289.
G. M. Cicuta and E. Montaldi, Lett. Nuovo Cimento **4**(1972)289.

[53] R. Gastmans and R. Meuldermans, Nucl. Phys. **B63**(1973)277. V. A. Smirnov,Theor. Math. Phys.**44**(1980)761;Theor. Math. Phys. **46**(1981)17; Fortsch. Phys. **33**(1985)495. V. A. Smirnov and K. G. Chetyrkin,Theor. Math. Phys. **56**(1984)770.

[54] F. V. Tkachov Phys. Lett.**B100**(1981)65.
K. G. Chetyrkin and F. V. Tkachov, Nucl. Phys. **B192**(1981)159.

[55] T. Gehrmann and E. Remiddi, Nucl. Phys. B **580**, 485 (2000) [hep-ph/9912329].

[56] S. Laporta and E. Remiddi, Phys. Lett. B **379**, 283 (1996) [hep-ph/9602417].

[57] C. G. Bollini and J. J. Giambiagi, Nuovo Cim. B **12**, 20 (1972).

[58] E. Remiddi and J. A. M. Vermaseren, Int. J. Mod. Phys. A **15**, 725 (2000) [hep-ph/9905237].

[59] T. Gehrmann and E. Remiddi, Nucl. Phys. B **601**, 248 (2001) [hep-ph/0008287].

[60] A. V. Kotikov, Phys. Lett. B**254**(1991)158. Phys. Lett. B**259**(1991)314. Phys. Lett. B**267**(1991)123. E. Remiddi, Nuovo Cim. A **110**(1997)1435.

[61] C. Anastasiou and K. Melnikov, Nucl. Phys. B **646**, 220 (2002) [hep-ph/0207004].

[62] C. Studerus, Comput. Phys. Commun. 181 (2010) 1293;

[63] R. E. Cutkosky, J. Math. Phys. **1**, 429 (1960).

[64] C. Anastasiou, S. Buehler, C. Duhr and F. Herzog, JHEP **1211**, 062 (2012) [arXiv:1208.3130 [hep-ph]].

[65] C. Anastasiou, F. Herzog and A. Lazopoulos, JHEP **1103**, 038 (2011) [arXiv:1011.4867 [hep-ph]].

[66] T. Gehrmann and E. Remiddi, Nucl. Phys. B **580**, 485 (2000) [hep-ph/9912329].

[67] J. D. Bjorken, Phys. Rev. **179**, 1547 (1969).

[68] J. D. Bjorken and E. A. Paschos, Phys. Rev. **185**, 1975 (1969).